

“Investigation of Photodetector Optimization in Reducing Power Consumption by a Noninvasive Pulse Oximeter Sensor”

A Thesis

Submitted to the Faculty

of the

WORCESTER POLYTECHNIC INSTITUTE

in partial fulfillment of the requirements for the

Degree of Master of Science

by

Chirag J. Pujary

Date: Jan 16, 2004

Approved:

Professor Yitzhak Mendelson, Ph.D., Major Advisor

Associate Professor, Biomedical Engineering

Professor Ross D. Shonat, Ph.D., Committee Member

Assistant Professor, Biomedical Engineering

Professor Peder C. Pedersen, Ph.D., Committee Member

Professor, Electrical and Computer Engineering

ABSTRACT

Noninvasive pulse oximetry represents an area of potential interest to the army, because it could provide cost-effective, safe, fast and real-time physiological assessment in a combat injured soldier. Consequently, there is a need to develop a reliable, battery-powered, wearable pulse oximeter to acquire and process photoplethysmographic (PPG) signals using an optimized sensor configuration. A key requirement in the optimal design of a wearable wireless pulse oximeter is low power management without compromising signal quality. This research investigated the advantage gained by increasing the area of the photodetector and decreasing the light emitting diode (LED) driving currents to reduce the overall power requirement of a reflectance mode pulse oximeter sensor. *In vitro* and preliminary *in vivo* experiments were conducted to evaluate a multiple photodetector reflectance sensor setup to simulate a varying detection area. It was concluded that a reflection pulse oximeter sensor employing a large area photodetector is preferred over a similar transmission type sensor for extending the battery life of a wireless pulse oximeter intended for future telemedicine applications.

ACKNOWLEDGEMENTS

I wish to extend my deepest appreciation to the following:

Prof. Yitzhak Mendelson for his assistance, guidance, and patience throughout the course of this work as well as his confidence in my abilities.

Prof. Ross Shonat and Prof. Peder Pedersen for their valuable comments and, for taking time to review this work.

Mark Savage, for his valuable contributions throughout this project especially, during initial design and brainstorming sessions.

My parents, Jayakar and Chitra Pujary, for their support, care, love and strong upbringing, which has greatly helped me to follow my dream and achieve goals in life.

My sister, Apeksha, for keeping me in touch with my parents and, for her words of encouragement and love.

Samta and her family, for all the love, and support.

Last, but never the least, my friends and room-mates, for their friendship and support.

This work is supported by the U.S. Army Medical Research and Materiel Command under Contract No. DAMD17-03-2-0006. The views, opinions and/or findings contained in this report are those of the author and should not be construed as an official Department of the Army position, policy or decision unless so designated by other documentation.

TABLE OF CONTENT

ABSTRACT	ii
ACKNOWLEDGEMENTS	iii
TABLE OF CONTENT	iv
LIST OF FIGURES	vii
LIST OF TABLES	xiii
1. INTRODUCTION	1
1.1 Significance of Oxygen Saturation	1
1.2 Pulse Oximetry.....	2
1.3 Principle of Pulse Oximetry	3
1.4 Pulse Oximeter Sensors	7
1.4.1 <i>Transmission Mode</i> :.....	7
1.4.2 <i>Reflection Mode</i> :.....	8
1.5 Advantages and Disadvantages of Reflectance and Transmittance Pulse Oximetry	9
1.6 Types of Pulse Oximeter Probes.....	10
1.6.1 <i>Reusable Probes</i> :	10
1.6.2 <i>Disposable Probes</i> :.....	10
1.7 Applications of Pulse Oximetry.....	11
1.7.1 <i>Surgery and Post Anesthetic Care Units</i> :	12
1.7.2 <i>Fetal and Neonate Care</i> :	12
1.7.3 <i>Future Applications in Combat Casualty Care</i> :	13
2. SENSOR COMPONENTS	14
2.1 Light Emitting Diodes (LED)	14
2.1.1 <i>Principle of Operation</i> :	15
2.1.2 <i>LED Characteristics</i> :	16
2.1.3 <i>Light Emitting Diodes vs Solid-State Lasers</i> :	17
2.1.4 <i>Depth of Light Penetration</i> :	19
2.1.5 <i>LED Power Consumption Concerns</i> :.....	20

2.2 Photodiode	21
2.2.1 Photocurrent and photovoltaic operation modes:	21
2.2.2 Characteristics of Silicon-Photodiodes (Si-PD):.....	24
2.2.3 Noise Current:	25
2.3 Optimum LED/PD Separation Distance	29
3. RESEARCH OBJECTIVES	31
4. DESIGN DECISION MATRIX.....	34
4.1 Objective Tree.....	34
4.2 Pairwise Comparison Technique	38
4.3 Initial Decision Matrix	40
4.4 Final Decision Matrix	46
5. MATERIALS	50
5.1 Experimental Sensor Setups	50
5.1.1 Prototype Ring Sensor:	50
5.1.2 Prototype 6-PD Disc Sensor:.....	51
5.1.3 Prototype 12-PD Reflectance Disc Sensor:	52
5.1.4 Central Hub Connector (Multiple DB-9 Female Interfaces):	52
5.2 Pulse Oximetry Instrumentation	54
5.2.1 Photoplethysmogram Signal Processing Unit (PSPU):	55
5.2.2 Reference Pulse Oximeter (RPO):	56
5.2.3 Experimental Pulse Oximeter (EPO):	56
6. METHODOLOGY	58
6.1 Sensor Mode Studies.....	58
6.2 Estimation of Power Consumption in Transmission and Reflection Modes	60
6.3 Testing Multiple PD Performance Using a Prototype 6-PD Reflectance Sensor.....	61
6.3.1 Dark Tests:.....	61
6.3.2 Multiple PD Tests:	61
6.3.3 In-Vivo Experiments:	61
6.4 Effects of PD Size and Measurement Site on Power Consumption	62
6.4.1 In Vivo Experiments:.....	62

6.5. Multiple PD Prototype Sensor Evaluation.....	63
7. RESULTS	67
7.1 Sensor Mode Studies.....	67
7.2 Estimation of Power Consumption in Transmission and Reflection Modes	74
7.3 Testing Multiple PD Performance Using a Prototype 6-PD Reflectance Sensor.....	78
7.4 Effects of PD Size and Measurement Site on Power Consumption	81
7.5 Multiple PD Evaluations.....	84
8. DISCUSSION	88
8.1 Decision Matrix	88
8.2 Sensor Mode Studies.....	90
8.3 Effect of Large PD Area on Power Consumption for Different Sensor Modes.....	93
8.4 Effect of Measurement Site on Power Consumption.....	96
8.5 Effect of Varying LED-PD Separation on Power Consumption	97
8.6 Evaluation of Large Area PD Sensor Prototype	99
9. CONCLUSIONS AND RECOMMENDATIONS.....	104
APPENDIX A	107
APPENDIX B-1.....	110
APPENDIX B-2.....	112
APPENDIX B-3.....	113
REFERENCES.....	115

LIST OF FIGURES

Figure 1.1.	Optical absorbance spectra of Hb, HbO ₂ in the visible and near-infrared wavelength region [2]	3
Figure 1.2.	Variations in light attenuation by tissue, illustrating the rhythmic effect of arterial pulsation [12].	5
Figure 1.3.	Normalization of R and IR wavelengths to remove the effects of variation in the incident light intensity or detector sensitivity [2].	6
Figure 1.4.	Empirical relationship between arterial SaO ₂ and normalized (R/IR) ratio[2].....	7
Figure 1.5.	Transmission mode sensor showing the relative position of the LEDs and PD.	8
Figure 1.6.	A typical commercial reflection mode sensor showing the relative position of the LEDs and PD.	9
Figure 1.7.	Different types of clinical probes.	11
Figure 2.1.	Photon generation due to electrons dropping into the valence band in a forward-biased p-n junction [2]	16
Figure 2.2.	Range of mean penetration depth for different wavelengths for high (100%) and low (40%) saturations [23].	20
Figure 2.3.	(a) Photovoltaic and (b) Photoconductive mode of the photodiode [2]	22
Figure 2.4.	I-V characteristics for a typical Si-PD [2].	23
Figure 2.5.	Spectral response of a typical Si-PD as a function of wavelength [2].	24
Figure 2.6.	Equivalent circuit of the photodiode.	26

Figure 2.7.	<i>Effect of increase in photodiode active area on dark current (I_d) and Noise Equivalent Power (NEP)[32]</i>	<i>28</i>
Figure 2.8.	<i>The effect of LED/PD separation on the DC (\square) and AC (\circ) components of the reflected IR PPGs. Measurements were performed at skin temperature of 43°C [33].....</i>	<i>30</i>
Figure 2.9.	<i>Effect of LED/PD separation on the relative pulse amplitude of R (+) and IR (\blacksquare) PPG. The driving currents of the R (\square) and the IR (*) LED's required to maintain a constant DC reflectance from the skin [33].....</i>	<i>30</i>
Figure 4.1.	<i>An objective tree showing non-hierarchical structuring of the sensor characteristics (objectives in rectangles and constraints in oval).</i>	<i>35</i>
Figure 4.2.	<i>A Venn diagram representing common attributes between sensor characteristics and sensor location.....</i>	<i>38</i>
Figure 4.3.	<i>Anatomic positions identified by site number for which basal cutaneous perfusion measurements were performed using photoplethysmogram [40].....</i>	<i>41</i>
Figure 4.4.	<i>Basal cutaneous perfusion measurements assessed by PPG, where locations (represented by site numbers) are ranked according to the mean values obtained [40]. (PPG units for signal amplitude in mm where 1mm = 10mV).....</i>	<i>42</i>
Figure 4.5.	<i>Markers representing the quality of PPG signals (PPG amplitude in volts) obtained in our laboratory from different body locations. (\bullet: Strong \blacksquare: Medium \blacktriangle: Weak).</i>	<i>45</i>
Figure 5.1.	<i>Light propagation in tissues surrounding a finger phalanx for different PDs configuring a variety of sensor modes.....</i>	<i>51</i>
Figure 5.2.	<i>Prototype ring sensor configuration showing the relative positions of the PDs in reflection, transflection and transmission modes.....</i>	<i>51</i>
Figure 5.3.	<i>Sensor configurations in reflection (a) and transmission (b) modes.....</i>	<i>52</i>

Figure 5.4.	<i>Prototype 12-PD reflectance disc sensor configuration showing the relative positions of the rectangular PDs and the LEDs.....</i>	<i>53</i>
Figure 5.5.	<i>Parallel configuration of DB9 female connectors used to construct a sensor interface.</i>	<i>54</i>
Figure 5.6.	<i>A simple circuit diagram of a I-V converter used to convert PD output from a current (I_p) to voltage (V_p).....</i>	<i>54</i>
Figure 5.7.	<i>Block diagram of the PSPU for obtaining the PPG signals from the prototype sensors.....</i>	<i>55</i>
Figure 5.8.	<i>Experimental setup to control the LED drive current supplied by the EPO to the LEDs.</i>	<i>57</i>
Figure 6.1.	<i>(a) Sensor assembly mounted on a finger and (b) a closer section of the finger phalanx with the prototype ring sensor.....</i>	<i>59</i>
Figure 6.2.	<i>Different sensor setups used for various experiments (a) single control sensor and (b) multiple PD prototype sensor [42].</i>	<i>63</i>
Figure 6.3.	<i>Sensors attachment to the forehead [42].</i>	<i>63</i>
Figure 6.4.	<i>Block diagram of the experimental setup.....</i>	<i>64</i>
Figure 6.5.	<i>Block diagram of the sensor connection in Case 1 and 2.....</i>	<i>65</i>
Figure 6.6.	<i>Block diagram of sensor connections in Case 3.</i>	<i>65</i>
Figure 6.7.	<i>Block diagram of the sensor connection with the current divider circuit used in Case 4.</i>	<i>66</i>
Figure 7.1.	<i>Relative LED peak drive currents required to maintain a constant PPG AC amplitude of about 0.55V RMS in reflection, transflection and transmission modes.</i>	<i>67</i>

<i>Figure 7.2(a).</i>	<i>Typical PPG AC magnitudes measured in reflection mode with 7mA IR LED peak drive current.</i>	<i>68</i>
<i>Figure 7.2(b).</i>	<i>Typical PPG AC magnitudes measured in transflection mode with 26mA IR LED peak drive current.</i>	<i>68</i>
<i>Figure 7.2(c).</i>	<i>Typical PPG AC magnitudes measured in transmission mode with 44.5mA IR LED peak drive current.</i>	<i>68</i>
<i>Figure 7.3(a).</i>	<i>Typical PPG AC magnitudes measured in reflection mode with 24.1mA IR LED peak drive current.</i>	<i>69</i>
<i>Figure 7.3(b).</i>	<i>Typical PPG AC magnitudes measured in transflection mode with 77.8 mA IR LED peak drive current.</i>	<i>69</i>
<i>Figure 7.3(c).</i>	<i>Typical PPG AC magnitudes measured in transmission mode with 143.8 mA IR LED peak drive current.</i>	<i>69</i>
<i>Figure 7.4(a).</i>	<i>Typical PPG AC magnitudes measured from the left index finger in different sensor modes with a constant IR LED peak drive current of 31mA.</i>	<i>70</i>
<i>Figure 7.4(b).</i>	<i>Typical PPG AC magnitudes measured in different sensor modes with a constant R LED peak drive current of 82.5mA.</i>	<i>71</i>
<i>Figure 7.5.</i>	<i>RMS values calculated from typical PPG amplitudes measured in reflection, transflection and transmission modes at constant IR and R LEDs peak drive currents of 31.0mA and 82.5mA, respectively.</i>	<i>71</i>
<i>Figure 7.6.</i>	<i>Increment in RMS noise with varying number of PDs connected in parallel.</i>	<i>74</i>
<i>Figure 7.7.</i>	<i>PPG signals obtained in transmission mode from varying number of PDs (a): IR peak current drive = 19.6 mA (b): R peak current drive = 46.0 mA.</i>	<i>75</i>
<i>Figure 7.7.</i>	<i>PPG signals obtained in reflection mode from varying number of PDs (c): IR peak drive current = 1.9 mA (d): R peak drive current = 3.0 mA.</i>	<i>76</i>

<i>Figure 7.8(a).</i>	<i>SNR improvement observed with increasing PD area in transmission mode.</i>	<i>77</i>
<i>Figure 7.8(b).</i>	<i>SNR improvement observed with increasing PD area in reflection mode.....</i>	<i>77</i>
<i>Figure 7.9.</i>	<i>Individual PD performance under complete darkness and a constant light illumination.</i>	<i>79</i>
<i>Figure 7.10.</i>	<i>Signal improvement observed in-vitro with multiple photodetectors.....</i>	<i>80</i>
<i>Figure 7.11.</i>	<i>Signal improvement observed in vivo with multiple photodetectors.....</i>	<i>80</i>
<i>Figure 7.12.</i>	<i>PPG signals measured from the forehead (a and b) and wrist (c and d) for constant LED driving currents.</i>	<i>81</i>
<i>Figure 7.13.</i>	<i>RMS values calculated from the PPG signals measured by the near (N), far (F) and combination (N+F) PDs from the wrist and forehead for constant R and IR LED drive currents corresponding to 8.5mA (a) and 4.2mA (b), respectively.</i>	<i>82</i>
<i>Figure 7.14.</i>	<i>Relative LED peak driving currents required to maintain a constant PPG amplitude of 0.840V RMS for the near (N), far (F) and combination (N+F) PD configurations. Measurements were obtained from the forehead.....</i>	<i>83</i>
<i>Figure 7.15(a).</i>	<i>SpO₂ obtained from the RPO and EPO using similar control sensors.</i>	<i>85</i>
<i>Figure 7.15(b).</i>	<i>HR readings obtained from the RPO and EPO pulse oximeters using similar control sensors.</i>	<i>85</i>
<i>Figure 7.16(a).</i>	<i>Comparison of SpO₂ readings for case-2 obtained from the control sensor (RS-10) connected to the EPO vs. a control sensor (RS-10) connected to the RPO.....</i>	<i>86</i>

<i>Figure 7.16(b).</i>	<i>Comparison of SpO₂ (%) readings obtained from the prototype sensor (6-PDs) with 100% LED current drive (case-3) connected to the EPO vs. a control sensor (RS-10) connected to the RPO.....</i>	<i>86</i>
<i>Figure 7.17(a).</i>	<i>Comparison of HR (bpm) measured from the control sensor (RS-10) and prototype 6-PD reflectance sensor with varying number of PDs at different LED drive currents.</i>	<i>87</i>
<i>Figure 7.17(b).</i>	<i>Comparison of SpO₂ measured from the control sensor (RS-10) and prototype 6-PD reflectance sensor with varying number of PDs at different LED drive currents.....</i>	<i>87</i>
<i>Figure 8.1.</i>	<i>(a) Multiple PDs simulating a large PD area (b) equivalent configuration utilizing ring-shaped continuous PDs.....</i>	<i>99</i>
<i>Figure 9.1.</i>	<i>Forehead reflectance sensor using a continuous ring-shaped PD for SpO₂ and HR measurements with low LED intensity for optimum power budgeting.</i>	<i>106</i>

LIST OF TABLES

<i>Table.2.1.</i>	<i>Characteristics of most common red / infrared LED materials [21].</i>	<i>14</i>
<i>Table 2.2.</i>	<i>Comparison of typical parameters of interest for LEDs and Laser diodes [22].</i>	<i>19</i>
<i>Table 4.1.</i>	<i>Pairwise comparison chart for an assorted set of primary objectives considered for a pulse oximeter sensor design.</i>	<i>40</i>
<i>Table 4.2.</i>	<i>Multiple comparisons of cutaneous perfusion measurements for the anatomical positions grouped in different tables [40].</i>	<i>43</i>
<i>Table 4.3.</i>	<i>Initial decision matrix created to shorten the list of possible locations (with site numbers) for sensor attachment.</i>	<i>44</i>
<i>Table 4.4.</i>	<i>Final decision matrix selects an appropriate location for the sensor placement on the soldier based on the highest score.</i>	<i>47</i>
<i>Table 7.1(a).</i>	<i>RMS values calculated using constant PPG signals with varying IR drive currents from different sensor modes for 3 replicate tests.</i>	<i>72</i>
<i>Table 7.1(b).</i>	<i>RMS values calculated using constant PPG signals with varying R drive currents from different sensor modes for 3 replicate tests.</i>	<i>72</i>
<i>Table 7.2(a).</i>	<i>Summary of ‘ratio of ratio’ (R/IR) calculated using constant PPG signals with varying currents from different sensor modes for 3 replicate tests.</i>	<i>73</i>
<i>Table 7.2(b).</i>	<i>Summary of ‘ratio of ratio’ (R/IR) calculated using PPG signals with constant LED drive currents from different sensor modes for 3 replicate tests.</i>	<i>73</i>
<i>Table 7.3.</i>	<i>Comparison of LED peak drive currents and power consumption for different sensor modes.</i>	<i>78</i>

<i>Table 7.4.</i>	<i>Comparison of estimated battery life for different PD configurations. Values based on forehead measurements for a typical 220mAh coin size battery.</i>	<i>84</i>
<i>Table 7.5.</i>	<i>Optical powers for different PD areas corresponding to a drop in peak LED drive currents.</i>	<i>85</i>
<i>Table 8.1.</i>	<i>Comparison of estimated battery life for different operating modes.</i>	<i>92</i>
<i>Table 8.2.</i>	<i>Equivalent detections area calculated for the inner and outer ring-shaped reflectance sensor configuration illustrated in Figure 8.1.</i>	<i>99</i>
<i>Table 8.3.</i>	<i>Statistical analysis of SpO₂ values obtained during various breathing maneuvers for different sensor setups.</i>	<i>100</i>
<i>Table 8.4.</i>	<i>Statistical analysis for low LED drive current and its effect on SpO₂ accuracy.</i>	<i>101</i>
<i>Table 8.5.</i>	<i>Estimated battery life for different LED operating currents.</i>	<i>102</i>

1. INTRODUCTION

1.1 Significance of Oxygen Saturation

Oxygen (O₂) is vital for the proper functioning of each cell in the human body. Lack of O₂ can quickly lead to irreversible damage to cells having a high metabolic rate. Thus, O₂ delivery to the cells is an important indicator of a person's health. Several methods have been developed to analyze O₂ delivery. Oximetry, for example, refers to the optical measurement of oxyhemoglobin (HbO₂) saturation in the blood. The basic concept of oximetry is to transmit light through a blood sample, and determine the amount of light absorbed by oxygenated and deoxygenated hemoglobin. About 2% of O₂ present in blood is dissolved in the plasma, and 98% is attached to hemoglobin (Hb), which is present in red blood cells. Hence, Hb is required for efficient O₂ transport from the lungs to the cells. HbO₂ is formed when Hb binds to O₂. In addition, Hb can also bind with carbon monoxide (CO) to form carboxyhemoglobin (HbCO). A small amount of methemoglobin (MetHb) is also present, which is unable to bind with O₂. Thus, percent oxygen saturation (%SaO₂) is a measurement of how much of the hemoglobin in the arterial blood is in the form of HbO₂, and is defined as:

$$\%SaO_2 = \frac{[HbO_2]}{[Hb] + [HbO_2] + [HbCO] + [MetHb]} * 100 \quad (1.1)$$

In healthy individuals, the normal range for SaO₂ is between 90-100%. Low SaO₂ can lead to the degeneration or death of cells and tissues [1]. There are many possible reasons for the decline in SaO₂, including low inspired O₂, difficulties in O₂ transport from the lungs to the blood, a low hematocrit, or decreased cardiac output.

1.2 Pulse Oximetry

Pulse oximetry is a common non-invasive method used in clinical medicine to estimate SaO_2 in arterial blood and provides vital information about the cardiorespiratory function of a patient [2] [3]. During World War II, a major advancement in noninvasive oximetry was made by Millikan et al [4] and Wood and Gearci [5] who described an ear oximeter designed specifically for use by pilots. This helped in monitoring the condition of war-fighter pilots who were flying at high altitudes in pressurized cockpits. A commercial ear oximeter, developed by the Hewlett Packard (HP) Company in the early 70s, was the first widely used device for measuring SaO_2 [6]. More recently, Aoyagi et al [7], Nakajima et al [8] and Yoshiya et al [9], combined optical plethysmography with the spectrophotometric determination of SaO_2 by developing the first pulse oximeter. It is based on the assumption that the change in the light absorbed by tissue during systolic cardiac cycle is caused primarily by the arterial blood. They showed that changes in light transmission through a pulsating vascular bed can be used to obtain an accurate noninvasive measurement of SaO_2 . With advancement in microelectronics, miniaturized pulse oximeters have been developed, which can be used occasionally for monitoring Navy Seals and Special Forces [10]. But these miniaturized pulse oximeters are not compatible for remote monitoring of soldiers on the battlefield. Currently, researchers are focused on development of a miniaturized wireless pulse oximeter with optimized power consumption, which can be used for physiological monitoring of military casualties or civilian mass casualties.

1.3 Principle of Pulse Oximetry

Pulse oximetry is based on spectrophotometric measurements of changes in blood color. Oxygenated blood is distinctively red, whereas deoxygenated blood has a characteristic dark blue coloration. The optical property of blood in the visible (i.e. between 400 and 700nm) and near-infrared (i.e. between 700 and 1000nm) spectral regions depends strongly on the amount of O₂ carried by blood. The method exploits the fact that Hb has a higher optical absorption coefficient in the red region of the spectrum around 660nm compared with HbO₂, as illustrated in Figure 1.1. On the other hand, in the near-infrared region of the spectrum around 940nm, the optical absorption by Hb is lower compared to HbO₂. At the isobestic wavelength (i.e. 805nm), where the two curves cross over, the absorbance of light is independent of oxygenation level.

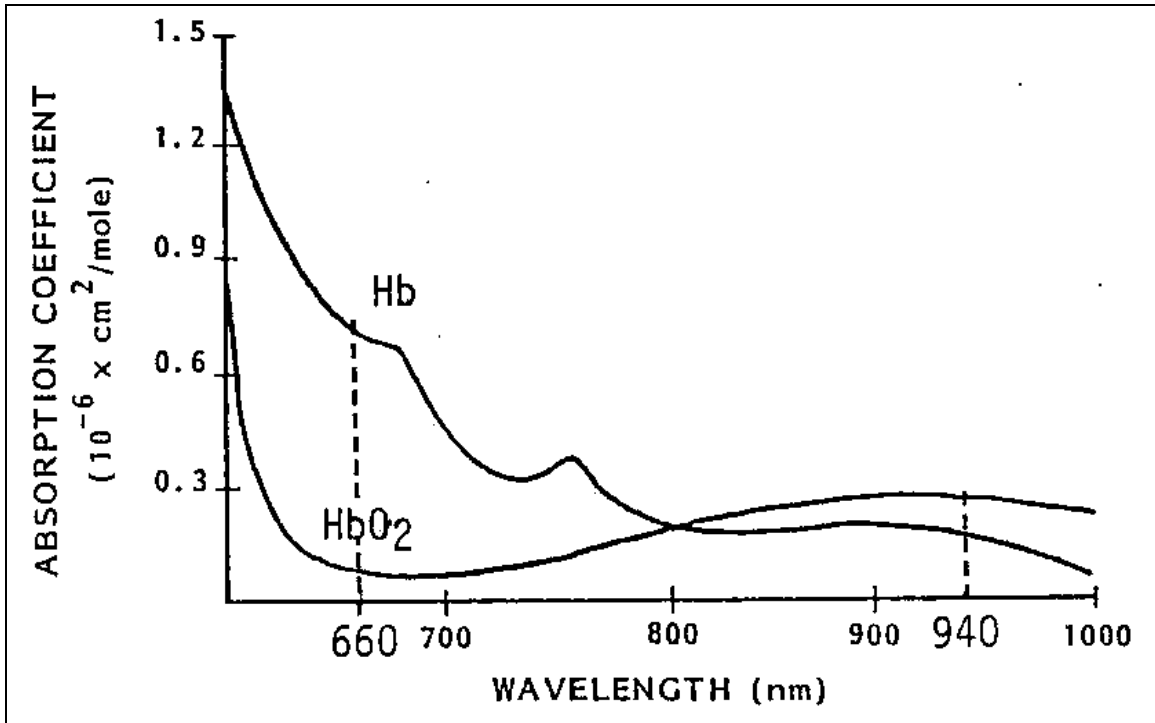


Figure 1.1. Optical absorbance spectra of Hb, HbO₂ in the visible and near-infrared wavelength region [2].

The absorbance of light at a specific wavelength by a homogenous solution can be accurately determined by the Beer-Lambert's law, using the equation (1.2).

$$I_t = I_o * e^{-\alpha cd} \dots\dots\dots (1.2)$$

where I_t is the transmitted light intensity, I_o is the incident light intensity, α is the specific absorption coefficient of the sample, c is the concentration of the sample, and d is the path length of light transmission. In oximetry, it is assumed that a hemolyzed blood sample consists of a two-component homogeneous mixture of Hb and HbO₂ and that light absorbance by the mixture of these components is additive. However, other variables in the biological media such as bone, skin, tissue, muscle and blood also scatter light. The absorption of light also depends on both skin thickness and color. Therefore, Beer-Lambert's Law is unable to account for all of these variables. Modern pulse oximetry relies on the detection of a photoplethysmographic (PPG) signal produced by variations in the quantity of arterial blood associated with periodic contractions and relaxations of the heart. As shown in Figure 1.2, the magnitude of the PPG signal depends on the amount of blood ejected from the heart with each systolic cycle, the optical absorption of blood, absorption by skin and various tissue components, and the specific wavelengths used to illuminate the vascular tissue bed. During systole, when the arterial pulsation is at its peak, the volume of blood in tissue increases. This additional blood absorbs more light, thus reducing the light intensity which is either transmitted or backscattered. During diastole, less blood is present in the vascular bed, thus increasing the amount of light transmitted or backscattered. The pulsatile part of the PPG signal is considered as the "AC" component, and the non-pulsatile part, resulting mainly from the venous blood, skin, and tissue, is referred to as the "DC" component. A deviation in the

LED brightness or detector sensitivity can change the intensity of the light detected by the sensor. This dependence on transmitted or backscattered light intensity can be compensated by using a normalization technique where the AC component is divided by the DC component, as given in equation (1.3).

$$(R/IR) = \left(\frac{\frac{AC_R}{DC_R}}{\frac{AC_{IR}}{DC_{IR}}} \right) \dots\dots\dots(1.3)$$

Thus, the time invariant absorbance due to venous blood or surrounding tissues does not have any effect on the measurement. This normalization is carried out for both the red (R) and the infrared (IR) wavelengths, as shown in Figure 1.3. The normalized R/IR “ratio of ratios” can then be related empirically to SpO₂, as shown in Figure 1.4. When the ratio is 1, the SpO₂ value is about 85% [11]. Most pulse oximeters measure absorbance at two

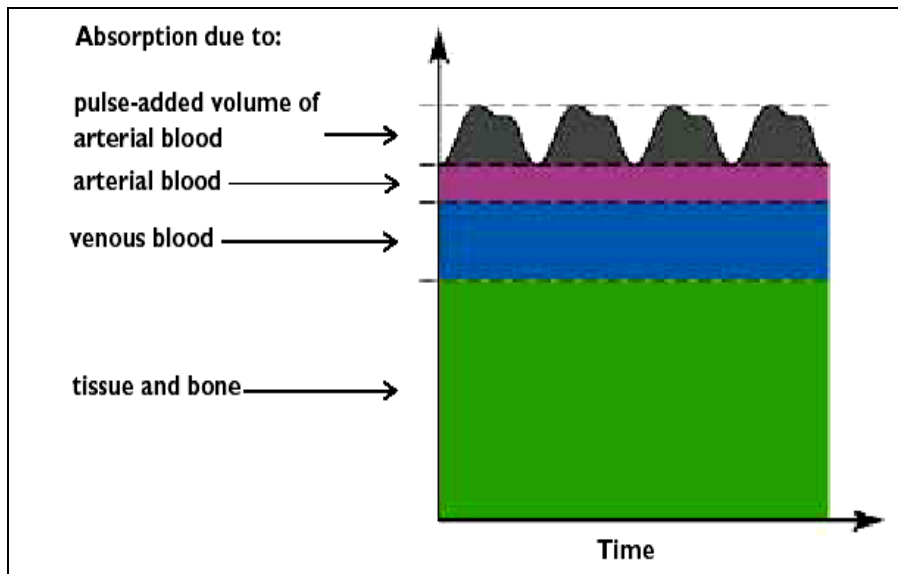


Figure 1.2. Variations in light attenuation by tissue, illustrating the rhythmic effect of arterial pulsation [12].

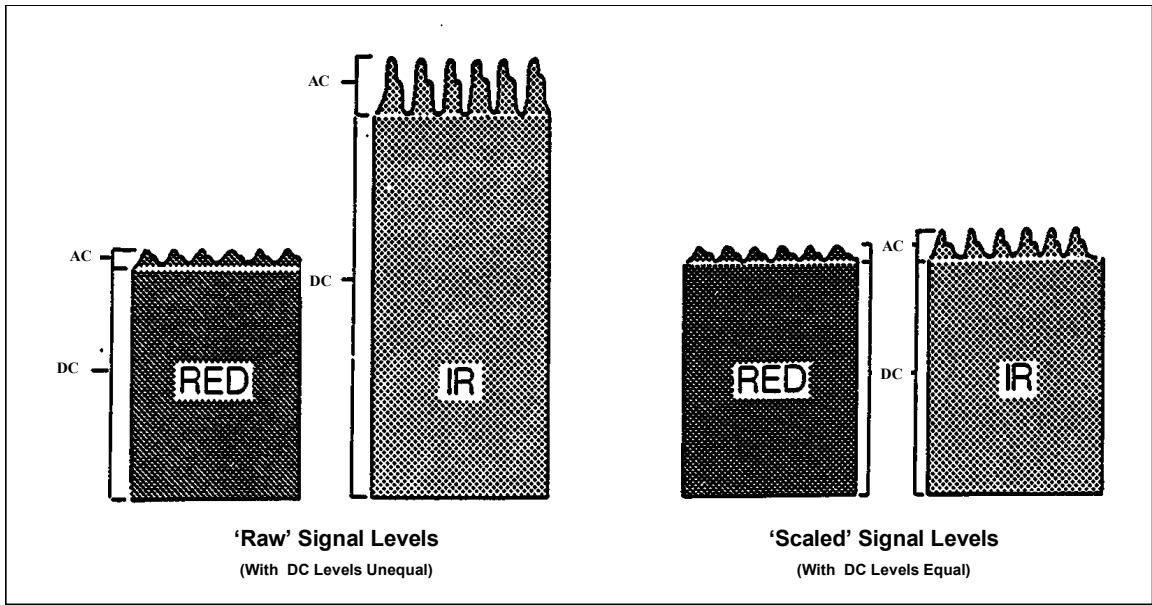


Figure 1.3. Normalization of R and IR wavelengths to remove the effects of variation in the incident light intensity or detector sensitivity [2].

different wavelengths and are calibrated using data collected from CO-oximeters by empirically looking up a value for SpO₂, giving an estimation of SaO₂ using the empirical relationship given by equation 1.4.

$$\text{SaO}_2 \% = A - B * (\text{R/IR}) \dots\dots\dots (1.4)$$

where R/IR is based on a normalization where the pulsatile (AC) component is divided by the corresponding non-pulsatile (DC) component for each wavelength, and A and B are linear regression coefficients which are related to the specific absorptions coefficients of Hb and HbO₂. The constants A and B are derived empirically during in-vivo calibration by correlating the ratio calculated by the pulse oximeter against SaO₂ from arterial blood samples by an in vitro oximeter for a large group of subjects. Pulse oximeters read the SaO₂ of the blood accurately enough for clinical use under normal circumstances because they use a calibration curve based on empirical data shown in figure 1.4.

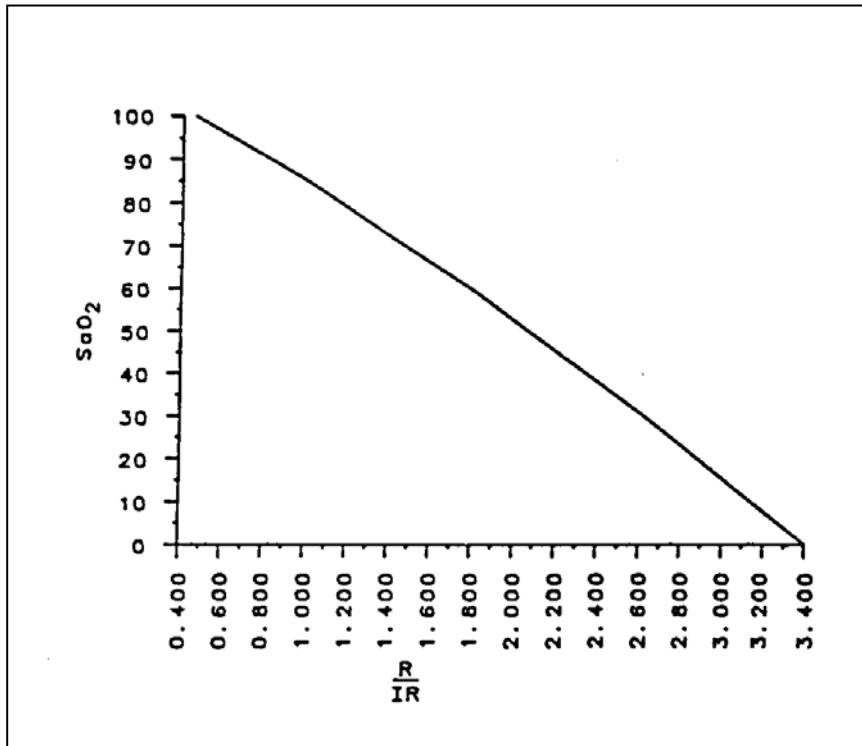


Figure 1.4. Empirical relationship between arterial SaO₂ and normalized (R/IR) ratio[2].

1.4 Pulse Oximeter Sensors

The main advantage of employing a photoplethysmographic technique is that only two wavelengths are required, thereby greatly simplifying the optical sensor [11]. A basic optical sensor of a noninvasive pulse oximeter consists of a red and infrared light emitting diode (LED) and a silicon photodiode (PD). Light emitted by the LEDs is partially reflected, transmitted, absorbed, and scattered by the skin, surrounding tissues, and the blood before it reaches the PD. Thus, noninvasive measurement by pulse oximetry can be performed in either transmission or reflection modes depending on the relative position of the sensor components.

1.4.1 Transmission Mode: In transmission pulse oximetry, the sensor is usually attached to a fingertip, foot, or earlobe, such that the LED and PD are placed on opposite sides of

a peripheral pulsating vascular bed, as illustrated in Figure 1.5. In this mode, the PD detects transmitted and predominantly forward scattered light. Transmission mode pulse oximetry is obviously limited to areas of the body where transmitted light can be readily detected. Most of the accessible locations are peripheral areas of the body such as finger tips, ear lobes and toes in adults, and the foot or palms in infants.

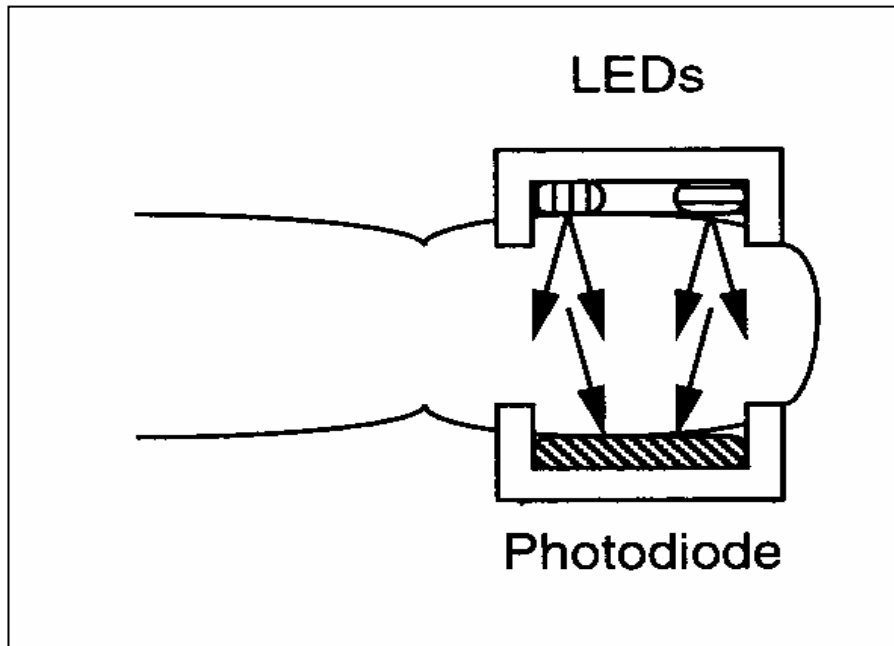


Figure 1.5. Transmission mode sensor showing the relative position of the LEDs and PD.

1.4.2 Reflection Mode: In reflection pulse oximetry, the LEDs and PD are both mounted side-by-side on the same planar surface, as shown in Figure 1.6. This alternative idea of using light reflection instead of light transmission was first described by Brinkman and Zijlstra [13]. In this mode, the PD detects reflected or back scattered light which enables measurements from multiple locations on the body where transmission measurements are not feasible. Normally, the sensor is applied to the forehead region, but is not restricted to this location. Reflection pulse oximetry has recently become an important new clinical

modality with potential benefits in fetal monitoring where the only accessible location is the fetal head.

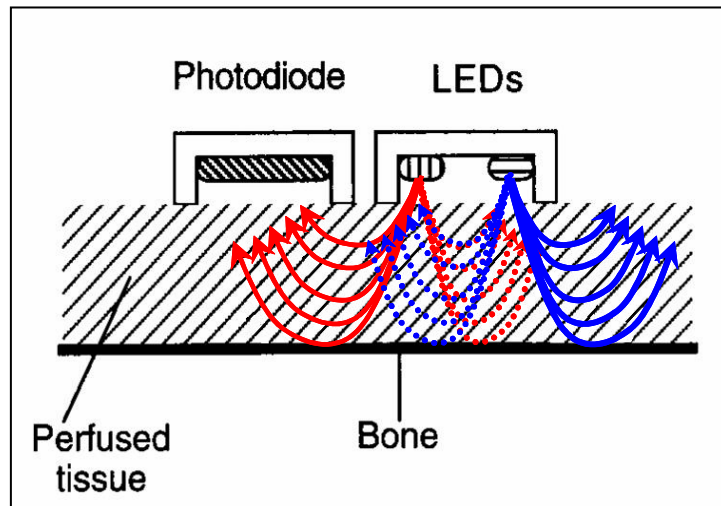


Figure 1.6. A typical commercial reflection mode sensor showing the relative position of the LEDs and PD.

1.5 Advantages and Disadvantages of Reflectance and Transmittance Pulse

Oximetry

The major advantage of transmittance over reflectance pulse oximetry is the increased intensity of the light detected by the PD. As the amount of light transmitted through the tissue is greater than the amount of light reflected or backscattered, the signal quality is generally much better in transmittance compared to reflectance mode. But this is true only if a strong light intensity is concentrated over a particular area. If the incident light intensity is reduced considerably, chances of light photons being reflected are much higher in comparison to them being transmitted through a relatively thick tissue volume. In addition, the major disadvantage of transmission probes is that the sensor application is limited to peripheral parts of the body such as finger tips, toes, earlobes in adults or the foot or palms of infants. In contrast, reflectance sensors can measure SaO_2 from virtually

any location of the body, but variation in AC PPG signal depends on the amount of blood perfusion, tissue thickness, bone and the intensity of light emitted from the LEDs.

1.6 Types of Pulse Oximeter Probes

Depending on the duration of clinical monitoring, there are different types of probes available, as illustrated in Figure 1.7.

1.6.1 Reusable Probes: Probes that can be used more than once in monitoring SpO₂ are called reusable probes. These probes are used without an adhesive sensor, as shown in Figure 1.7 (a). Reusable sensors are available in transmission as well as reflection mode, as illustrated in Figure 1.7 (b) and (c). They are used for short time monitoring (i.e. less than 4 hours or spot checks). As per the duration of use (i.e. long term or short term) and condition of the patient (excessive sweating), adhesive tapes of reusable sensor are frequently changed to avoid measurement errors due to lack of contact between the sensor and the patient's skin.

1.6.2 Disposable Probes: Typically, adhesive sensors are used for both short term and long term monitoring but must be repositioned at least every 8 hours. Disposable sensors illustrated in Figure 1.7 (d) are used on a single patient and discarded afterwards.

Available clinical pulse oximeter sensors are not useful for monitoring SpO₂ during physical exercise or in the case of a soldier in combat. Due to dirt-filled and sweaty environment, repeated replacement of adhesive tapes as well as the sensor is not feasible, especially when the soldier is mobile or in combat. Modified sensors (disposable or reusable) as well as innovative attachment techniques must be designed for intended application while considering features such as performance, functionality and regulations.

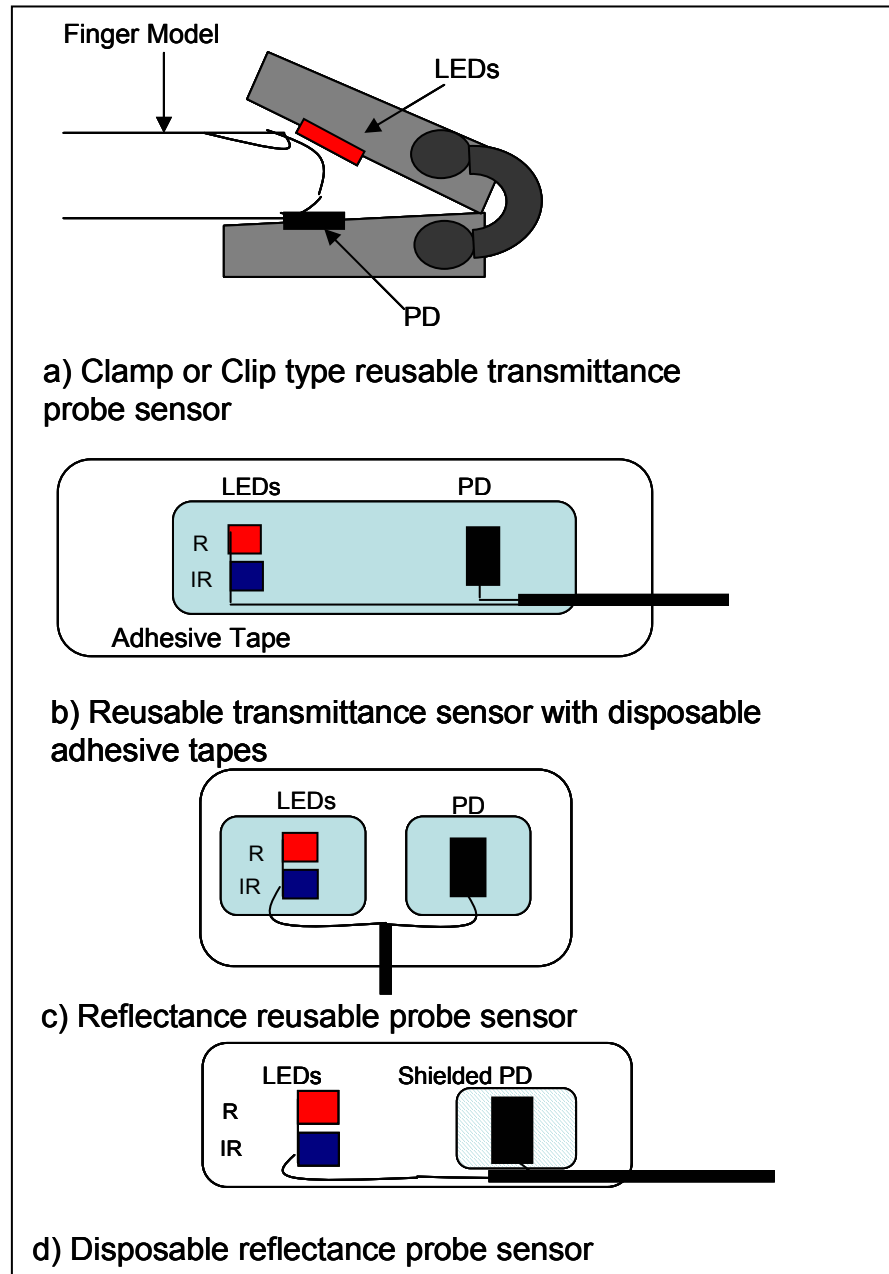


Figure 1.7. Different types of clinical probes.

1.7 Applications of Pulse Oximetry

Being an integral part of a surgical theater, the pulse oximeter finds its use in many clinical applications such as in an Intensive Care Unit (ICU), during anesthesia, hypoxemia screening, and transport from the operating room to the recovery room.

1.7.1 Surgery and Post Anesthetic Care Units: Pulse oximetry is used routinely as an early indicator of physiological change during post or pre-surgery and also under anesthesia. Desaturation is often a problem encountered during the induction of anesthesia. Most anesthetics cause respiratory depression, which reduces ventilation and thus might be causing desaturation. This may also occur due to equipment failures. For example, blockage in the flowmeter or leaks in the anesthesia machine or breathing apparatus can cause cyanosis, which is a bluish tint to the skin caused by lack of O₂ that may not be detected by a physician until the SaO₂ is around 80% [14]. Early detection of hypoxic episodes could lead to earlier corrective measures and prevent adverse consequences of hypoxemia, such as arrhythmias, myocardial ischemia, and brain ischemia [15].

1.7.2 Fetal and Neonate Care: Pulse oximetry has also found its mark in the care of fetuses and neonates [16]. Continuous monitoring (as opposed to intermittent blood gas measurements) allows ongoing assessment of neonate's stability. Blood gas determinations only reflect discrete moments in time and may not reflect information concerning ongoing status of a neonate. Pulse oximeter is a more reliable device for both unstable and chronically ill infants when evaluated against a transcutaneous oxygen tension (TcPO₂) monitor. In comparing simultaneous measurements of both TcPO₂ and SaO₂, Mendelson and Peura [17] found that TcPO₂ readings lagged SaO₂ by approximately 12 seconds. Also, it is less cumbersome to apply than the heated sensor of transcutaneous monitors and does not require calibration to initiate monitoring in routine use. A pulse oximeter can be extremely valuable when caring for any neonate requiring oxygen therapy. Although arterial blood gas determinations is still necessary, use of a

pulse oximeter decreases the number of blood gases needed and allows for rapid determination of proper amounts of O₂ required by the neonate.

1.7.3 Future Applications in Combat Casualty Care: In severe environments characterized by limited supplies, limited diagnostic and life-support equipment, combat casualties may wait for hours before definitive health care can be provided [18]. Efforts must be made to minimize the mortality rate of a wounded soldier by providing remote triage, initial treatment and subsequent evacuation. An efficient way is to optimize the medical treatment for those who are not fatally wounded. Diagnostics help the combat life saver (CLS) and medics on the battlefield to determine which casualties require immediate resuscitation. Novel diagnostic tools are needed to identify locations of foreign bodies, determine the extent of injury (trauma), monitor vital signs and ascertain the adequacy of resuscitation. To be effective with such a demand, it's essential to have improved techniques for high-tech diagnosis and treatment. Penetrating injury to the chest can cause extensive damage to the lung parenchyma [19]. Punctured lung can cause injury to a blood vessel causing hemothorax i.e. collection of blood in the pleural cavity or pneumothorax i.e. a condition developed due to collection of air or gas in the pleural cavity. Typically, a traumatic soldier would suffer from hypovolemic shock where the cardiovascular system is unable to supply blood flow due to massive external or internal bleeding [20]. The symptoms that are associated with such conditions are chest pain, rapid heart rate and shortness of breath leading to a drop in SpO₂. Early detection of irregular physiological signs of an injured soldier can help a CLS to take corrective steps to prevent any adverse effect. Some of these changes might be diagnosed earlier by using a pulse oximeter which provides information about SpO₂ and pulse rate.

2. SENSOR COMPONENTS

For practical application of pulse oximetry, the light source must be powerful enough to penetrate through a biological medium without causing any tissue damage. LEDs are small and have excellent drive characteristics, with high light intensity output for a relatively narrow bandwidth. The wavelengths of 660nm and 930nm used in pulse oximetry are within the range of LED availability. Thus, LEDs fulfill all the requirements for a light source in a pulse oximeter sensor [2].

2.1 Light Emitting Diodes (LED)

Luminescence is a general term used to describe the emission of radiation from a solid due to excitation from some form of energy. The type of luminescence generated by a LED is termed electroluminescence, and is due to the excitation resulting from the application of an electric field. LEDs are commercially constructed from semiconductor alloys such as Gallium Arsenide (GaAs), Gallium Phosphide (GaP), Gallium Aluminum Arsenide (GaAlAs), and Gallium Arsenic Phosphide (GaAsP). Table 2.1 summarizes the characteristics of the most common LED materials [21].

Table.2.1. Characteristics of most common red / infrared LED materials [21].

Material	Dopant	Peak Emission (nm)	Color	Quantum Efficiencies (%)
GaAs	Si	910 – 1020	Infrared	10
Ga _x Al _{1-x} As	Si	879 – 890	Infrared	15
GaP	Zn,O	700	Red	4
GaAs _{0.35} P _{0.65}	Zn	650	Red	15

2.1.1 Principle of Operation: An LED is an optoelectronic semiconductor which generates light from recombination of excess concentrations of electrons and holes. The energy difference between the hole state and the electron state before recombination is equal to the energy of the photon emitted, which also governs the wavelength of the emitted light. With addition of a doping material, a semiconductor becomes more conductive as extra atoms change the balance, either by adding electrons or creating holes. In a N-type material, extra electrons are present, and free electrons move from a negatively-charged area to a positively charged area. Semiconductors with extra holes are called P-type materials, where electrons jump from hole to hole, moving from a negatively-charged area to a positively-charged area. When a section of N-type and P-type are bonded together, a diode is created which conducts electricity in only one direction. With no voltage applied to the diode, the extra electrons from the N-type material fill the holes present in the P-type material along the junction between the layers. A depletion zone is created, and no charge flows through the semiconductor. When voltage is supplied to the diode with the positive (+ve) terminal of the circuit connected to the P-type material and the negative (-ve) terminal connected to the N-type material, current will flow. The depletion zone would disappear, with the electrons moving towards the +ve terminal and away from the N-type material. As the electrons fill the excess holes in the P-type material, energy is emitted in the form of photons, as shown in Figure 2.1. This release of energy is due to electrons jumping from the conduction band (higher orbital) to the valence band (lower orbital). The greater the drop in energy level, the greater is the energy of the photon, which is characterized by a higher wavelength.

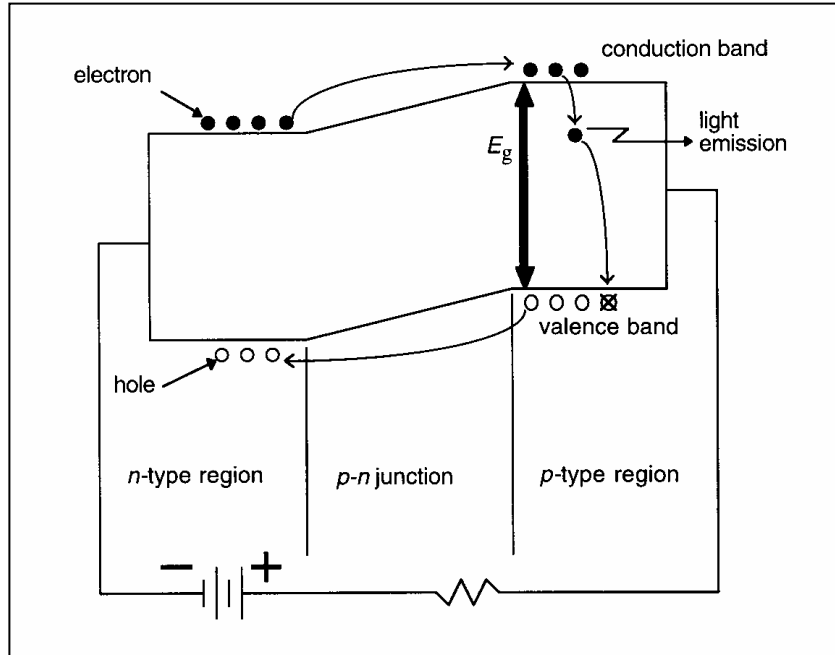


Figure 2.1. Photon generation due to electrons dropping into the valence band in a forward-biased p-n junction [2] .

2.1.2 LED Characteristics: The predominant factors for application of LEDs in pulse oximetry are listed below.

(a) *Forward Current (I_f):* The current flowing in the LED from the anode to the cathode.

Typical values for forward current range from 2 to 50 mA.

(b) *Forward Voltage (E_g):* A potential drop across the p-n junction of the diode. The values for LED's forward voltage can range from 0.9 to 2.5 V.

(c) *Wavelength (λ):* Typical wavelengths used in pulse oximetry are 660nm for the R LED and 940nm for the IR LED. The wavelength of light emitted from an LED is determined by

$$E_g = hc/\lambda \quad (2.1)$$

where, E_g is the forbidden bandwidth in the electrons (i.e. forward voltage),

h is Planck's constant (6.626×10^{-34} Js),

c is the speed of light in a vacuum ($3.0 \times 10^8 \text{ m/s}$), and

λ is the wavelength of emitted photons.

(d) *Radiant Power*: The radiant power of LEDs used in pulse oximetry depends on the dc current supplied, and typically range from 1mW-10mW. The radiant power of LEDs varies linearly with the forward current over a range of currents used in pulse oximeters.

(e) *Power Dissipation*: It is important to guarantee that the LED's maximum power is maintained within the safe operating conditions. The majority of power dissipated by a LED produces heat which is absorbed by the skin serving as the primary heat sink in a pulse oximeter sensor. The power dissipated is directly proportional to the drive current of the LED according to equation 2.2.

$$P=VI \quad (2.2)$$

(f) *LED Packaging*: Modern manufacturing techniques have minimized the LED size. Commercial pulse oximeter sensors have two LEDs encased in a single package with miniaturized dimensions. To withstand vibration and shock, and to provide superior mechanical strength, optically clear resins are used for LED encapsulation.

2.1.3 Light Emitting Diodes vs Solid-State Lasers: An alternative light source that is commercially available and can be considered for application in pulse oximetry is a solid-state laser diode. Lasers have found an important place in medical applications. For example, as CO₂ lasers in general surgery, treatment of cancer using photodynamic therapy and in ophthalmology where detached retinas are treated using light from ruby laser. It is valuable to compare the advantages and disadvantages of using a laser diode as an alternative light source for pulse oximetry. Solid-state lasers are available in the wavelength required for pulse oximetry, and have light intensities strong enough to

penetrate biological tissues. But the disadvantages are the package size of each laser which is typically larger than a LED. Most solid-state lasers are constructed with a photodiode assembly to provide a constant light intensity output and invariably increase the total package size.

Another significant difference between solid-state laser diodes and LEDs is the power output. Similar to the minimum forward voltage required for LEDs to emit photons, a threshold current is required by the solid-state laser before it can lase. Unlike LEDs, Laser diodes will not operate below a threshold current. In comparison to the forward voltage required by the LEDs for spontaneous emission, a laser's threshold current is much higher, as shown in table 2.2. Thus, a large amount of power will be consumed if a laser diode is used as a light source for pulse oximetry. This is a major drawback for wireless pulse oximetry. Also, the peak power output of LEDs is significantly lower in comparison to solid-state laser diodes. The highly concentrated power output of laser diodes could cause damage to biological tissues by causing extensive burn in the applied region. LEDs, on the contrary, do not deliver enough power to damage the tissue, but they do deliver enough energy to be transmitted, reflected or scattered by biological tissues. With a low peak power output but high duty cycle, LEDs provide a much gentler delivery of the same wavelengths of light compared to a laser diode. For this reason, LEDs do not have the same risk factors to cause accidental eye damage as compared to laser diodes. Solid-state lasers have a higher depth of penetration as the beam width is smaller in comparison to the LEDs. In contrast, energy from the LEDs is dissipated over a wider area, which enables a better interaction of photons with a

larger region of blood vessels. Thus, it can be concluded that LEDs are appropriate light sources for pulse oximetry compared with solid-state laser diodes.

Table 2.2. Comparison of typical parameters of interest for LEDs and Laser diodes [22].

Attribute/Parameter	LEDs	Solid-state Laser diodes
Type of Radiation	Spontaneous Emission	Stimulated Emission
Particle Phase	Incoherent	Coherent
Polarization state	Randomly polarized	Linearly polarized
Direction	Random	Linear
Significant Parameters	Band Width increases at the expense of power	Threshold current, (10 to 30 mA),
Output Power	10 - 50 (high power) mW	1 - 1000 mW

2.1.4 Depth of Light Penetration: The depth of penetration of light is the distance at which the radiant power decreases to $1/e$ of its incident value. It is inversely related to the absorption coefficient (α). The greater the absorption, the lower is the depth of penetration of light in a biological medium. The penetration depth of the probing light in pulse oximetry should be closely correlated at the two wavelengths in order to minimize the effects of tissue heterogeneity. Distribution of penetration of depths for 660nm and 890nm light were computed by Mannheimer et al [23] using the Monte Carlo modeling by Bonner *et al.* [24] and equations derived by Schmitt [25] from photon diffusion theory in order to measure 100% SaO₂. As illustrated in figure 2.2, an estimated 4.3 mm mean penetration depth is evident for R (660nm) and IR (930nm) spectral regions while calculating high (100%) as well as low (40%) SpO₂ values. Hence, the tissue thickness underneath the pulse oximeter sensor should be 4 to 5 mm in order to achieve optimum depth of penetration (4.3mm). This information is critical for selecting the location for

sensor attachment. For example, reflectance sensor locations like the forehead, finger and ear lobe with tissue thickness of approximately 3 to 5 mm will result in stronger PPG signals whereas regions such as the inner thigh and chest that have greater tissue thickness (>5mm) and lower vascularization will result in diminished PPG amplitudes.

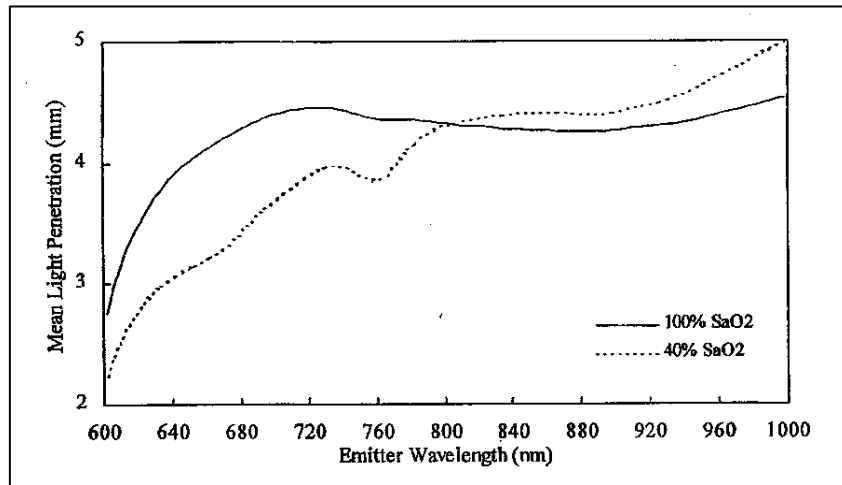


Figure 2.2. Range of mean penetration depth for different wavelengths for high (100%) and low (40%) saturations [23].

2.1.5 LED Power Consumption Concerns: A significant proportion of the overall power consumed in a portable battery-operated pulse oximeter is attributed to the red and infrared LEDs in the sensor. About 70% of the power is consumed by the LEDs and the RF transmitters whereas the other 30% is consumed by the microcontroller that is used for computing SpO₂ and HR [26]. As there are 2 LEDs and a single PD present in a pulse oximeter, each of the LEDs must be turned ‘ON’ alternatively using a timing system. This enables the PD to synchronously recognize the transmitted or reflected light from the R and IR LEDs and split those signals.

One approach in optimizing power consumption is to decrease the duty-cycle of the switching signals delivered to the LEDs [26-28]. After reducing the duty cycle to a

minimum, the only other alternative to further reduce power consumption is to lower the current delivered to the LEDs. However, due to the high optical absorption by tissues and blood, decreasing the driving current supplied to the LEDs will lower the incident light intensity, and therefore could result in a significantly degraded PPG signal. It has been shown that with deteriorated signal quality, there is an increase in errors related to the SpO₂ value [26-28].

2.2 Photodiode

Photodiodes transform light into an electrical signal, typically a current. Silicon is the most commonly used photodiode material, because it is sensitive to a range of wavelengths including visible light. A silicon photodiode can absorb photons that have energy greater than the band gap [$E_g(\text{Si}) = 1.1 \text{ eV}$ at room temperature]. This absorption of photons creates an electron-hole pair. As minority carriers diffuse through the p-n junction, it converts to majority carriers. This conversion process contributes to the photocurrent.

2.2.1 Photocurrent and photovoltaic operation modes: A typical p-n PD can be operated in either photovoltaic or photoconductive mode, as shown in Figure 2.3. In photovoltaic mode, a light induced voltage is produced by an unbiased PD which is not a linear function of incident light. In an open circuit condition ($I=0$), the output voltage (V_{oc}) is given by

$$V_{oc} = \frac{kT}{q} \ln\left(\frac{I_p}{I_D} + 1\right) \quad (2.3)$$

where, I_D is the diode current,

I_p is the photocurrent,

T is the Absolute temperature (K),

k is the Boltzmann's constant ($1.38 \times 10^{-23} \text{ J K}^{-1}$) and,

q is the electron charge (1.6×10^{-19} coulombs).

In the photoconductive mode, the PD is reverse biased so as to produce a light induced current. The I-V characteristic of an “off-the-shelf” silicon photodiode subjected to illumination is shown in Figure 2.4. The graph indicates an increase in relative current with an increase in illumination at $V=0$ (short circuit current). The illumination response is linear to the incident light intensity until the photodiode becomes forward biased; at this point, the generated current starts to flow through the diode. The output current (I_{SC}) varies linearly with the incident light power according to equation 2.4.

$$I_{SC} = SE \quad (2.4)$$

where, S is the sensitivity or the unit of the photocurrent produced per unit of input light.

E is the incident illumination from the light source.

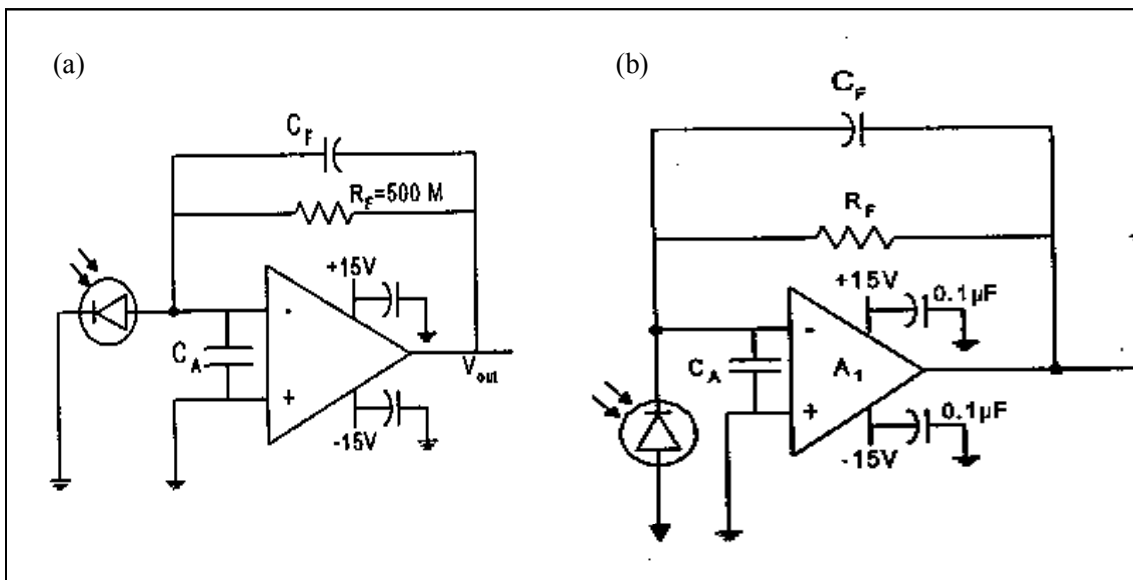


Figure 2.3. (a) Photovoltaic and (b) Photoconductive mode of the photodiode [2].

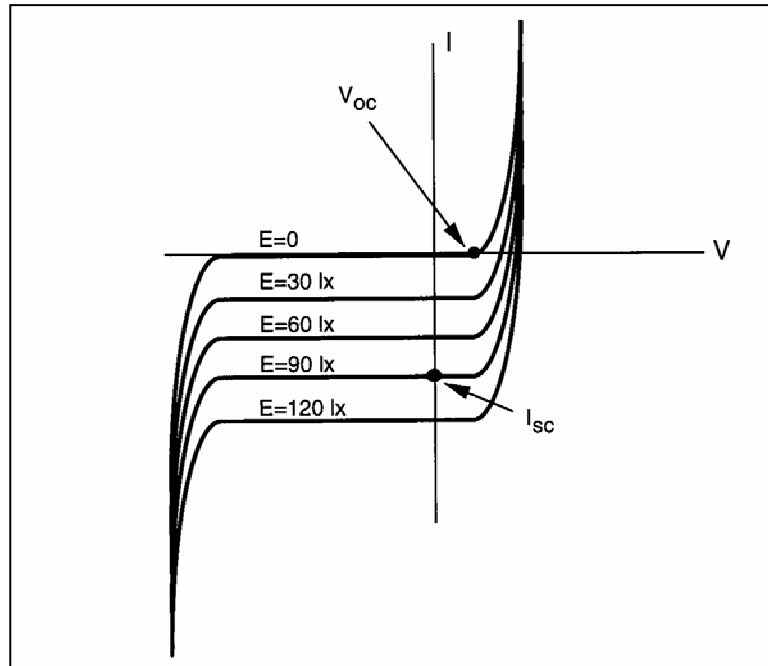


Figure 2.4. *I-V characteristics for a typical Si-PD [2].*

Even though a reverse bias will generate a dark current (I_d), a photoconductive mode will enhance the photodiode speed requirement as the junction capacitance is reduced with increase in reverse bias. In pulse oximetry, dual LEDs are monitored using a single Si-PD to obtain SpO_2 values. Figure 2.4 shows the spectral response of Si-PD, indicating that a Si-PD works well with the wavelengths of interest to pulse oximetry. Thus, a photoconductive mode is used as the output current is directly proportional to the incident light.

2.2.2 *Characteristics of Silicon-Photodiodes (Si-PD)*: The performances required from a photodiode are high sensitivity, low noise, high detection speed, wide bandwidth, high reliability, and low cost.

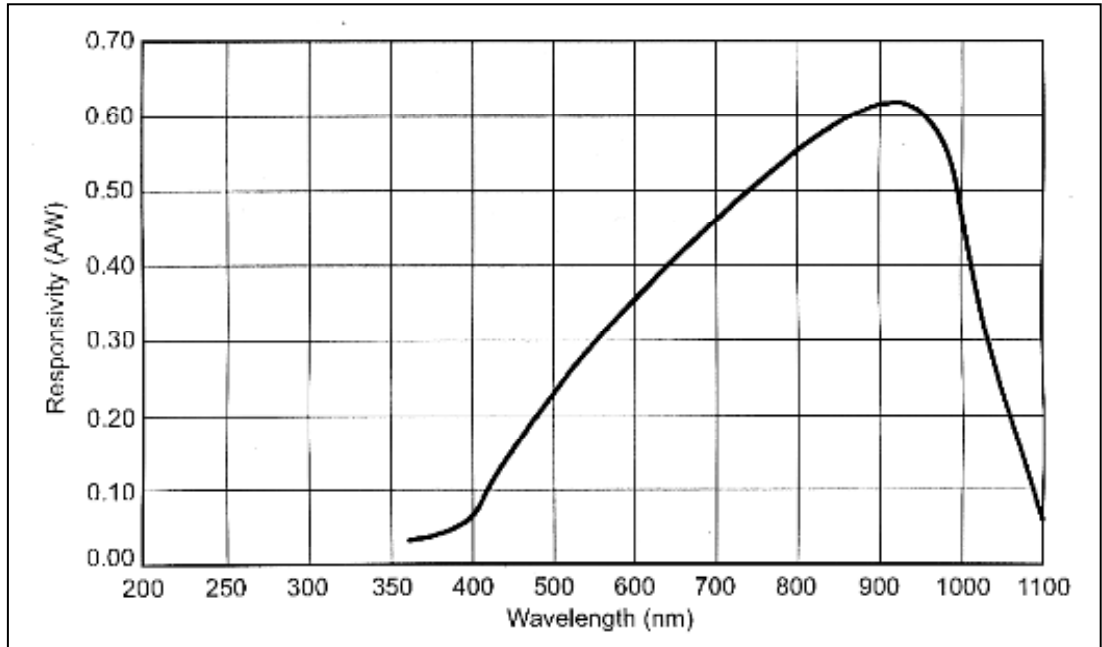


Figure 2.5. Spectral response of a typical Si-PD as a function of wavelength [2].

2.2.2(a) *Spectral Sensitivity*: The output current level observed for a known incident light level at a specific temperature is termed spectral sensitivity. The spectral sensitivity is determined when the center frequency of the detected light is specified. The unit for the spectral sensitivity of a photodiode is (mW/cm²).

2.2.2(b) *Responsivity (R)*: The responsivity of a silicon PD in (A/W) is a measure of the sensitivity to light as shown in Figure 2.5. It is defined by the ratio of the photocurrent (I_P) to the incident light power (P) at a give wavelength, as given by equation 2.5.

$$R = \frac{I_P}{P} \quad (2.5)$$

2.2.2(c) *Quantum Efficiency (Q.E.):* The percentage of the incident light that contributes to the photocurrent is called quantum efficiency. Equation 2.6 shows the relation between responsivity and quantum efficiency.

$$Q.E. = \frac{R_{Observed}}{R_{Ideal}} \quad (2.6)$$

2.2.3 *Noise Current:* The noise current observed in a silicon PD is the sum of a number of sources. The most fundamental source, (I_s), is the noise associated with the random arrival of photons, called shot noise. The second, (I_t), is the noise generated by a PD in the dark as a result of its temperature, called thermal (Johnson) noise. The electronic circuit used to measure the photocurrent can also introduce a noise under certain conditions, as shown in Figure 2.6.

The total noise current (I_n) is given as:

$$I_n = (I_s^2 + I_t^2)^{1/2} \quad (2.7)$$

Shot noise (I_s) is the dominant component of the noise current of a reversed biased PD which relies on the dark current (I_d) value, as shown in equation 2.8

$$I_s = (2qI_d df)^{1/2} \quad (2.8)$$

where, df is the noise bandwidth, and q is the charge of an electron.

The thermal noise increases as a function of the square root of the value of the shunt resistance (R_{SH}), as shown in equation 2.9 [21].

$$I_t = (4kTdfR_{SH})^{1/2} \quad (2.9)$$

where, T is the Absolute temperature (K),

k is the Boltzmann's constant (1.38×10^{-23} J K⁻¹) and,

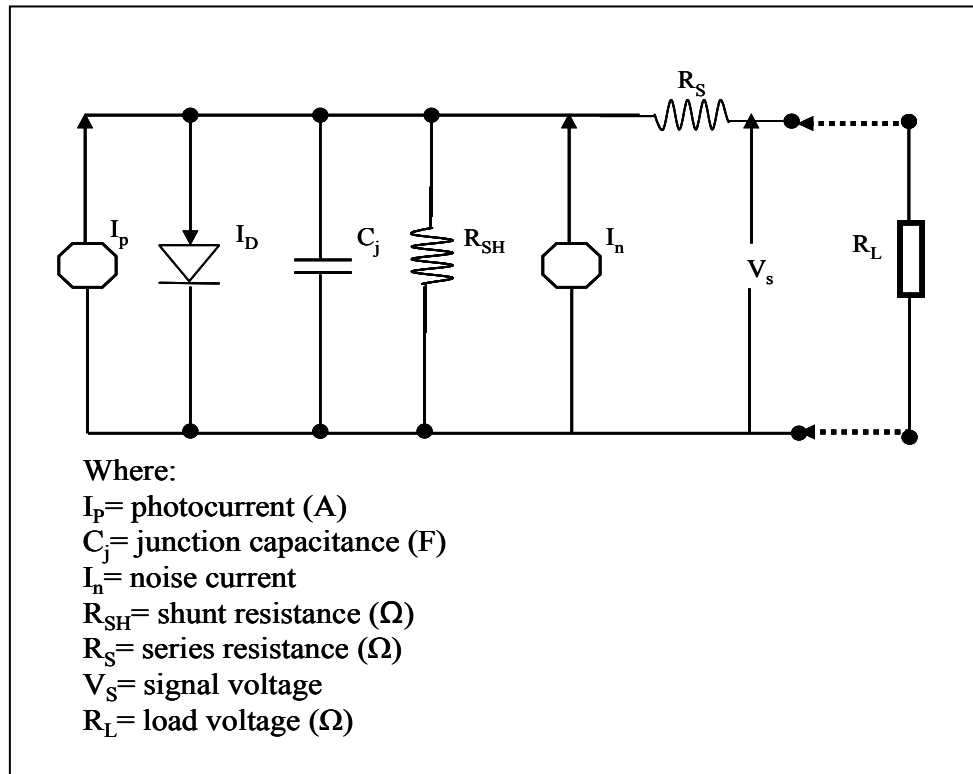


Figure 2.6. Equivalent circuit of the photodiode.

Mendelson *et al* [29] developed a multiple PD reflectance sensor using 6 PDs which improved the SNR of PPG signals. But the effect of increment in noise due to application of discrete PDs was not investigated. Theoretically, thermal noise (I_n) depends on R_{SH} that remains unaltered with addition of multiple PDs. But dark current noise is dependent on the junction capacitance (C_j) that increases as more PDs are attached in parallel. It can be concluded that dark current noise forms a key component of total PD noise. Thus, the dark current is extremely crucial for SNR calculations of a large area PD. As it was not feasible to custom build an annular large area PD with LEDs in the epicenter, discrete PDs have been used in this research to simulate large area PD. Thus, it is important to investigate the effect of increment in number of PDs (i.e. larger

active area) on the noise level. The sensitivity of a PD is directly related to noise. Any photocurrent that is less than a few standard deviations of the noise current will be masked by that current and thus will not be detectable except by averaging over a longer period of time. Therefore, a PD has to be designed with the requirement of minimum detectable light power. The incident power on a PD required to generate a current equivalent to the total PD noise current is defined as noise equivalent power [21, 30, 31], NEP (W). The relationship is given by

$$\text{NEP} = \frac{I_n}{R} \quad (\text{Unit: A/Hz}^{1/2}) \quad (2.10)$$

where, I_n = Noise current (A),

R = Responsivity (A/W).

If we assume that the noise power generated in a detector is proportional to its sensitive area, then noise current will vary as the square root of its area (i.e. $A^{1/2}$) [21]. Thus, we can define a unit NEP* which takes into account the effects of variable bandwidth (Δf) and detector area (A). The relationship is given by

$$\text{NEP}^* = \frac{\text{NEP}}{(A * \Delta f)^{1/2}} \quad (\text{Unit: W/cmHz}^{1/2}) \quad (2.11)$$

The NEP is also dependent on the bandwidth which is limited by the application of the band pass filter (0.5-15Hz) in the initial stages of PPG signal acquisition. NEP values can vary from 10^{-11} W/Hz, for large active area PDs, down to 10^{-15} W/Hz for small active areas. By increasing the detector size, more photons are intercepted. Figure 2.7 shows the effect of increase in active area on the dark current (I_d) and NEP [32]. It is evident that with the increase in the active area of the silicon PD, the dark current

increases, which leads to an increase in the shot noise. Similarly, NEP increases due to increase in the noise current (I_n) according to equation 2.10.

As the focus of this research project is to design a sensor with a larger PD area for improved power optimization, it was important that all factors governing noise were considered. NEP and I_d are the only relevant components of noise that directly relate to the increase in noise as a factor of PD area, as illustrated in the Figure 2.7. As dark noise was found to be a major component of PD noise, it was used to evaluate SNR as a function of increments in PD area.

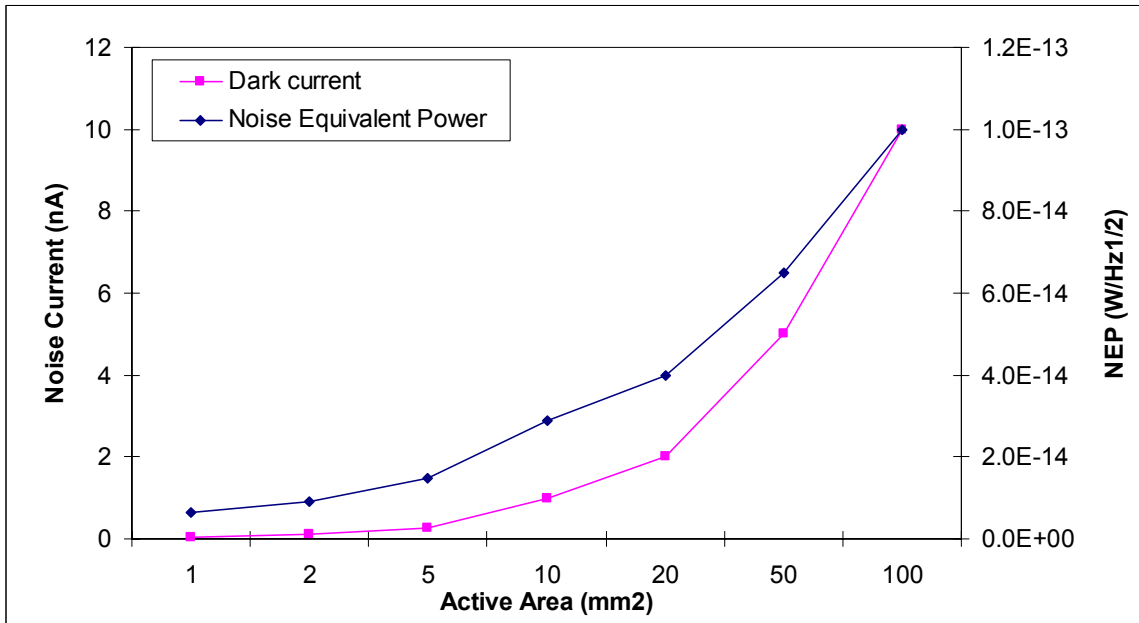


Figure 2.7. Effect of increase in photodiode active area on dark current (I_d) and Noise Equivalent Power (NEP)[32] .

2.3 Optimum LED/PD Separation Distance

One of the major considerations required while designing a reflectance pulse oximeter sensor is determining the optimum separation distance between the LEDs and PD. The light emanating from the LEDs in the reflectance sensor is diffused by the skin and subcutaneous tissues in a lateral direction. This suggests that to detect most of the backscattered radiation from the skin, the PD must be able to detect light from an area concentric with the LEDs. If the PD is positioned too close to the LED's, the large DC component, which is mainly due to multiple scattering of the incident photons by the blood free corneum and epidermis layers in the skin, will cause the pre-amplifier to saturate. But, it is also know that the intensity of the backscattered light decreases in direct proportion to the LED/PD separation distance. As illustrated in figure 2.8, Mendelson et al [33] experimentally proved a two-fold increase in the pulse amplitude of the PPG. They observed that the PPG signals became progressively more stable as the LED/PD separation was increased from 4 to 11mm, but only by incrementing in the LED drive current, as observed in figure 2.8. Hence, the selection of the LED driving current depends on the LED/PD separation distance. As shown in figure 2.9, they also found that a minimum separation distance of 4-6mm between the LEDs and the PD was required to obtain the best sensitivity in terms of detecting adequately large pulsatile components at low LED drive currents. Thus, while designing the prototype reflectance sensors, the optimum separation distance between the LED and the PD is kept within the range of 4mm to 10mm in order to obtain high quality PPG signals for accurate SpO₂ measurements.

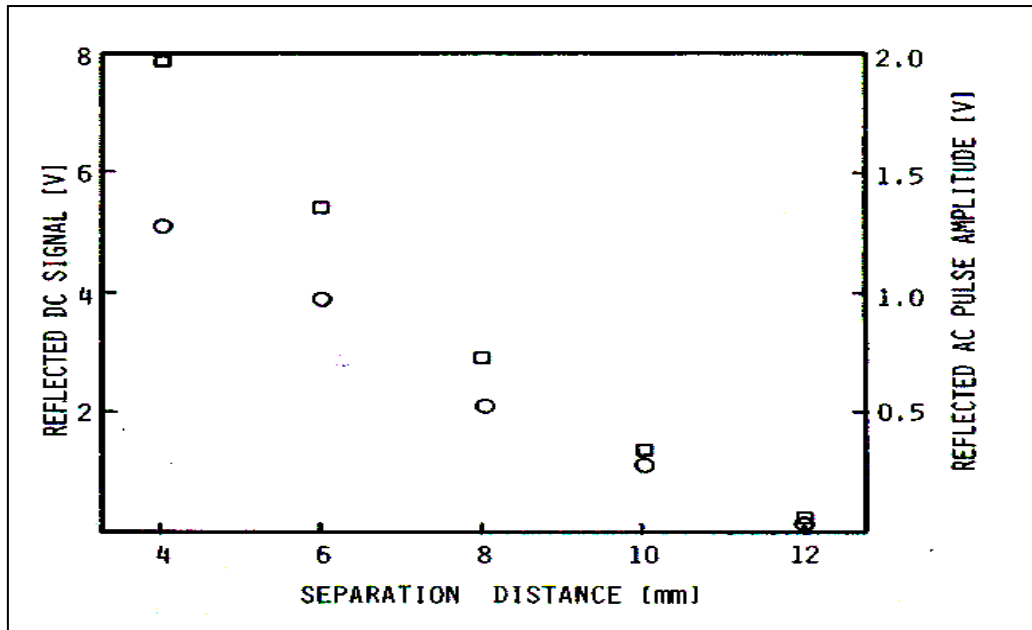


Figure 2.8. The effect of LED/PD separation on the DC (□) and AC (○) components of the reflected IR PPGs. Measurements were performed at skin temperature of 43°C [33].

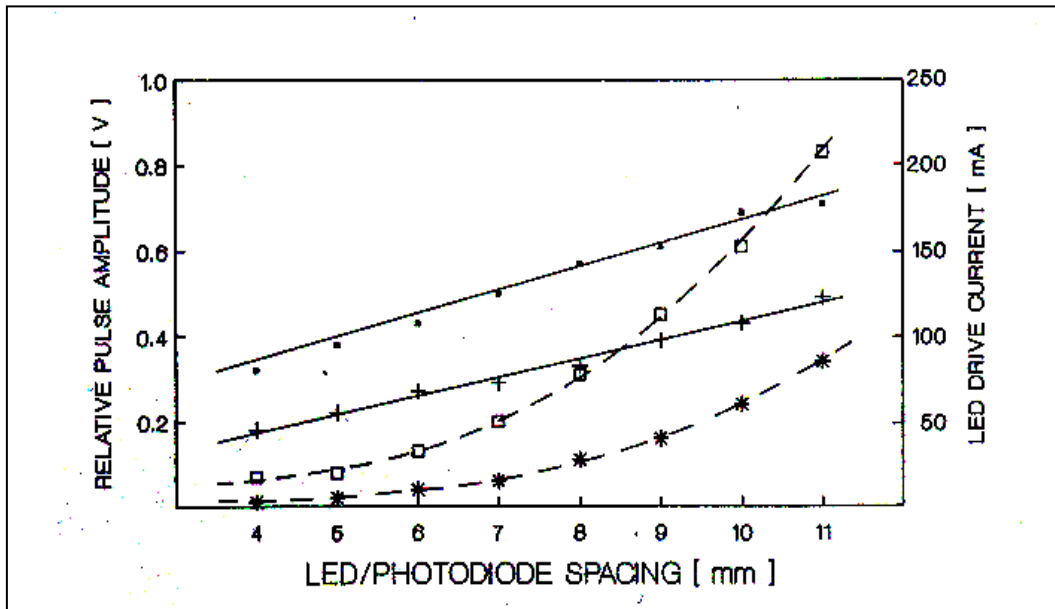


Figure 2.9. Effect of LED/PD separation on the relative pulse amplitude of R (+) and IR (■) PPG. The driving currents of the R (□) and the IR (*) LED's required to maintain a constant DC reflectance from the skin [33].

3. RESEARCH OBJECTIVES

The U.S. military has long been interested in incorporating hand-held pocket-sized personal digital assistant (PDA) computers and a Warfighter Personnel Status Monitor (WPSM) into its telemedicine applications for improved combat casualty care [34, 35]. By combining noninvasive physiological sensors with innovative microelectronics, a wireless communication link, and global positioning, the WPSM will be able to monitor the soldier's vital signs in real-time. It is envisioned that in the near future a frontline medic would be able to utilize this technology to read a soldier's medical history and assess the soldier's status on the battlefield, using advanced biomedical sensors. This technology could be used not only to improve far-forward diagnosis and treatment of combat casualties (i.e. performing remote triage), but also to predict the physiological performance of healthy soldiers or the likelihood of potential serious medical consequences that could be developed if certain medical conditions are left undetected or untreated. However, to gain better acceptability and address the unmet demand for long-term continuous monitoring, several technical issues must be solved in order to design more compact sensors and instrumentation that are power efficient, low-weight, reliable and comfortable to wear before they could be used routinely by soldiers as part of their regular combat equipment.

Despite the steady progress in the miniaturization of pulse oximeters, to date, the most significant limitation is battery longevity and wireless communication. For instance, real-time continuous physiological monitoring of mobile soldiers during combat using existing pulse oximeters is unavailable because commercial oximeters involve unwieldy wires connected to the sensor and sensor attachment to a finger restrains normal activity.

Therefore, there is a need to develop an advanced battery-efficient, noninvasive, remote monitoring device that is able to monitor crucial physiological information such as oxygen saturation and heart rate from different locations on the body.

For battlefield medical applications, features such as small size, light weight, being completely untethered and low power consumption are critical features of the sensor and instrumentation design. The pulse oximeter sensor is an integral part of the instrumentation design where primary power optimization can be achieved. Therefore, the long-term objectives of this research project are focused towards the future development of a low power, wireless pulse oximeter sensor. The specific objectives of this thesis are as follows:

Aim 1: Investigate different sensor modalities that would be suitable for monitoring combat soldiers.

Rhee *et al* developed a prototype ring sensor utilizing reflectance configuration, but the reason for the selection of a reflectance mode remains unclear [26-28, 36]. With signal quality and power consumption considered as design criteria different sensor modes must be evaluated. Hence, it was important to

- Construct a prototype ring sensor to test different sensor configurations.
- Test different sensor configurations to obtain quality PPG signals.
- Estimate and compare power consumption for different sensor modes.

Aim 2: Construct multiple PD sensor prototypes for different measurement modes.

Application of multiple PDs has a significant effect on the signal quality as observed by using an earlier sensor configuration developed by Mendelson et al [29, 33]. This

objective is focused on testing the potential power reduction achieved by the combination of multiple PDs. Specifically, the goal was

- To construct a multiple PD sensor prototype in transmission as well as reflection mode.
- To demonstrate that by increasing the area of the PD it is possible to reduce the overall power requirement of a wireless sensor and still maintain good signal quality.

Aim 3: Test the effects of lowering LED drive current on signal quality and measurement accuracy.

One approach in optimizing power consumption is to reduce the peak LED current drives. Thus, it was important to investigate the effects of lowering peak LED current drive on measurement accuracy. Specifically, the objective was

- To perform comparative experiments and statistical analysis where SpO₂ and HR values obtained from different prototype sensors are compared with a commercially available reflectance sensor (based on a single PD design).
- To calculate SNR improvement as a function of PD

4. DESIGN DECISION MATRIX

4.1 Objective Tree

It is important to understand and identify some of the key parameters that are required for the effective design of a wireless pulse oximeter sensor. Sensor site, length of monitoring (long term, short term or spot checks) and patient characteristics, such as activity level, represent primary considerations in an effective pulse oximeter sensor design [37]. To achieve a well designed product, an objective tree was used to create a list of characteristics that are necessary for the design.

An objective tree is an important graphical designing tool, which reflects a hierarchical structure of different goals and sub-goals that must be tackled before the final product is designed [38]. In this design project, the objective tree was used to generate a list of features that are deemed critical in the development of a pulse oximeter sensor considering its future battlefield applications. Some of the common questions noted from an initial brainstorming session are listed below.

- Does size of the sensor matter?
- What would be the most suitable location for mounting the sensor on a soldier during active combat?
- What type of sensor mode would be preferred for military applications?
- How much power can be consumed by the sensor?

Based on the questions, an objective tree was constructed as illustrated by the tree diagram shown in Figure 4.1.

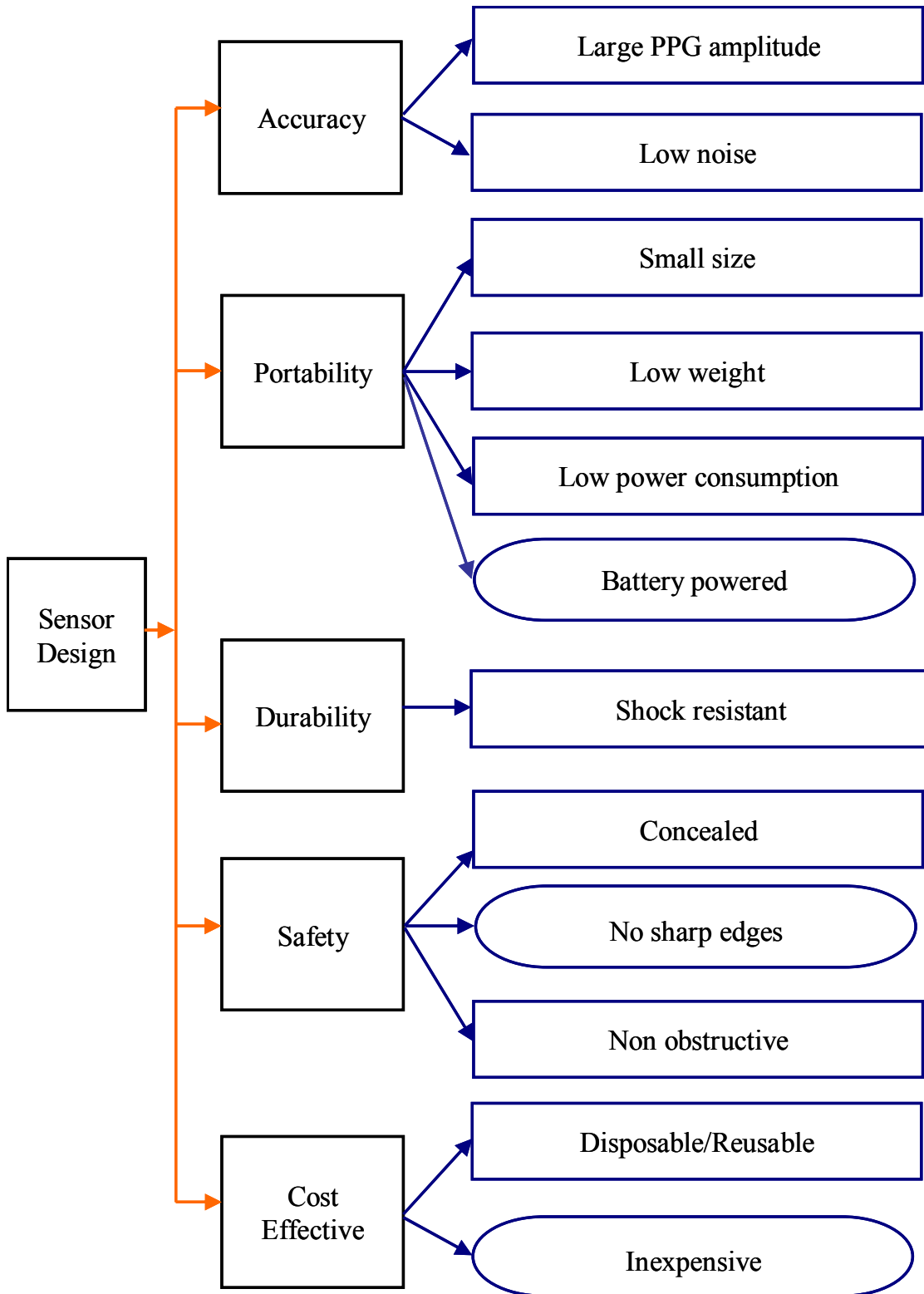


Figure 4.1. An objective tree showing non-hierarchical structuring of the sensor characteristics (objectives in rectangles and constraints in oval).

The main objectives were placed in a rectangular box while the constraints were denoted by an oval-shaped box. Constraints are features that shouldn't be included in the final product. In this particular case, constraints were defined as restrictions on a certain aspect of the design. Objectives such as portability, safety and cost generate the constraining factors. Some of the constraints faced during the design of a pulse oximeter sensor are no sharp edges, cost and battery powered design. Some design objectives can be defined either in the form of 'HIGH' or 'LOW', such as, the accuracy of detecting a PPG signal should be 'HIGH', whereas the power consumption should be "LOW". Some design questions can be answered in a definite fashion such as a "YES" or "NO" based on common sense, while others require in depth research in the form of literature review or experiments, for example, to determine power consumption and sensor mode selection. The objectives illustrated in Figure 4.1, are explained below.

Accuracy: The primary objective of a pulse oximeter sensor is to acquire a high quality PPG signals for accurate SpO₂ and HR measurement. Thus, accuracy can be further divide into large PPG signal amplitude and low noise.

Portability: Portability of a pulse oximeter sensor can be attained by objectives such as small sized, light weight and low power consumption. Commercial sensors are generally small (10 x 30 mm²) and light weight (<10gms), so modifying it for our design requirement would be simple, provided they can be powered by a battery.

Durability: The durability of the sensor design depends on objectives such as resistant to shocks. As the ultimate pulse oximeter design goal would be to develop a wireless unit with a small built-in battery, low power budgeting is considered as a crucial design objective.

Safety: One of the most important objectives of the sensor design is not have any sharp edges on the sensor which might cause injuries to the soldier. Thus, the sensor design or packaging should be rounded. In addition, since the sensor emits light, it is important to conceal it in order to prevent detection of the soldier wearing the device in the dark.

Cost: Battery replacement can be costly and inconvenient. It depends on long-term or short-term physiological monitoring of the soldier's condition and the power consumed by the pulse oximeter. Furthermore, the total cost of the sensor design would vary, depending on the type of sensor (reusable or disposable). The most effective design would be a reusable sensor, as it would reduce the production cost.

Additional design considerations for mounting a pulse oximeter sensor on a soldier during active combat include:

Sensor mode: Selection of the sensor mode (transmission or reflection mode) has common attributes to the sensor characteristics and the selection of location where the sensor should be mounted on a soldier. Features such as low power consumption and convenient attachment techniques define characteristics that are required for selecting a particular sensor mode. Improper attachment techniques can increase motion artifacts, which has direct impact on signal quality.

Sensor location: While selecting an appropriate attachment site, factors such as cutaneous circulation and anatomical location are important considerations. Abundant blood supply is present in highly vascularized regions thus, facilitating accurate SpO₂ measurement from these locations. Similarly, certain attachment areas provide flexibility in designing the sensor for maximum concealment, convenient application and minimum side-effects such as potential pressure necrosis to the measurement site.

Features such as power consumption, signal quality, accuracy and attachment technique are also crucial and, therefore are considered as common attributes for sensor design characteristics as well as selection of sensor attachment site on soldiers engaged in active combat, as shown in the Venn diagram (Figure 4.2). Easy attachment, sensor attachment using different methods, power consumption as well as the sensor modes are common design attributes.

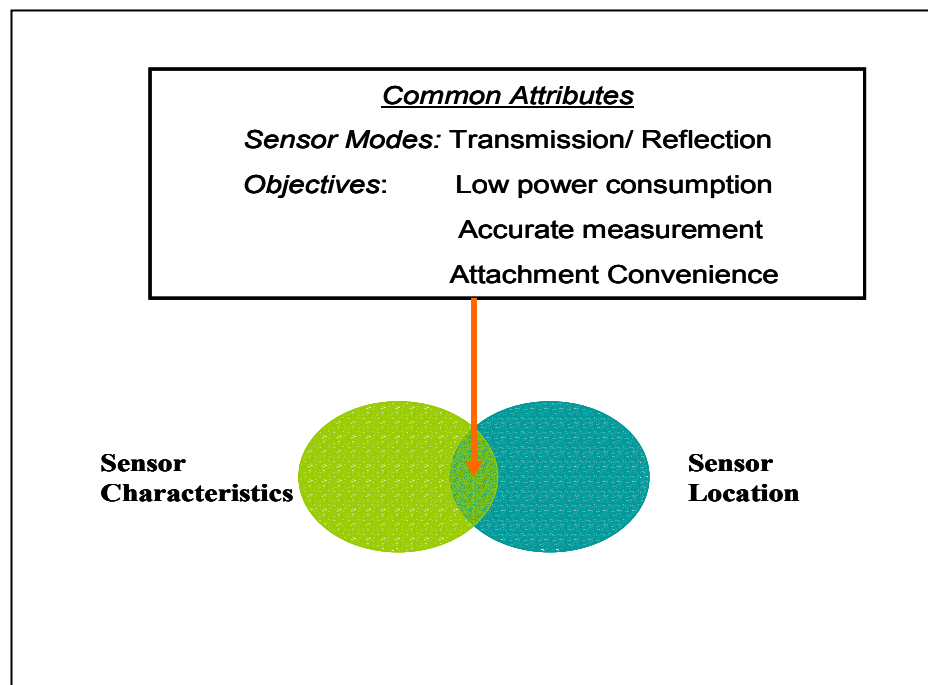


Figure 4.2. A Venn diagram representing common attributes between sensor characteristics and sensor location.

4.2 Pairwise Comparison Technique

The quality of the PPG signal, physiological and anatomical advantages and sensor attachment play a powerful role in the development of a wireless pulse oximeter sensor for monitoring SpO₂ during combat. But each feature has certain precedence over one another which are relative to the sensor design. Parameters such as signal quality and sensor attachment have a higher priority over the physiological advantage or physical

characteristics such as portability, durability and cost. Thus, it would be convenient to identify the values of (rank) each parameter comparative to one another. A pairwise comparison technique allows us to determine the relative order (ranking) of a group of items and can be used as part of a process of assigning weights to each goal in the design. The primary features from the objective tree in Figure 4.1 were considered in the pairwise comparison table. The features were placed in the first column and first row of the table. Once the comparison matrix was created, as shown in table 4.1, for each row (excluding the first row), features listed in the first column were compared with respect to each feature in the first row. If a column feature is important in comparison to the row feature, then a '0' value was assigned in the corresponding column; otherwise, if it was considered less important, then a '1' was assigned. For example, signal quality was considered more important than portability or durability. Thus, a '0' was assigned to portability and durability. When a feature was compared against itself, 3 asterisks ('***') were assigned. After comparing each feature, values assigned to each row were summed up. The summation of values from each row provided the ranking of the corresponding column feature. The most important feature is equivalent to a ranking of zero. To avoid the use of rank '0' for the most important feature, the row total was incremented by one.

From the pairwise comparison table shown in table 4.1, it was concluded that the following ranking of features was important

Signal quality > Attachment > Location > Safety > Portability > Durability > Cost

where > denotes the order of importance

Table 4.1. Pairwise comparison chart for an assorted set of primary objectives considered for a pulse oximeter sensor design.

Factors for sensor design	Signal Quality	Portability	Durability	Safety	Cost	Attachment	Location	Score (Row total +1)
Signal Quality	***	0	0	0	0	0	0	1
Portability	1	***	0	1	0	1	1	5
Durability	1	1	***	1		1	1	6
Safety	1	0	0	***	0	1	1	4
Cost	1	1	1	1	***	1	1	7
Attachment	1	0	0	0	0	***	0	2
Location	1	0	0	0	0	1	***	3

4.3 Initial Decision Matrix

Before comparing each ranked factor for a particular location, it was essential to list the locations where the sensor could be located. Application of an initial decision matrix is also a preliminary step towards shortening a vast list of possible locations where the sensor can be positioned. In order to select a suitable location, features such as clinical acceptability, military acceptability and available sensor modes were considered. Questions related to acceptance of the sensor location for military application, and the clinical availability of a pulse oximeter sensor were answered by a simple ‘Yes’ or ‘No’.

Regional variations in skin perfusion are the main reasons for the difference in signal quality observed at various locations. After reviewing a number of publications, the clinical acceptability for a particular location was justified. Mendelson *et al* have recently demonstrated the application of a reflectance pulse oximeter sensor on the forehead, chest and back to obtain accurate SpO₂ values [39]. The finger tips, forehead and earlobes are suitable sites for application of pulse oximeter sensors in clinical medicine. Tur *et al* compared measurement of the basal perfusion of the cutaneous

microcirculation as a function of anatomical position using non invasive photoplethysmography [40]. The 52 anatomical sites used in the comparative experiment were identified by site numbers, as shown in Figure 4.3. Various anatomical sites identified by site numbers illustrated in Figure 4.3 are ranked according to the mean PPG amplitudes obtained, as shown in Figure 4.4. As shown in table 4.2, the groups were multiply compared using the Newmans-Keuls statistical test where difference were assessed at $p=0.05$ and $p=0.01$ levels of significance [41]. The entry N means that the perfusion of the 2 compared groups is not significant whereas the presence of 1 or 2 asterisks means that the group in the left-hand column has significantly lower perfusion

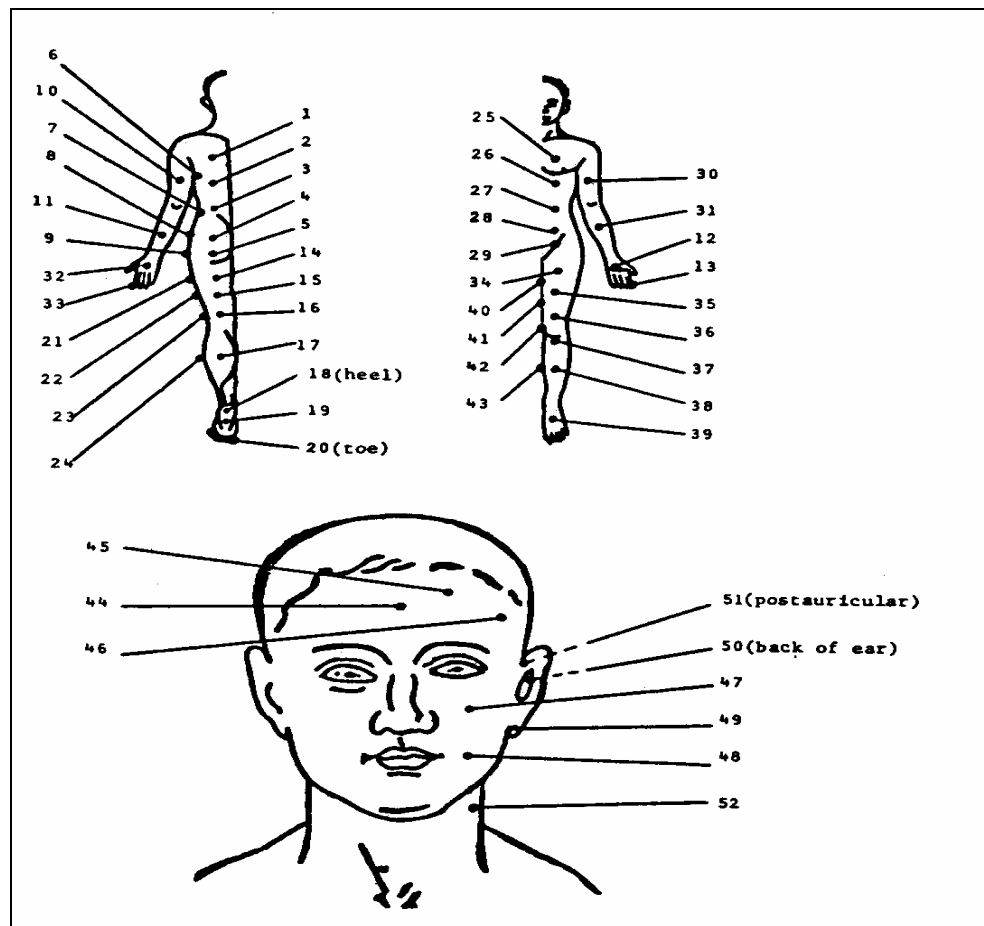


Figure 4.3. Anatomic positions identified by site number for which basal cutaneous perfusion measurements were performed using photoplethysmogram [40].

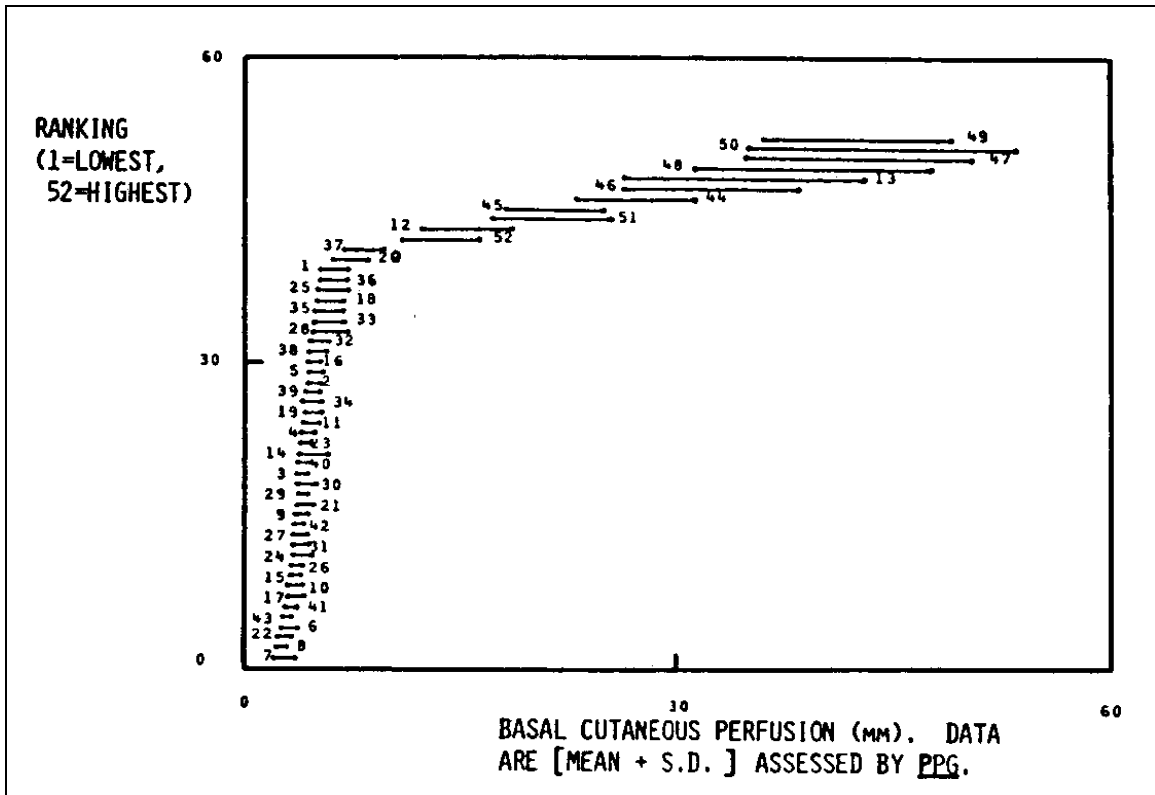


Figure 4.4. Basal cutaneous perfusion measurements assessed by PPG, where locations (represented by site numbers) are ranked according to the mean values obtained [40]. (PPG units for signal amplitude in mm where 1mm = 10mV)

than the paired group in the top row of the table. Results from the study showed that anatomical locations such as the finger, face or ear have a higher cutaneous perfusion in comparison to other locations [40].

A shortened list of locations from the initial decision matrix simplifies the final decision matrix for selection of the most appropriate site for sensor placement. The human model depicted in Figure 4.5 has been marked with green circle markers which represent locations where strong PPG signals are typically obtained. Similarly, blue (square) and red (triangular) markers suggest locations with unreliable or weak signals, respectively. The pros and cons associated with each of the selected locations are mentioned in Appendix A. Table 4.3 lists the locations that were considered for the

Table 4.2. Multiple comparisons of cutaneous perfusion measurements for the anatomical positions grouped in different tables [40].

	Upper Limb	Lower limb	Foot	Hand	Face
Trunk	N	N	N	**	**
Upper Limb		N	N	**	**
Lower Limb			N	**	**
Foot				**	**
Hand					*,N

	Lower Leg	Arm	Upper Leg	Lower Trunk	Upper trunk
Side	**	**	**	**	**
Lower leg		N	N	N	**,*
Arm			N	N	N,*
Upper leg				N	N
Lower trunk					N,*

	PAR	Finger	Face	Back of ear	Earlobe
Hand	N	*,N	N	**,N	**,N
PAR		N	N	**,N	**,N
Finger			N	N	N
Face				N	N
Back of ear					N

application of a wireless pulse oximeter sensor. Selected sites with the respective rank numbers are listed in the table 4.3. Five best sites are required for inclusion in the final decision matrix and further experimental investigation. The finger, forehead and earlobe are standard locations that are clinically accepted [42]. The forehead, chin and wrist form a set of locations where reflectance sensor placement and attachment is relatively easy using articles that are a part of the soldier’s gear. For example, the kevlar helmet, or chin strap, are potential means for attaching a reflectance sensor without using disposable adhesive tape. Based on the performance required and keeping in mind the end user’s activities, locations such as forehead, finger base, ear lobe, chin and wrist were considered in the final decision matrix. These locations are highlighted in red in table 4.3 and termed as “pre-selected locations” in the final decision matrix.

Table 4.3. Initial decision matrix created to shorten the list of possible locations (with site numbers) for sensor attachment.

Anatomical Location (Site Number from Figure 4.3)	Literature reference	Sensor clinically available (Yes/No)	Potential acceptability for military applications (Yes/No)	Possible sensor mode R-reflection T-transmission
Head Region				
Forehead (44,45,46)	Mendelson <i>et al</i> [39], Tur <i>et al</i> [40]	Yes	Yes	R
Temple (46)	Tur <i>et al</i> [40]	Yes	Yes	R
Nose	Nellcor Tyco Healthcare [42]	Yes	Yes	R and T
Chin		No	Yes	R
Ear Lobe (49)	Mendelson <i>et al</i> [11, 39] Tur <i>et al</i> [40]	Yes	Yes	R and T
Nape (47)	Tur <i>et al</i> [40]	No	Yes	R
Jaw line (48)	Tur <i>et al</i> [40]	No	Yes	R
Upper Torso				
Chest (25)	Mendelson <i>et al</i> [39], Tur <i>et al</i> [40]	No	Yes	R
Abdomen (27)	Tur <i>et al</i> [40]	No	Yes	R
Back (2,3)	Mendelson <i>et al</i> [11, 39] Tur <i>et al</i> [40]	Yes	Yes	R
Upper Extremities				
Arm (10,30)	Tur <i>et al</i> [40]	No	No	R
Forearm (31)	Tur <i>et al</i> [40], Mendelson <i>et al</i> [33]	No	No	R
Wrist (11)	Tur <i>et al</i> [40]	Yes	Yes	R
Palm (12)	Tur <i>et al</i> [40]	No	No	R
Finger Base (13)	Tur <i>et al</i> [40]	Yes	Yes	R and T
Finger tips (33)	Tur <i>et al</i> [40], Mendelson <i>et al</i> [33], Awad <i>et al</i> [43]	Yes	No	R and T
Lower Extremities				
Thigh(35,36)	Tur <i>et al</i> [40], Mendelson <i>et al</i> [33]	No	Yes	R
Calf(24,43)	Tur <i>et al</i> [40]	Yes	No	R
Foot(39)	Tur <i>et al</i> [40]	Yes	No	R
Toe(20)	Tur <i>et al</i> [40]	Yes	No	R and T

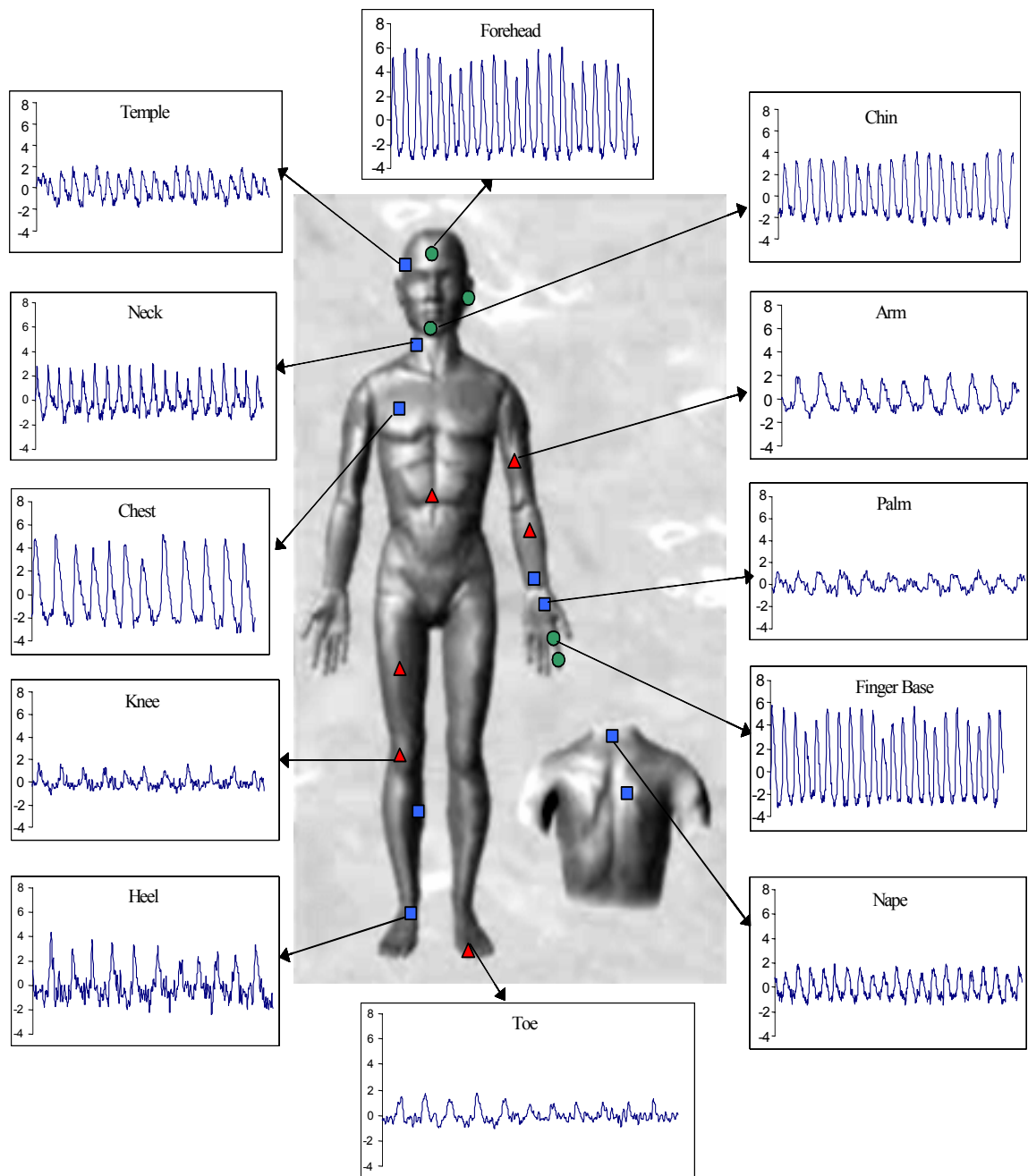


Figure 4.5. Markers representing the quality of PPG signals (PPG amplitude in volts) obtained in our laboratory from different body locations. (●: Strong ■: Medium ▲: Weak).

4.4 Final Decision Matrix

The parameters from the objective tree and the shortened list from the initial decision matrix were combined in the development of a final decision matrix. Relative weights of the ranked objectives were obtained by normalizing the ranks after assigning the top objective to unity. The other method is by assigning a scale of 1 to 10 for each ranked objective with the top objective assigned to a 10. Thus, on a scale of 1 to 10, the seven objectives were assigned as follows: signal, 10; attachment, 9; location, 8; safety, 6; portability, 4; durability, 2; cost, 1. The normalization factor for these goals is the arithmetic total of the total points awarded to all the values, which in this case was 40. Thus, the normalized values for the objectives would be: signal, 0.25; attachment, 0.225; location, 0.2; safety, 0.15; portability, 0.1; durability, 0.05; and cost, 0.025. These objectives remain the same for the sensor at different locations, but the simplicity level for accomplishing an objective would vary with respect to different locations. Certain locations do not provide a good quality or accurate signal as shown in the Figure 4.5. Although SpO₂ is typically measured from locations such as digits and ears, the forehead is an excellent alternative site for patients with low peripheral perfusion [44, 45]. Keeping these factors in mind, each location was ranked for a particular objective. With this method it becomes possible to determine which sensor location provides the most convenient way of achieving the ranked objectives. After each location was scored against each other for a particular objective, the sum of the scores for each location row were calculated. In table 4.4, the product of the objective's normalized value and the weighted score of the location are shown in parenthesis. For example, signal quality has a weighted objective of 0.25 and using it for the location (ex: forehead), we obtain

weighted score (1.25) as the product of the score (5) and weighted objective (0.25), as summarized in table 4.4. These are weighted values of an objective in comparison to each location. The location with the highest score was selected to be the most suitable location for the sensor placement while keeping in mind the different objectives and challenges faced during the design of the sensor. For example, using a head band for the forehead sensor is the most convenient attachment technique in comparison to other locations.

Table 4.4. Final decision matrix selects an appropriate location for the sensor placement on the soldier based on the highest score.

Objective Rank	1	2	3	4	5	6	7	
Objectives	Accuracy	Attachment	Location	Safety	Portability	Durability	Cost	Total
Weighted Objectives	0.25	0.225	0.2	0.15	0.1	0.05	0.025	1.00
Pre-selected Locations								
Forehead	5 (1.25)	5 (1.125)	4 (0.8)	5 (0.75)	5 (0.5)	5 (0.25)	5 (0.125)	29 (4.8)
Wrist	1 (0.25)	2 (0.45)	1 (0.2)	5 (0.75)	2 (0.2)	2 (0.1)	5 (0.125)	18 (2.08)
Earlobe	2 (0.5)	3 (0.675)	2 (0.4)	5 (0.75)	1 (0.1)	3 (0.15)	5 (0.125)	21 (2.7)
Chin	3 (0.75)	4 (0.9)	3 (0.6)	5 (0.75)	3 (0.3)	4 (0.2)	5 (0.125)	27 (3.63)
Finger	4 (1.00)	1 (0.225)	5 (1.0)	5 (0.75)	4 (0.4)	1 (0.05)	5 (0.125)	25 (3.55)

But in terms of anatomical location, the finger is a much better location due the presence of a large vascular bed fed by digital arteries. This does not indicate that the forehead has low physiological advantage, as the supraorbital artery arising from the internal carotid artery supplies blood flow to the forehead skin which is not as prone to vasoconstriction during low perfusion conditions. Studies have confirmed that the forehead is less susceptible to vasoconstriction compared with the digits, and forehead sensors are more responsive to changes in SpO₂ when patients have a low pulse perfusion [44, 45].

Although the finger produces much stronger PPG signals in terms of quality, it is overshadowed by the noise produced due to motion associated with clenching, pressing, and hand shaking during routine activities [36, 46]. Hence the finger scores a point less than the forehead in the signal (accuracy) ranking.

Portability and durability features are essential when the complete design of the pulse oximeter is completed. But by considering the sub goals that further elaborate each objective, it is easier to score different locations. For example, locations such as fingers and the wrist score lower points than the other three locations as they are highly susceptible to shock. Safety and cost are factors that remain unchallenged with respect to the location for sensor placement. For this reason, scores for the safety and cost remain constant for all pre-selected locations. Ear sensors and finger sensors are affected by thermo-regulatory vasoconstriction and have slower response to changes in central oxygenation as compared to forehead sensors which maybe critical for rapid detection of hypoxemia [47, 48]. Therefore, from the final decision matrix, it was concluded that following ranked locations are important where > represents the order of importance.

Forehead > Chin > Finger > Earlobe > Wrist.

Thus, in this particular design case, it was concluded that the forehead is the most suitable location for sensor placement. But issues related to power budgeting still remain unanswered. Even though a forehead sensor requires the application of reflectance mode, it is crucial to evaluate the different sensor modes to justify the selection of reflectance mode on the basis of the lowest power consuming sensor mode. The finger has adequate physical area to accommodate different sensor modes which may be reconfigured with enlarged PD area for improved signal quality. Thus, for evaluating power consumption in

different sensor modes, a finger sensor is an appropriate sensor site where it is possible to configure different sensor geometries by altering the position of the LEDs relative to the PDs.

5. MATERIALS

5.1 Experimental Sensor Setups

Low power management without compromising signal quality is a key requirement for an optimal design of a wearable pulse oximeter. Thus, a number of prototype sensors were configured to investigate different sensor geometries.

5.1.1 Prototype Ring Sensor: A prototype sensor configuration consisting of 6 identical Si PDs (for each PD, active chip area: 2mm x 3mm) and a pair of R and IR LEDs was constructed and tested to study the potential power savings associated with different PD positions in a ring-shaped sensor and to select an appropriate sensor mode for further investigations. A suitable location to test the different sensor modes is the proximal phalanx of a volunteer's finger. The PDs and LEDs were arranged symmetrically along the inner circumference of the sensor using a black Velcro tape. As shown schematically in Figure 5.1 and Figure 5.2, two of the six PDs (PD-1 and PD-6) were positioned adjacent to the LEDs, typical of a reflection sensor configured for measuring backscattered light. Two PDs (PD-2 and PD-5) were positioned along a transverse plane to measure light that is emanating from both sides of the finger in a so-called transflection mode. The remaining PDs (PD-3 and PD-4) were positioned opposite the LEDs to measure the light transmitted through the finger. The ring sensor was attached to a volunteer's left index finger with an external clamp, which aided in securing the sensor on the finger. Power consumptions were estimated from the reduced LED drive currents supplied from the pulse oximeters to individual LEDs.

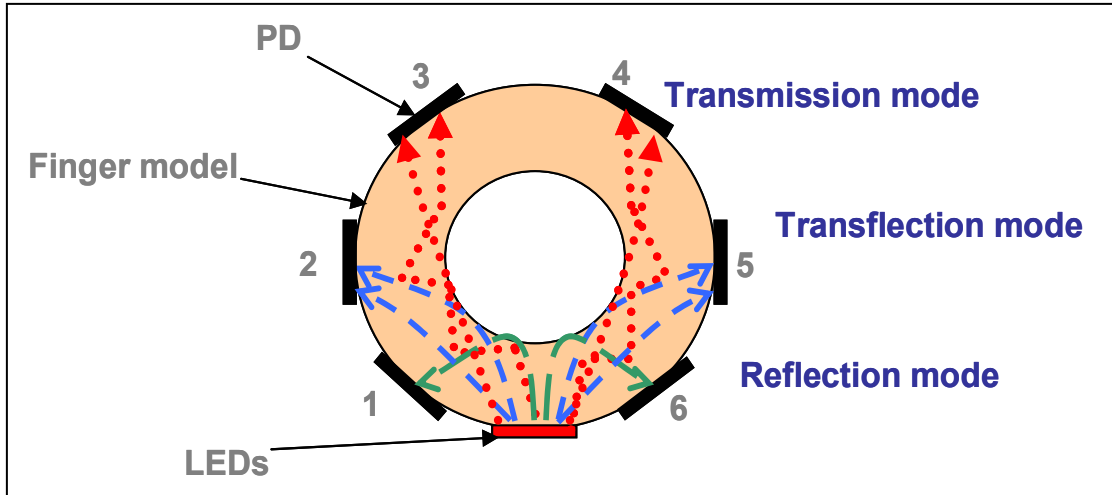


Figure 5.1. Light propagation in tissues surrounding a finger phalanx for different PDs configuring a variety of sensor modes.

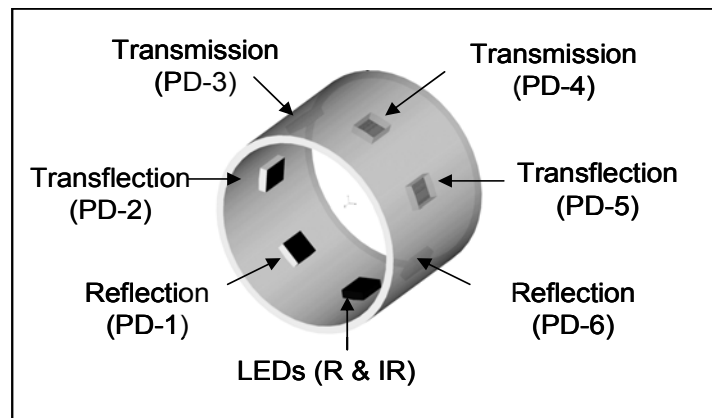


Figure 5.2. Prototype ring sensor configuration showing the relative positions of the PDs in reflection, transflection and transmission modes.

5.1.2 Prototype 6-PD Disc Sensor: A prototype sensor comprising six identical Si PD chips (active chip area: 2mm x 3mm) and a pair of R and IR LEDs were configured on a flat plastic disc to study the potential power savings associated with an increase in PD area for different sensor modes. As shown schematically in Figure 5.3(a), six PDs with a combined active area of 36mm² were positioned in a close ring configuration at a radial distance of 6.0mm from the LEDs. The LEDs in the center were positioned in a detachable mode, as shown in Figure 5.3(b). Thus, by changing the relative position of

the LEDs, the 6-PD prototype sensor could be configured to function in reflection or transmission mode.

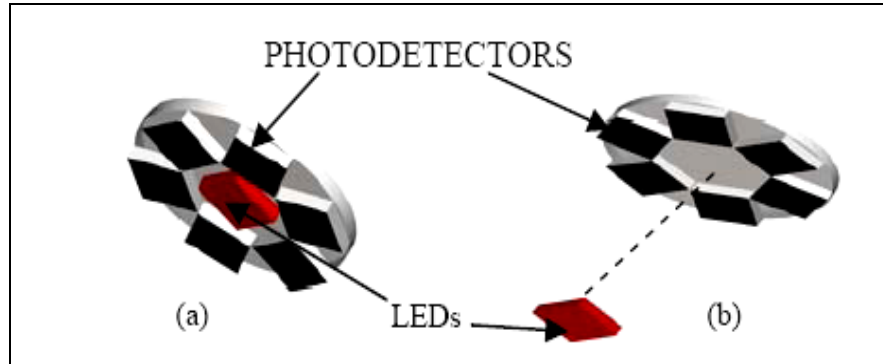


Figure 5.3. Sensor configurations in reflection (a) and transmission (b) modes.

5.1.3 Prototype 12-PD Reflectance Disc Sensor: A prototype reflectance sensor comprising 12 identical Si PD chips (active chip area: 2mm x 3mm) and a pair of R and IR LEDs was configured to study the effect of LED-to-PD separation distance on power consumption. As shown schematically in Figure 5.4, 6 of the PDs were positioned in a close inner-ring (N) configuration at a radial distance of 6.0mm from the LEDs. The second set of 6 PDs were spaced equally along an outer-ring (F) separated from the LEDs by a radius of 10.0mm. An optical guard was constructed around the LEDs using an insulated black wire which creates a non-reflective barrier between the LEDs and the PD. This prevents light from reaching the PDs without passing through the tissue. Each cluster of 6 PDs was arranged symmetrically in a concentric planar configuration and wired in parallel to represent a larger PD area compared to a smaller area (typically 2mm x 3mm) used in commercially available reflectance type sensors.

5.1.4 Central Hub Connector (Multiple DB-9 Female Interfaces): A central hub provided a convenient way to increase the amount of backscattered light collected by connecting several PDs in parallel. As shown schematically in Figure 5.5, the hub was built by

connecting six DB-9 female connectors in parallel to enable convenient and fast reconfiguration of the total detection area, thus, avoiding the need to remove and re-attach the sensor during *in-vivo* experiments.

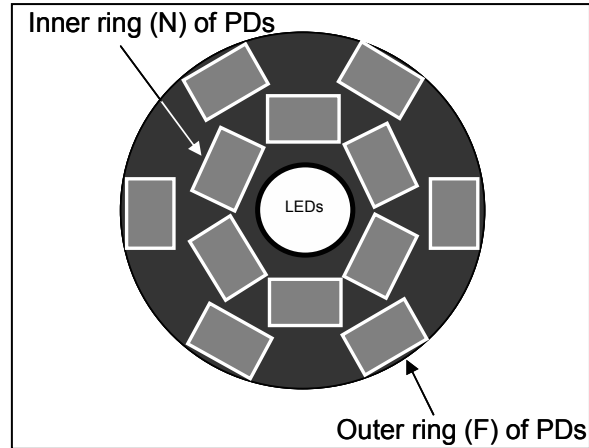


Figure 5.4. Prototype 12-PD reflectance disc sensor configuration showing the relative positions of the rectangular PDs and the LEDs.

Each PD in the prototype ring sensor was wired using a separate DB-9 male connector. The connector was attached through the hub that connected the PD directly to the common summing input of a current-to-voltage (I-V) converter, as shown in Figure 5.6. The hub provided a convenient way to connect in parallel two PDs simultaneously for each of the three modes (transmission, reflection and transfection) in the prototype ring sensor.

While using the prototype 6-PD disc sensor, individual PDs were evaluated. The hub provided a convenient technique to obtain output from a single PD or a combination of multiple PDs, without changing or removing the prototype sensor attached to the volunteer. Secondly, the total detection area of the multiple PDs sensor could be increased or decreased externally by connecting or disconnecting certain connectors from the hub.

5.2 Pulse Oximetry Instrumentation

Different pulse oximeters were used for a variety of experiments including evaluation of the final prototype sensor. The specification sheets for the different pulse oximeters are found in Appendix B.

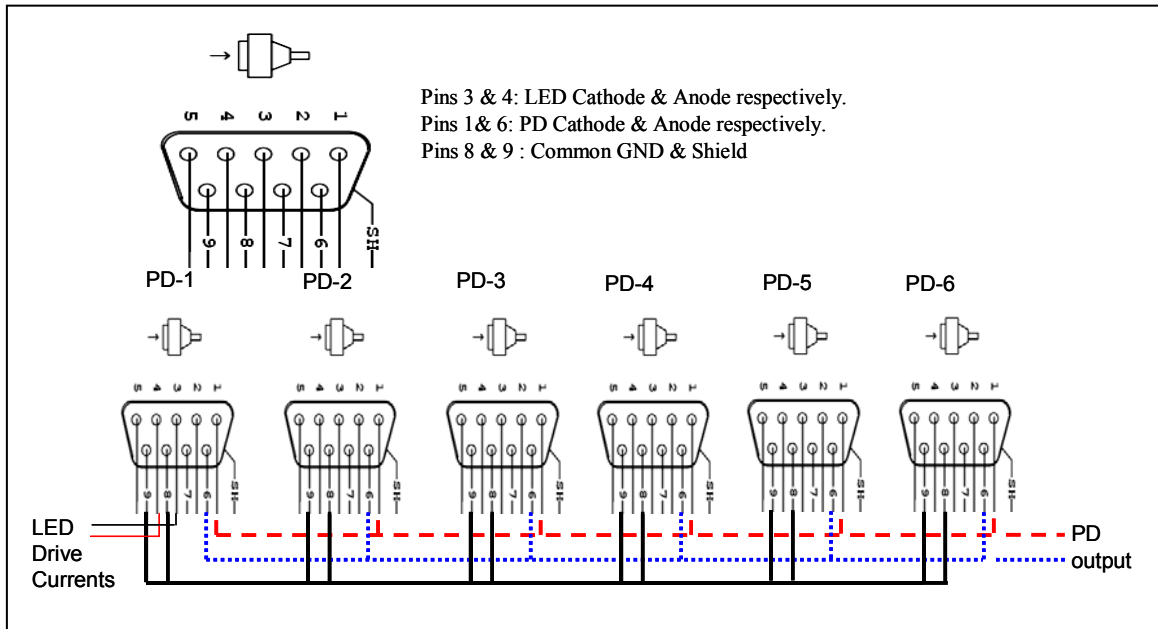


Figure 5.5. Parallel configuration of DB9 female connectors used to construct a sensor interface.

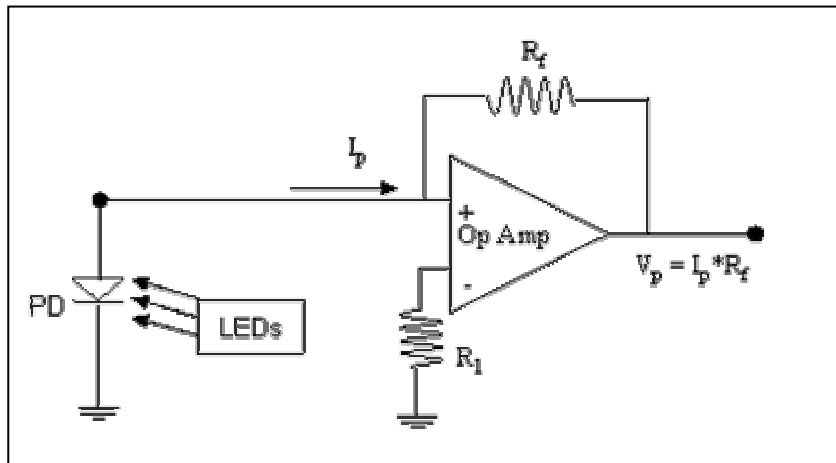


Figure 5.6. A simple circuit diagram of an I-V converter used to convert PD output from a current (I_p) to voltage (V_p).

5.2.1 Photoplethysmogram Signal Processing Unit (PSPU): A PPG signal processing unit (PSPU) was used to record raw PPG signal components (i.e. AC: R & IR and DC: R & IR). Analog signals obtained from the PSPU were used for off-line signal processing and computation of SpO₂ values. A block diagram of the PSPU is shown in Figure 5.7. A unipolar peak current supplied from the LED driver circuit is passed through the input module to the LEDs. The digital switching circuit generates a pulse sequence (T_{ON} : 128 μ sec and T_{OFF} : 896 μ sec) for turning ‘ON/OFF’ each LED sequentially. Thus, the timing circuit enables synchronous detection by splitting the PD output signal for individual LEDs using a sample-and-hold circuit (S/H). The PD generates a current proportional to the amount of light detected. The current drive supplied to each LEDs was adjusted externally using a potentiometer. The current-to-voltage (I-V) converter connects the PDs in the hub to the pulse oximeter. The S/H circuit stores the voltage for a specified period of time before processing. The S/H signals are separated to the different

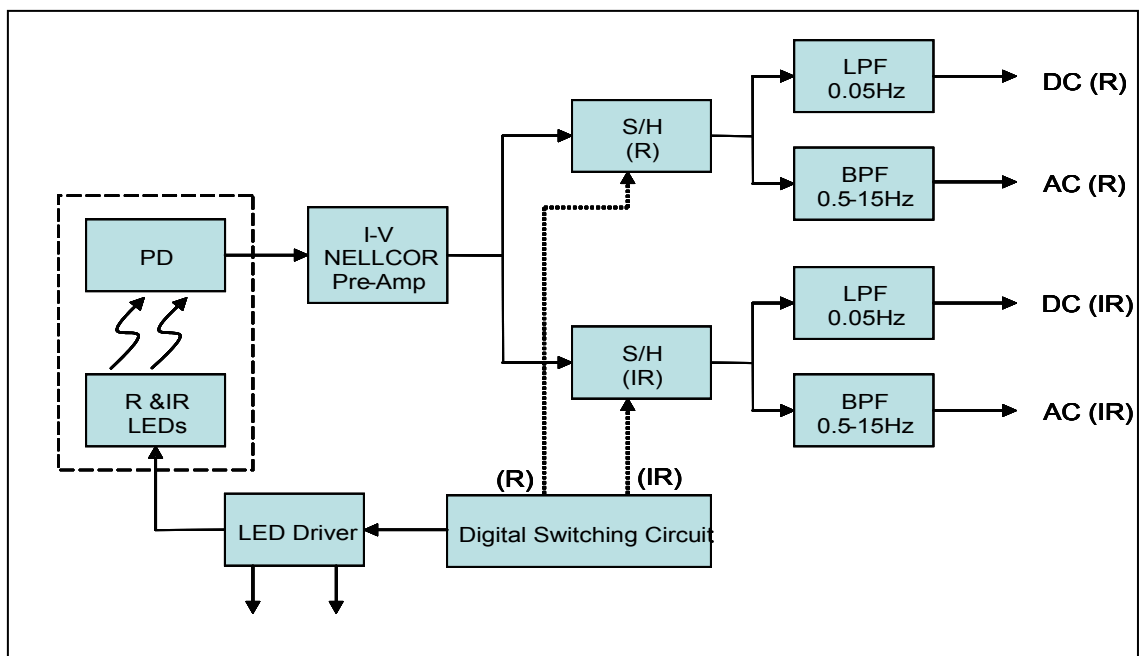


Figure 5.7. Block diagram of the PSPU for obtaining the PPG signals from the prototype sensors.

PPG signal components using analog filters. Low pass filtering (LPF) with a cutoff frequency of 0.05Hz provides the DC component of the PPG signal. The AC component of the PPG signal is acquired by band pass filtering (BPF) the PPG signal between ranges of 0.5 and 15 Hz.

5.2.2 Reference Pulse Oximeter (RPO): A noninvasive, commercially available, table-top pulse oximeter (Nellcor, Inc. Model N-100) connected to a Nellcor reflectance sensor (RS-10) were used to acquire reference measurements from the forehead during *in-vivo* experiments [49]. A fiber-optic cable connected the N-100 oximeter to the Nellcor Model N-8000 interface that converts the HR and SpO₂ measured by the RPO to analog voltage outputs [50]. The N-8000 interface was connected to a National Instrument (NI) BNC-2120 interface. The specifications for both units can be found in Appendix B-1 and B-2. The NI BNC-2120 connector block simplifies the connection of analog signals while maintaining the integrity of the measurements with a shielded enclosure. The data transferred to the PC were captured by a PCI-6024E data acquisition card.

5.2.3 Experimental Pulse Oximeter (EPO): A commercially available, portable, OEM evaluation kit (NONIN Inc, Xpod) with 3 wire interface and low power draw (60mW) was used as an experimental pulse oximeter (EPO). The EPO permitted a full range of sensor applications to obtain SpO₂ and HR values regardless of sensor configuration. It offered two different serial data formats for simple integration into the existing system, as shown in Appendix B-3. Using serial data format #2, digital data were serially transmitted at a baud rate of 9600 to a PC using a standard RS-232 serial interface at the rate of 5 bytes, 75 times per second. An external current divider circuit with a series of resistors was connected in parallel across the LEDs, as shown in Figure 5.8. This current

divider circuit provided a convenient way to vary the peak current supplied to the LEDs, from 6% (1.44mA) to 100% (24mA) of the nominal currents typically supplied by the EPO.

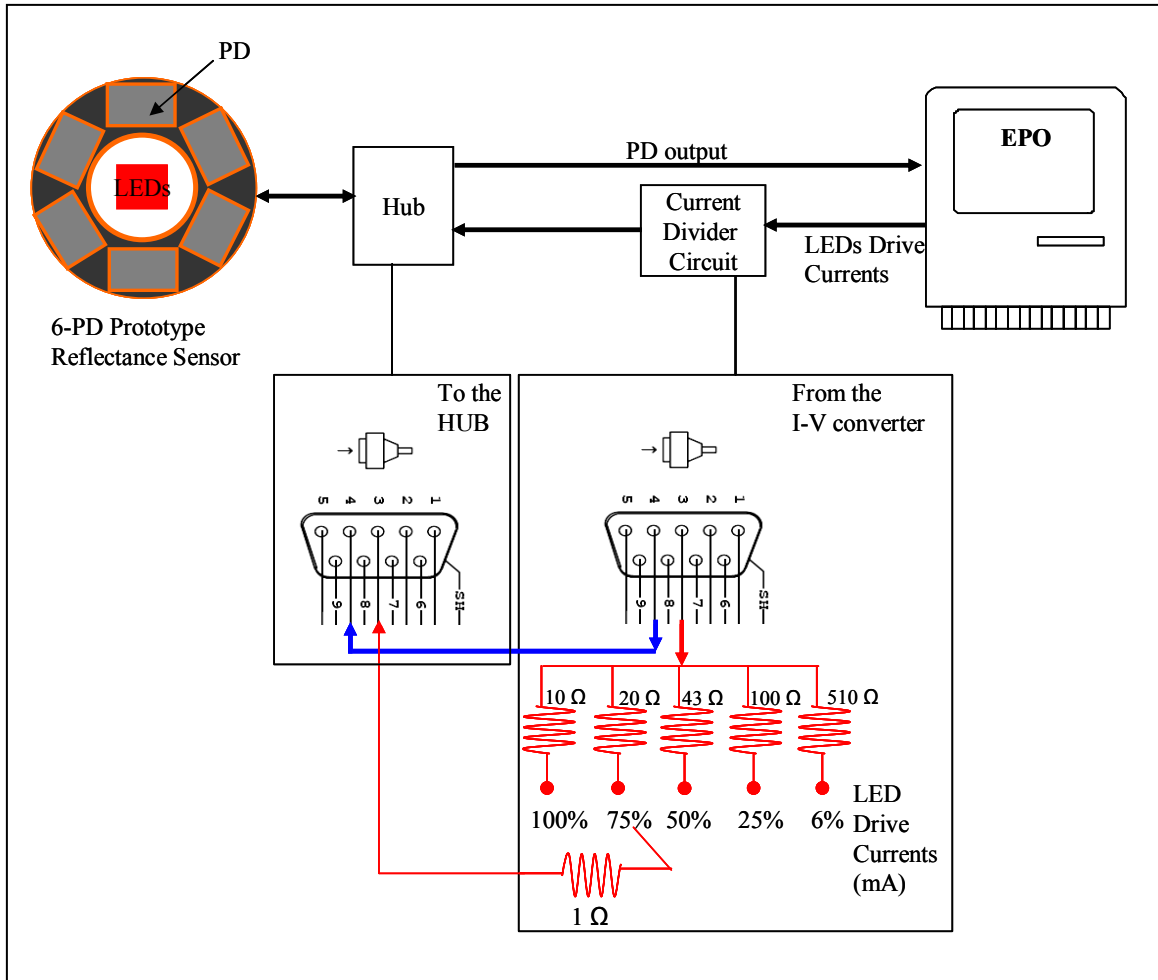


Figure 5.8. Experimental setup to control the LED drive current supplied by the EPO to the LEDs.

6. METHODOLOGY

6.1 Sensor Mode Studies

A series of *in vivo* experiments were performed to quantify and compare the magnitudes of the PPGs measured by each pair of PDs in reflectance, transflection and transmission modes. As illustrated schematically in Fig. 6.1(a) and (b), the prototype sensor was wrapped around the proximal phalanx of a volunteer's finger with the LEDs resting on the palm side of the index finger. After the sensor was securely attached to the finger, the minimum currents flowing through the LEDs were adjusted while the output of the amplifier was monitored to assure that distinguishable and stable PPGs were observed from each PD pair and the electronics were not saturated. The measurements were acquired in two sets with different conditions, as follows.

(a) *Constant PPG amplitude with varying LED currents:* In the first set of experiments, the LED drive currents were adjusted until the amplitude of each PPG signal reached approximately a constant magnitude of $2 V_{p-p}$. Before the data were digitized, it was important to test if constant PPG signal amplitude can be obtained by the different sensor modes using the PSPU. The raw PPG signals were monitored by a storage oscilloscope to determine that a constant $2 V_{p-p}$ signal magnitude was achieved for each sensor configuration. The experimental results were used to estimate the minimum current required to drive the LEDs in each sensor configuration. Also, these measurements helped in estimating the amount of power required for each sensor mode for a constant PPG signal, which is essential for accurate calculation of SpO_2 .

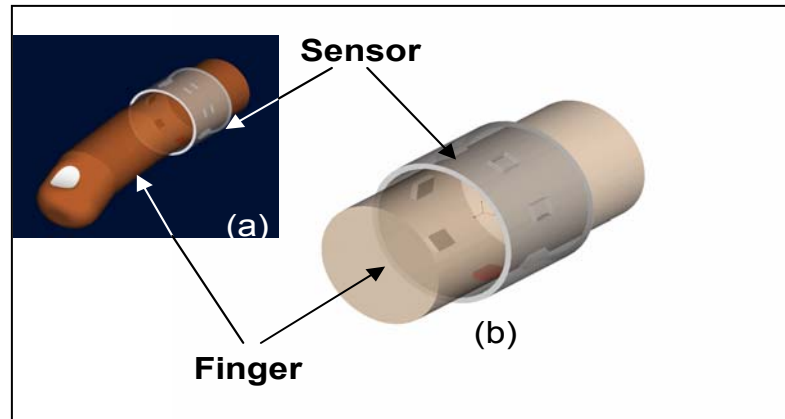


Figure 6.1(a). Sensor assembly mounted on a finger and **(b)** a closer section of the finger phalanx with the prototype ring sensor.

(b) Constant Current with varying PPG amplitude: Another series of measurements were performed where LED drive currents were maintained at a constant level (IR: 31mA and R: 85.2mA) while the average magnitude of the PPG signals from each pair of PDs were compared. These LED drive currents were used throughout the data acquisition for each sensor mode, thus enabling comparison of varying PPG signal amplitude, as each sensor mode had a varying signal quality at a specified LED drive current. These constant LED drive currents were determined by obtaining relatively strong PPG signals (R and IR) with low noise resolution, as observed on a storage oscilloscope. The transmission mode (PD-3 and PD-4) was tested with a gradual drop in current until the signal was about to deteriorate, which determined the largest quantity of current required during each sensor mode. The currents were reduced to a much lower level than normal because two PDs were attached for each sensor mode rather than the traditional single PD used in commercial pulse oximeter sensors.

6.2 Estimation of Power Consumption in Transmission and Reflection Modes

A series of experiments were performed to quantify the magnitudes of the transmission and reflection PPGs recorded from the index finger as a function of different detector areas while using a prototype 6-PD disc sensor. Initially, to estimate the background noise generated by the PDs and electronic circuitry, the R and IR LEDs were switched off, and the PDs were covered to shield them from ambient light. Then, after the sensors were attached to the finger, the minimum currents flowing through each LED (R and IR) were adjusted until distinguishable and approximately equal amplitude PPG waveforms were clearly noticeable when only one PD element was selected by the hub. Following initial current adjustments, the additional 5 PDs were connected in parallel while the PPG waveforms were observed to assure that the electronics were not saturated. After satisfactory driving conditions were established the LED driving currents remained unchanged for the duration of the experiments. The variation in the LED position relative to the location of the PDs enabled a convenient method to compare reflection and transmission modes in terms of the power consumption requirements.

(a) Reflection Mode: The prototype 6-PD disc sensor was configured by positioning the LEDs in the center of the 6 PDs, as illustrated in Figure 5.1(a). The sensor was attached to the base of the ventral side of the subject's index finger.

(b) Transmission Mode: The prototype 6-PD disc sensor was reconfigured, as depicted in Fig. 5.1(b). Accordingly, the LEDs were secured to the ventral side of the index finger and the PDs were positioned symmetrically across the LEDs on the dorsal side of the finger.

6.3 Testing Multiple PD Performance Using a Prototype 6-PD Reflectance Sensor

A series of *in-vitro* experiments were performed to quantify the effect of multiple PDs which simulate a large PD area. The factors considered during these experiment were dark current (I_d), effect of ambient light and increment in noise level.

6.3.1 Dark Tests: To test the background noise level generated by each PD, a series of dark measurements were performed by switching off the LEDs in the sensor and blocking ambient light from reaching the PDs. Each PD was attached to the central hub to estimate the noise increment due to dark current.

6.3.2 Multiple PD Tests: Each PD was randomly connected through the hub to determine the spatial uniformity of the illuminating field incident on the PDs. To produce a constant level background illumination, a signal composed of a DC bias voltage modulated by a small 1Hz AC sine wave was generated by a programmable function generator. The signal from the function generator was applied to a separate LED that was used to simulate a typical PPG signal. The external LED was mounted behind a translucent flat medium that served as an optical diffuser. The surface of the diffuser was positioned at a distance of 30cm away from the planar surface of the PDs.

6.3.3 In-Vivo Experiments: A series of *in vivo* experiments were performed to determine the signal improvement gained by using different PD areas. The prototype 6-PD disc sensor was attached to the base of a finger and the peak currents supplied to the R and IR LEDs were adjusted to 3mA and 1.9mA, respectively. As the driving currents were adjusted, the output of each amplifier was monitored to assure that (i) a distinguishable and stable PPG was observed when a single PD was employed, and (ii) maximal PPG signals were produced without causing amplifier saturation when all 6 PDs were

connected in parallel through the hub. It is important to note that the final currents selected were significantly lower compared to the typical peak driving currents employed in commercial pulse oximeters which normally range from 80mA-130mA.

6.4 Effects of PD Size and Measurement Site on Power Consumption

6.4.1 In Vivo Experiments: A series of *in vivo* experiments were performed to quantify and compare the PPG magnitudes measured by the two sets of six identical PDs. The prototype 12-PD reflectance disc sensor was mounted on the dorsal side of the wrist or the center of the forehead below the hairline. These representative regions were selected as two target locations for the development of a wearable telesensor because they provide a flat surface for mounting a reflectance sensor which for example could be incorporated into a wrist watch device or attached to a soldier's helmet without using a double-sided adhesive tape. After the sensor was securely attached, the minimum peak currents flowing through each LED were adjusted while the output of the amplifier was monitored continuously to assure that distinguishable and stable PPGs were observed from each set of PDs and the electronics were not saturated. Two sets of measurements were acquired from each body location as follows:

(a) Constant current with varying PPG amplitude: In the first set of experiments, the currents supplied to the LEDs were kept at a constant level and the magnitude of the PPGs measured from each set of six PDs were compared.

(b) Constant PPG amplitude with varying LED currents: A series of measurements were performed where the driving currents were adjusted until the amplitude of the respective PPG reached a constant amplitude. This provided an estimate of the minimum peak currents (I_p) required to drive the LEDs for the near and far-positioned PDs,

6.5. Multiple PD Prototype Sensor Evaluation

The 6-PD prototype disc reflectance sensor and the control RS-10 sensor were attached to the volunteer's forehead using a standard headband, as shown in Figure 6.2 and 6.3. To test SpO₂ and HR measurement accuracy at different LED driving currents, it was necessary to implement a stop breathing technique to vary SpO₂. In order to calculate the systemic error between the two different pulse oximeters, it was essential to collect SpO₂ values during normal breathing using the control sensor. As the breathing stopped for a brief period, the SpO₂ dropped accordingly. Thus, a range of SpO₂ was recorded and compared. The detailed block diagram of the experimental setup is shown in Figure 6.4.

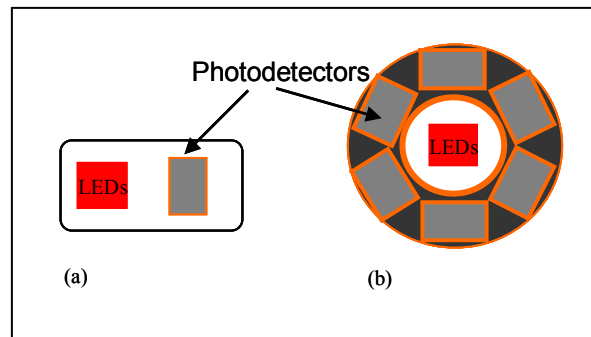


Figure 6.2. Different sensor setups used for various experiments (a) single control sensor and (b) multiple PD prototype sensor [42].

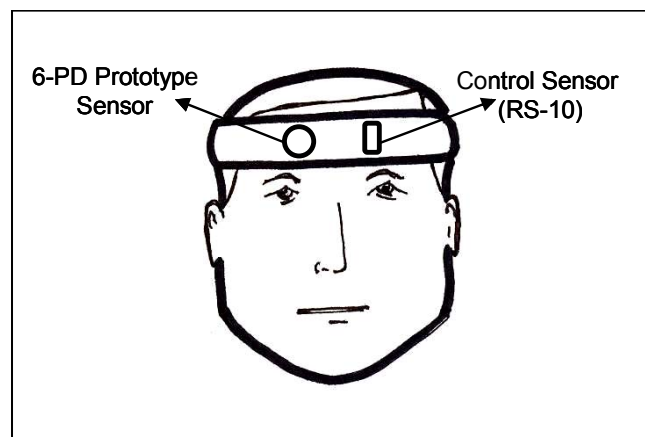


Figure 6.3. Sensors attachment to the forehead [42].

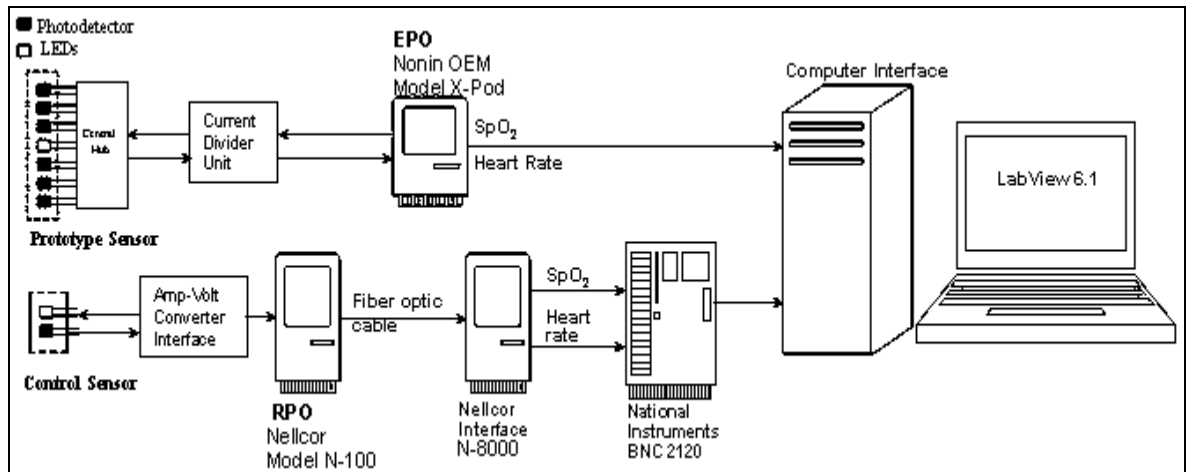


Figure 6.4. Block diagram of the experimental setup

Breathing Protocol: Initially, data were collected during normal ambient air breathing. Then, following a short period of hyperventilation for about 10 seconds, the subject held his breath for about 40 seconds and resumed normal breathing.

Case 1: To have a consistent SpO₂ data from the two pulse oximeters, it was necessary to test both devices with the control sensor attached, as shown in Figure 6.5. Hence, two RS-10 control sensors were connected to the RPO and EPO. During normal breathing, SpO₂ was measured from the two pulse oximeters. The difference between the readings of the pulse oximeters provided a systemic error (bias), which is the mean of the difference between the two readings using the same control sensors.

Case 2: The RS-10 control sensors were attached to the volunteer's forehead and the other end was connected to the RPO and EPO as shown in Figure 6.5. *Case 2* differed from *Case 1* because in *Case 2* the volunteer was asked to perform a stop-breathing maneuver. The systemic error was calculated using the difference in SpO₂ readings obtained from the two pulse oximeters connected to the same RS-10 control sensors.

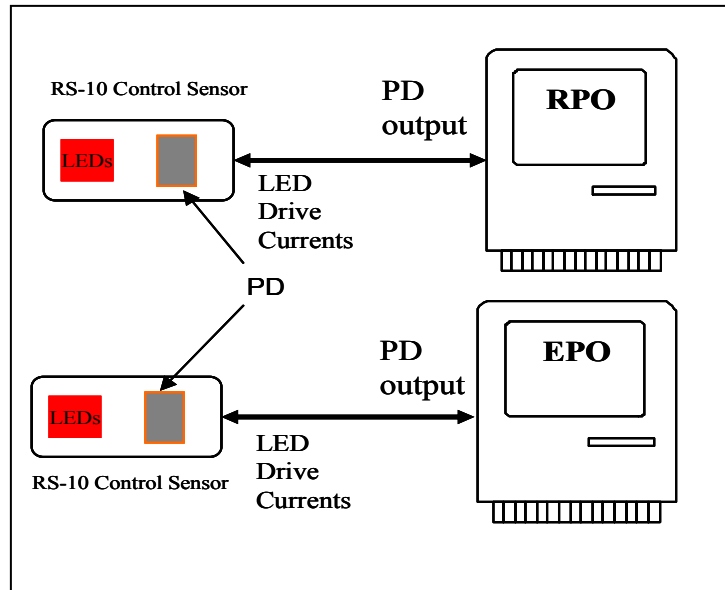


Figure 6.5. Block diagram of the sensor connection in Case 1 and 2.

Case 3: The RS-10 control sensor connected to the EPO oximeter in Case 2 was replaced by the 6-PD prototype reflectance sensor as shown in Figure 6.6. The 6-PD prototype reflectance sensor was attached to the forehead to collect data from the EPO while the control sensor (RS10) was connected to the RPO. After the sensors were attached and the

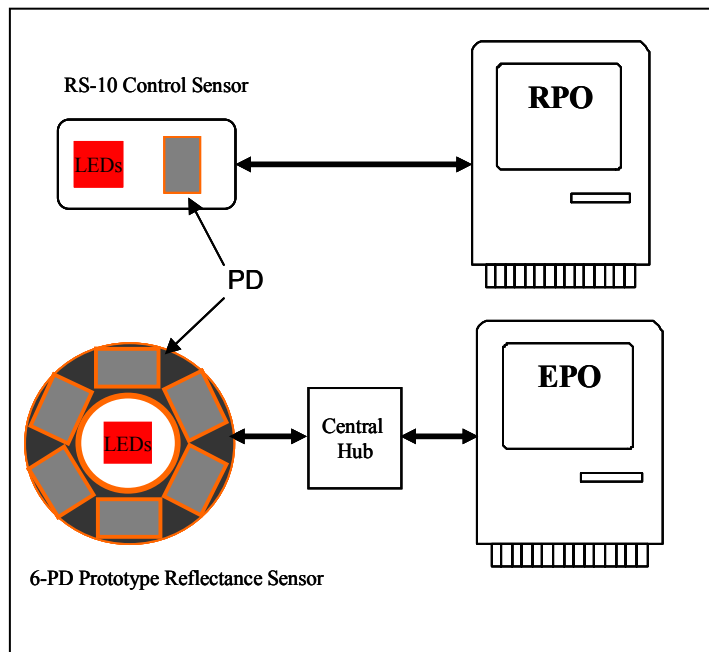


Figure 6.6. Block diagram of sensor connections in Case 3.

readings were stable, the drive current across each LED was monitored using a digital voltmeter. The LEDs currents were maintained at 100% of the nominal value set by the manufacturer. One set of data was collected for stop breathing. The systemic error was calculated using the difference in the SpO₂ readings obtained from the two pulse oximeters with different sensors.

Case 4: The 6-PD prototype reflectance sensor was connected to the EPO and attached to the volunteer's forehead. To simulate a large PD area, the number of PDs in the 6-PD prototype reflectance sensor was gradually increased. A current divider circuit was employed in order to control the LED drive current supplied from the EPO, as shown in Figure 6.7. With every addition of a PD to the central hub, data points were acquired for 100% (24mA) and 6% (1.44mA) peak current. Data analyzed from this experiment provided information correlated to the systemic error due to large modification in the LED drive current. It also provided information related to errors associated with an increase in the PD area.

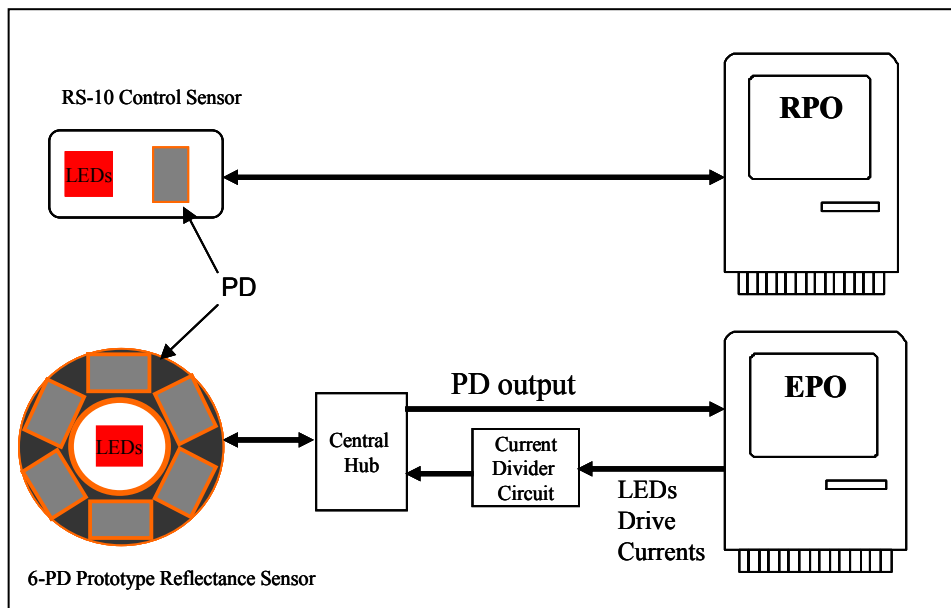


Figure 6.7. Block diagram of the sensor connection with the current divider circuit used in Case 4.

7. RESULTS

7.1 Sensor Mode Studies

Relatively constant AC amplitudes of 0.550V RMS PPGs were measured from each pair of PDs configured in reflection, transflection and transmission modes by varying the LED's peak drive currents. The LED peak drive currents for each sensor mode are noted in Figure 7.1. Typical PPG signals measured from the left index finger using different sensor modes are shown in Figures 7.2(a-c) and 7.3(a-c) for the R and IR LEDs, respectively. As noted, transmission mode required about 6 times more drive current in comparison to reflection mode to obtain a relatively constant PPG magnitude of 0.550V RMS. Similarly, transflection mode required approximately 3 times more current to obtain similar PPG amplitudes. From this data, it is evident that reflection mode required the least amount of driving current compared to transflection or transmission modes in order to generate similar PPG amplitudes.

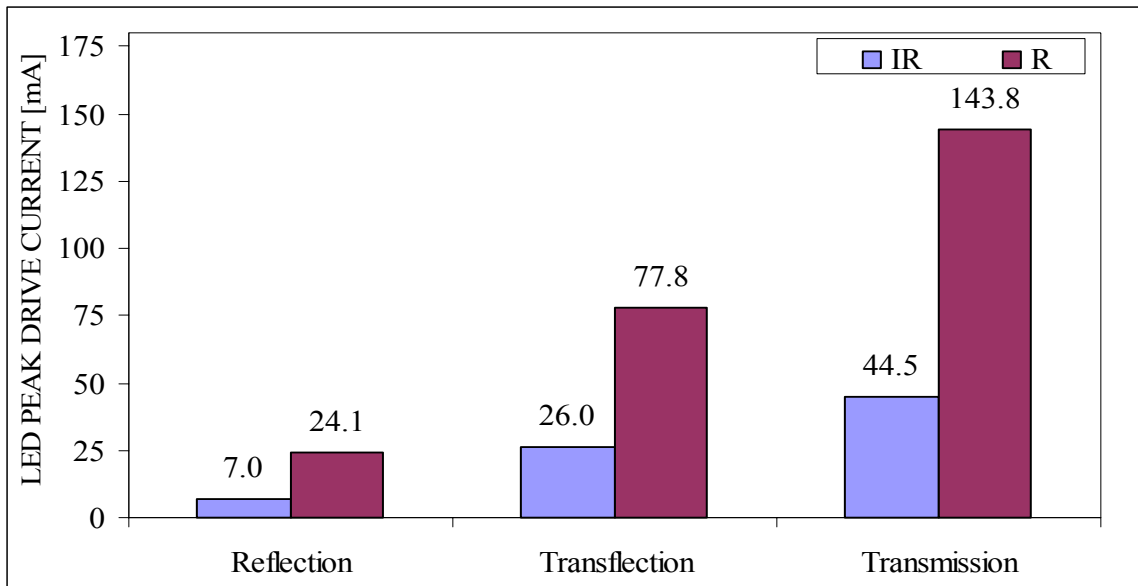


Figure 7.1. Relative LED peak drive currents required to maintain a constant PPG AC amplitude of about 0.55V RMS in reflection, transflection and transmission modes.

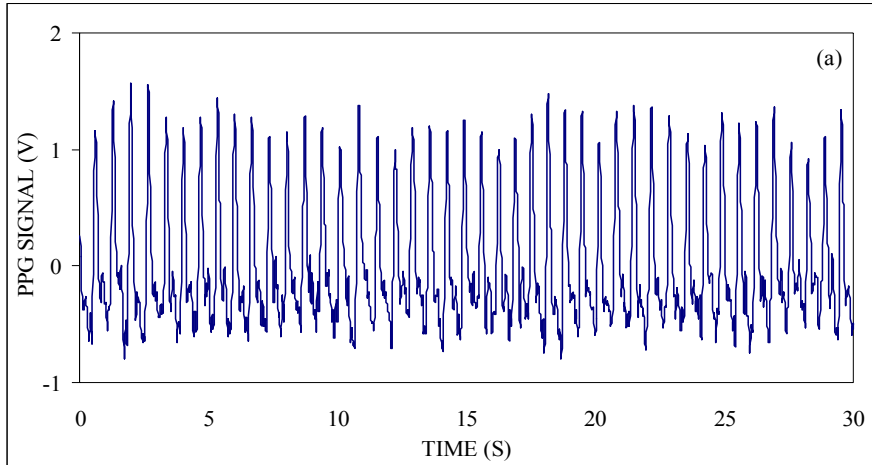


Figure 7.2(a). Typical PPG AC magnitudes measured in reflection mode with 7mA IR LED peak drive current.

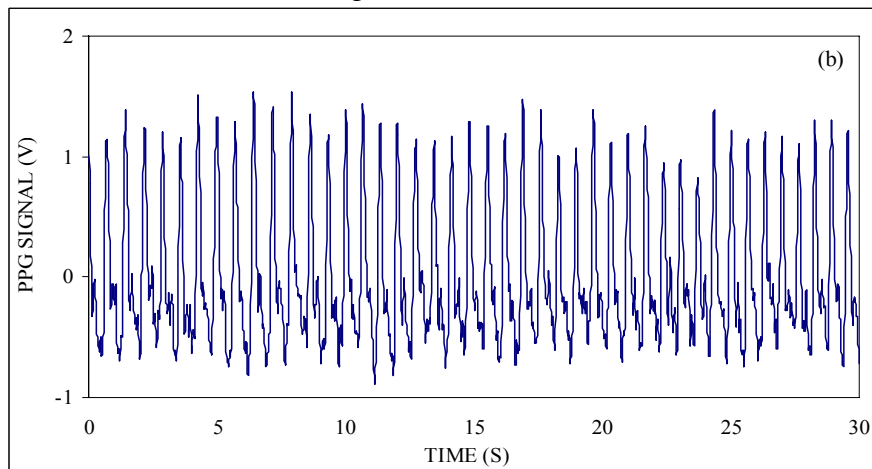


Figure 7.2(b). Typical PPG AC magnitudes measured in reflection mode with 26mA IR LED peak drive current.

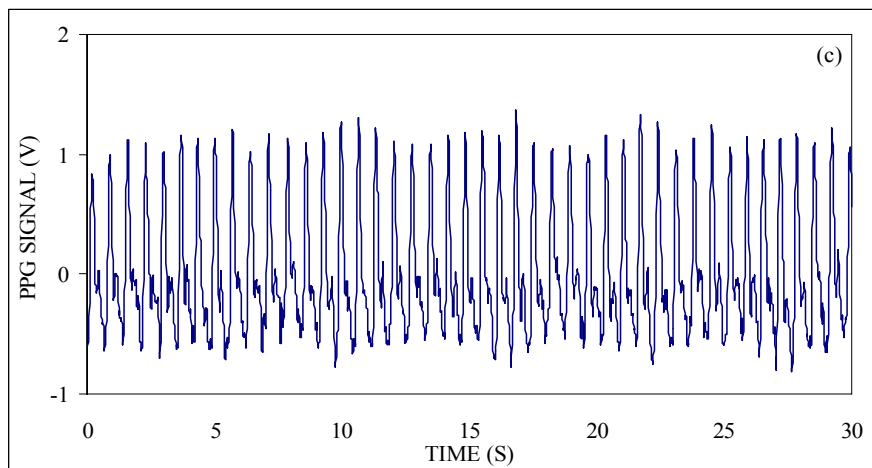


Figure 7.2(c). Typical PPG AC magnitudes measured in transmission mode with 44.5mA IR LED peak drive current.

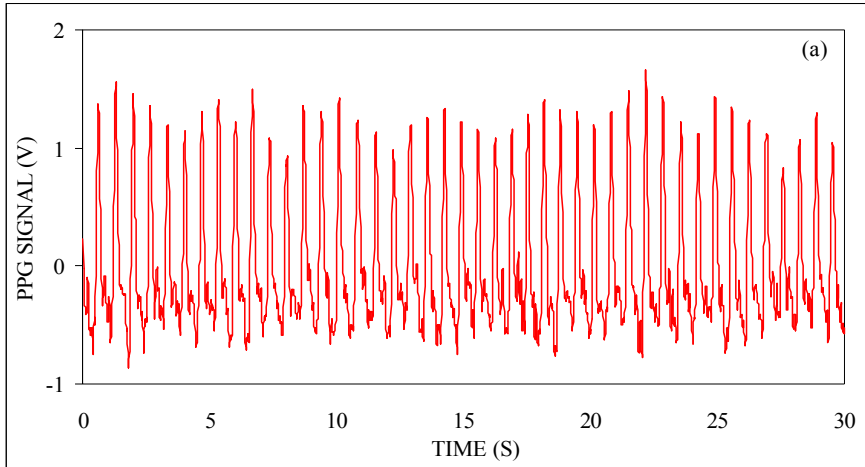


Figure 7.3(a). Typical PPG AC magnitudes measured in reflection mode with 24.1 mA IR LED peak drive current.

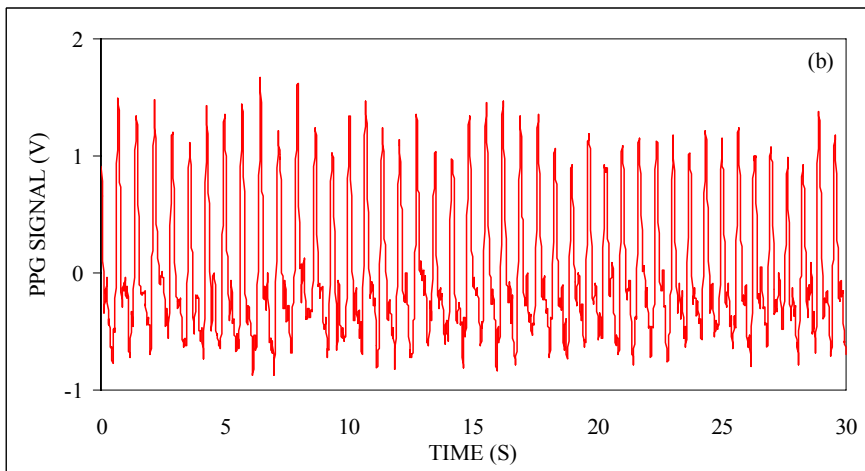


Figure 7.3(b). Typical PPG AC magnitudes measured in transfection mode with 77.8 mA IR LED peak drive current.

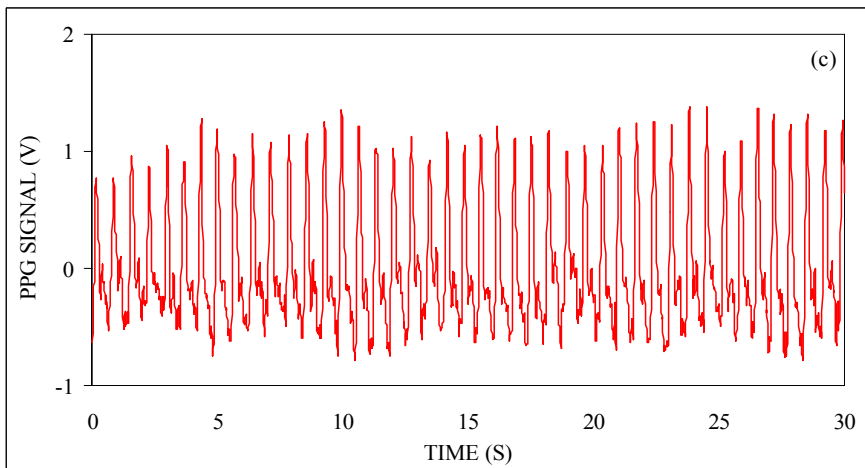


Figure 7.3(c). Typical PPG AC magnitudes measured in transmission mode with 143.8 mA IR LED peak drive current.

The relative amplitudes of the PPG signals measured from the left index finger by each pair of PDs configured in transmission, transflection and reflection modes are plotted in Figure 7.4(a) and (b). For comparison, the RMS values of the corresponding AC components for the three configuration modes that were tested in this study are also plotted in Figure 7.5. It was observed that the amplitude of the AC components depend on the relative locations of the PDs inside the ring. While keeping a constant LED drive current and the same active area for each PD pair to facilitate easy comparisons, it was found that the magnitude of the PPGs was the highest in reflection mode and their values decreased considerably when measurements were obtained in transflection or transmission modes. Also, data analysis clearly revealed that there was considerable SNR improvement in reflection mode compared to either transmission or transflection modes for constant LED peak drive currents.

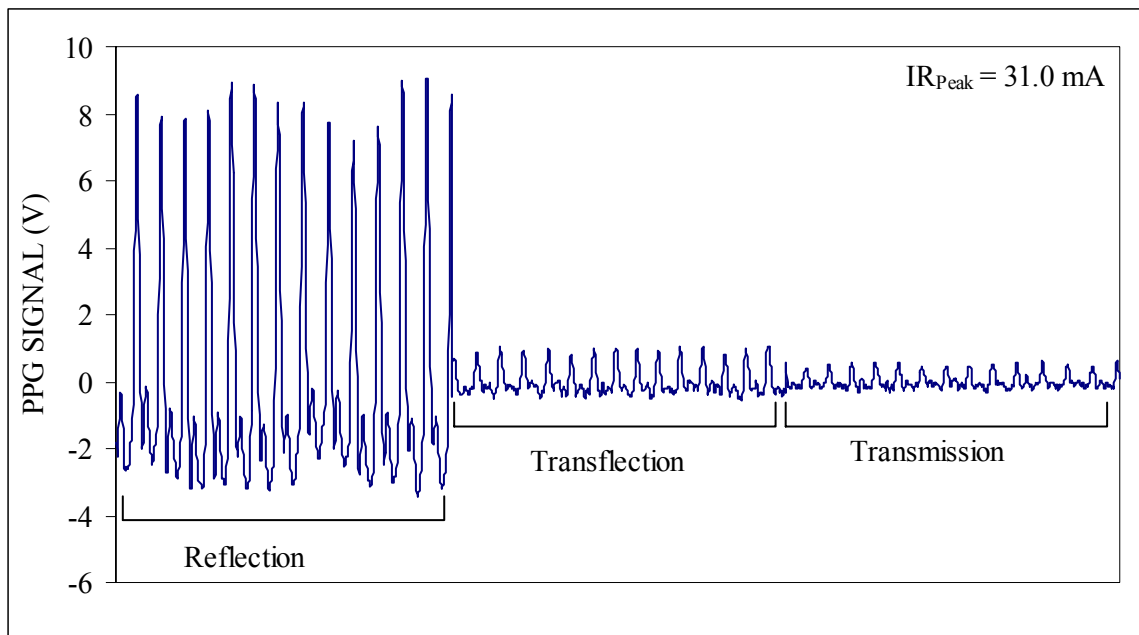


Figure 7.4(a). Typical PPG AC magnitudes measured from the left index finger in different sensor modes with a constant IR LED peak drive current of 31mA.

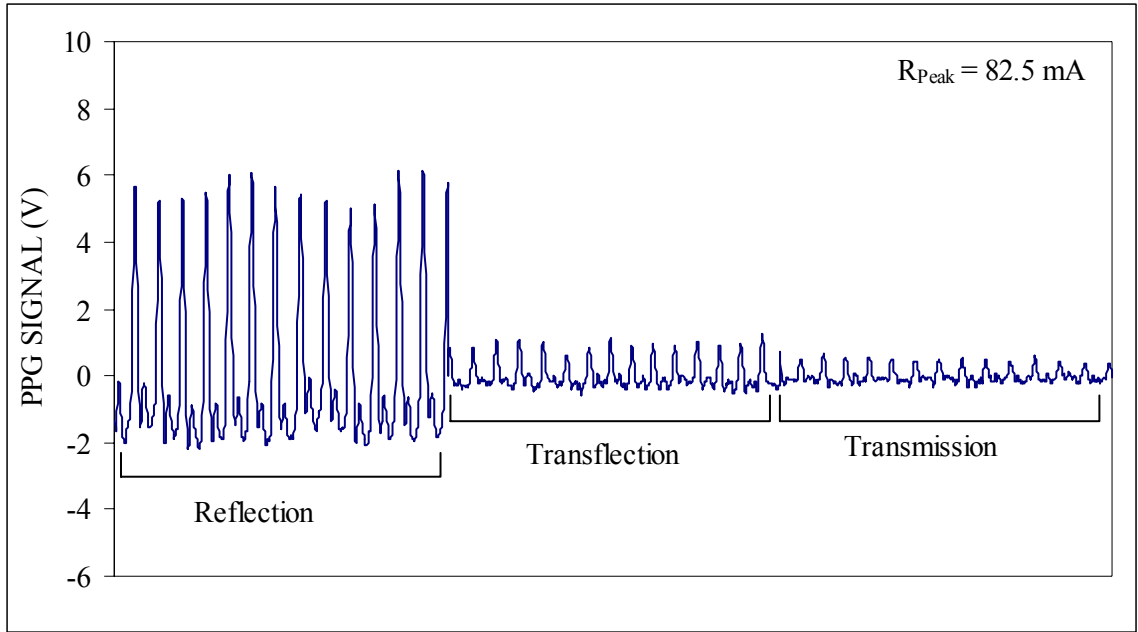


Figure 7.4(b). Typical PPG AC magnitudes measured in different sensor modes with a constant R LED peak drive current of 82.5mA.

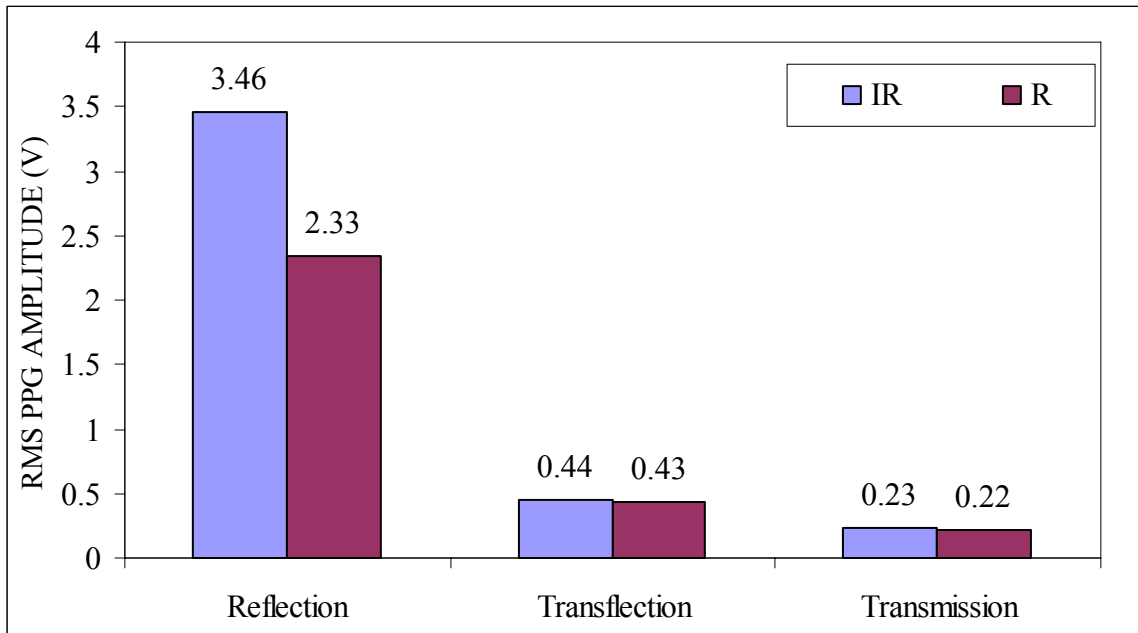


Figure 7.5. RMS values calculated from typical PPG amplitudes measured in reflection, transflection and transmission modes at constant IR and R LEDs peak drive currents of 31.0mA and 82.5mA, respectively.

A single factor ANOVA was performed to show that there was no significant variation in the constant RMS values calculated from the AC PPG signals with varying

LED drive currents for different sensor modes. The null hypothesis (H_0) was maintained consistent for all data analysis and was defined based on equal means ($\mu_1=\mu_2=\mu_3...=\mu_n$). The H_0 was accepted when the $F_0 < F_{crit}$, otherwise it was rejected. If H_0 is accepted, then the means have no significant variance. If H_0 is rejected, the means vary significantly and thus, show significant error. The statistical analyses are summarized in tables 7.1(a) and (b) for IR and R LEDs, respectively. The RMS values for constant PPG signals from different sensor modes with varying IR LED peak drive currents are summarized in table 7.1 (a) where the H_0 was accepted as $F_0 < F_{crit}$ (5.143249, $\alpha = 0.05$). Similarly, in table 7.1 (b), H_0 was accepted as $F_0 < F_{crit}$ (5.143249, $\alpha = 0.05$) which shows that the AC PPG magnitudes are consistent for different sensor modes and the only varying factor is the LED drive current.

Table 7.1(a). RMS values calculated using constant PPG signals with varying IR drive currents from different sensor modes for 3 replicate tests.

Groups	Count	Sum	Average	Variance
Reflection	3	1.5413	0.5138	0.0015
Transflection	3	1.9017	0.6339	0.0076
Transmission	3	1.4425	0.4808	0.0099

ANOVA

Source of Variation	Sum of Squares	Degree of freedom	Mean Squares	Test statistic F_0	P-value	Reference Distribution F_{crit}
Between Groups (SSA)	0.0389	2	0.0195	3.0715	0.1206	5.1432
Within Groups (SSE)	0.0380	6	0.0063			
Total (SST)	0.0770	8				

Table 7.1(b). RMS values calculated using constant PPG signals with varying R drive currents from different sensor modes for 3 replicate tests.

Groups	Count	Sum	Average	Variance
Reflection	3	1.5589	0.5196	0.0106
Transflection	3	1.9154	0.6385	0.0041
Transmission	3	1.3212	0.4404	0.0103

ANOVA

Source of Variation	Sum of Squares	Degree of freedom	Mean Squares	Test statistic F_0	P-value	Reference Distribution F_{crit}
Between Groups (SSA)	0.0596	2	0.0298	3.5773	0.0949	5.1432
Within Groups (SSE)	0.0500	6	0.0083			
Total (SST)	0.1096	8				

Also, a single factor ANOVA was executed to test the variation in the R/IR values calculated from PPG signals with varying as well as constant LED drive currents. The

R/IR values calculated from the replicated experiments are summarized in tables 7.2 (a) and (b). The P-value, or attained significance, is the smallest level of significance for α . So if an experimenter's choice of α is greater than or equal to the calculated P-value, then the H_0 is rejected. This is another technique to statistically monitor variation in the measured PPG signals. Throughout the statistical analysis, P-values show variation greater than the significance level (α) of 0.05. Thus, the results generate a confidence level of 95%. The R/IR values for constant PPG signals from different sensor configurations with varying LED drive currents were summarized in table 7.2 (a) where the H_0 was accepted as $F_o < F_{crit} (5.143249, \alpha = 0.05)$. Similarly, in table 7.2 (b), H_0 was accepted as $F_o < F_{crit} (5.143249, \alpha = 0.05)$. This suggests that with varying PPG signals for different sensor modes with constant LED drive currents, constant R/IR values can be obtained for SpO₂

Table 7.2(a). Summary of 'ratio of ratio' (R/IR) calculated using constant PPG signals with varying currents from different sensor modes for 3 replicate tests.

Groups	Count	Sum	Average	Variance
Reflection	3	1.8913	0.6304	0.0009
Transflection	3	1.8563	0.6188	0.0000
Transmission	3	1.9200	0.6400	0.0000

ANOVA

Source of Variation	Sum of Squares	Degree of freedom	Mean Squares	Test statistic F_o	P-value	Reference Distribution F_{crit}
Between Groups (SSA)	0.0007	2	0.0003	1.0570	0.4043	5.1432
Within Groups (SSE)	0.0019	6	0.0003			
Total (SST)	0.0026	8				

Table 7.2(b). Summary of 'ratio of ratio' (R/IR) calculated using PPG signals with constant LED drive currents from different sensor modes for 3 replicate tests.

Groups	Count	Sum	Average	Variance
Reflection	3	2.0731	0.6910	0.0002
Transflection	3	2.1517	0.7172	0.0004
Transmission	3	2.2043	0.7348	0.0044

ANOVA

Source of Variation	Sum of Squares	Degree of freedom	Mean Squares	Test statistic F_o	P-value	Reference Distribution F_{crit}
Between Groups (SSA)	0.0029	2	0.0015	0.8726	0.4649	5.1432
Within Groups (SSE)	0.0100	6	0.0017			
Total (SST)	0.0129	8				

calculation. Thus, assuming the physiological conditions remain unchanged, R/IR remains consistent even with variation in sensor modes regardless of LED drive currents. In other words, SpO₂ calculations will not be affected regardless of sensor configuration.

7.2 Estimation of Power Consumption in Transmission and Reflection Modes

First, a series of dark measurements were acquired to ascertain the noise increment observed by using multiple PDs. The noise level detected, which was assessed from the dark current measurement by varying the number of PDs connected in parallel, is shown in Figure 7.6. From this data, it is evident that the background noise depends on the number of active PDs connected in parallel. Analysis of the data in figure 7.6 also revealed that the total RMS noise generated by a single PD increased by about 50% when all 6 PDs were used. The AC amplitudes of the PPG signals measured by the sensor in transmission and reflection modes with varying numbers of PDs are plotted respectively in Figures 7.7 (a-d).

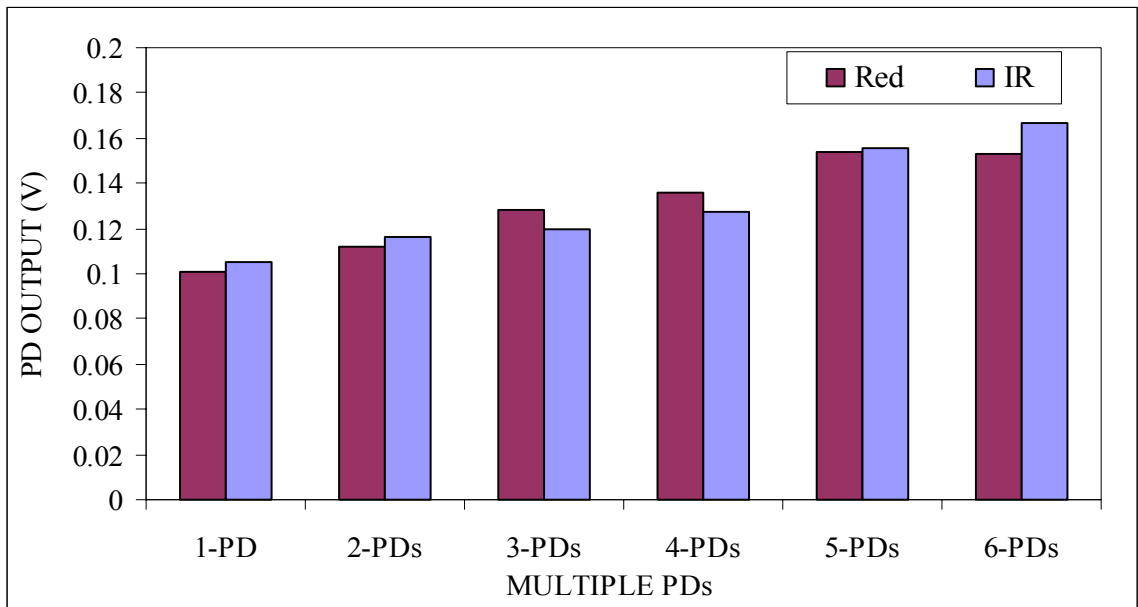


Figure 7.6. Increment in RMS noise with varying number of PDs connected in parallel.

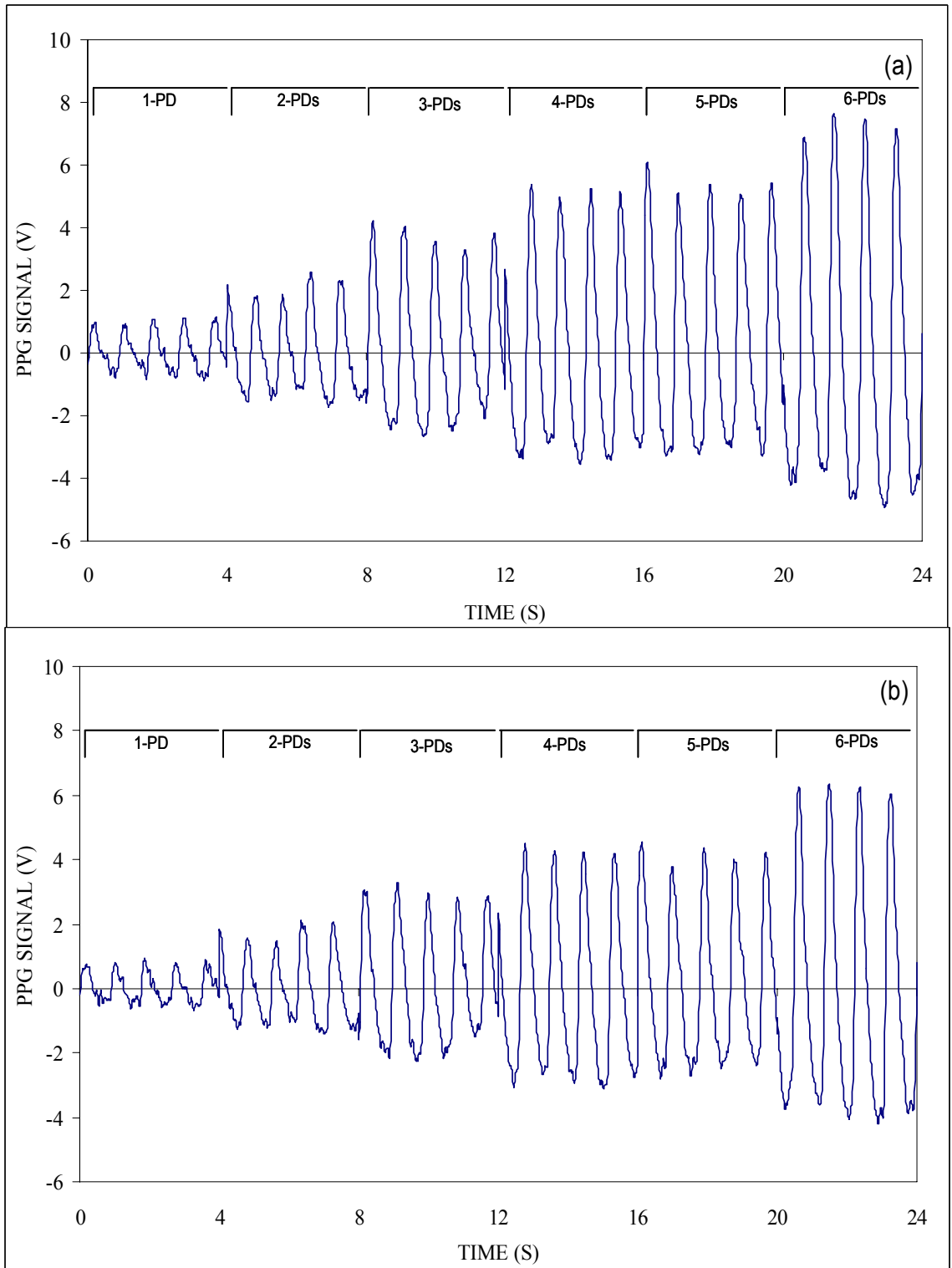


Figure 7.7. PPG signals obtained in transmission mode from varying number of PDs (a): IR peak current drive = 19.6 mA (b): R peak current drive = 46.0 mA.

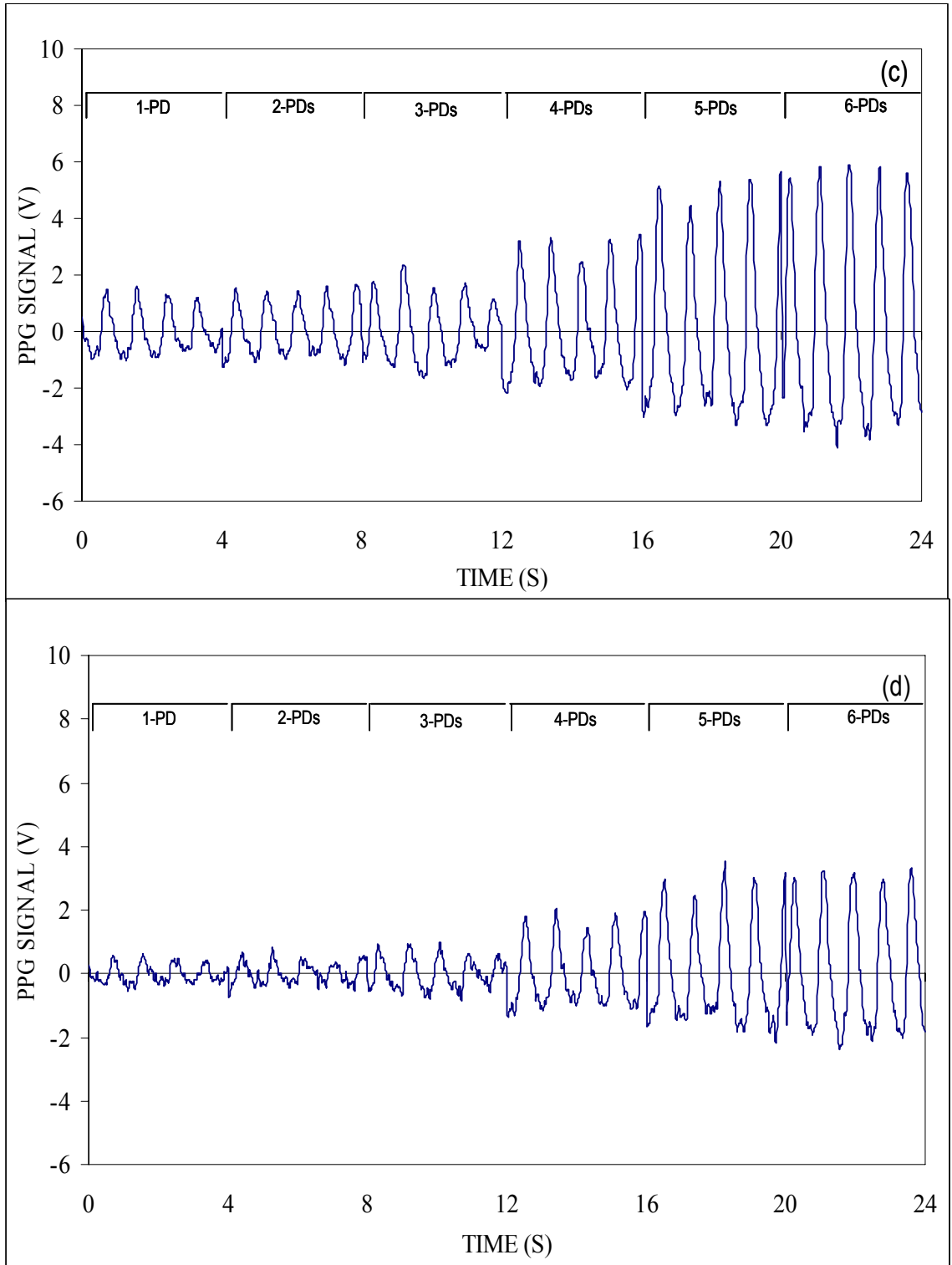


Figure 7.7. PPG signals obtained in reflection mode from varying number of PDs (c): IR peak drive current = 1.9 mA (d): R peak drive current = 3.0 mA.

As shown in Figures 7.7(a-d), by increasing the number of PDs (simulating progressively larger PD areas) the AC PPG signals tend to improve in both transmission and reflection mode. Analysis of the data clearly indicates that there is a considerable SNR improvement in both transmission and reflection modes as the total active area of the detector is increased, as shown in Figures 7.8 (a) and (b).

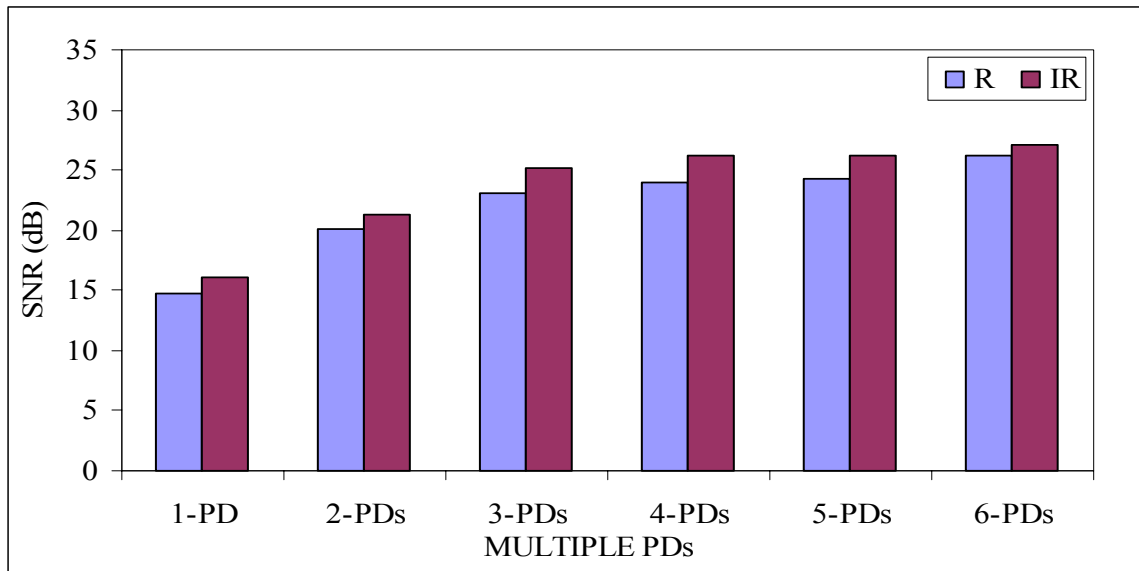


Figure 7.8(a). SNR improvement observed with increasing PD area in transmission mode.

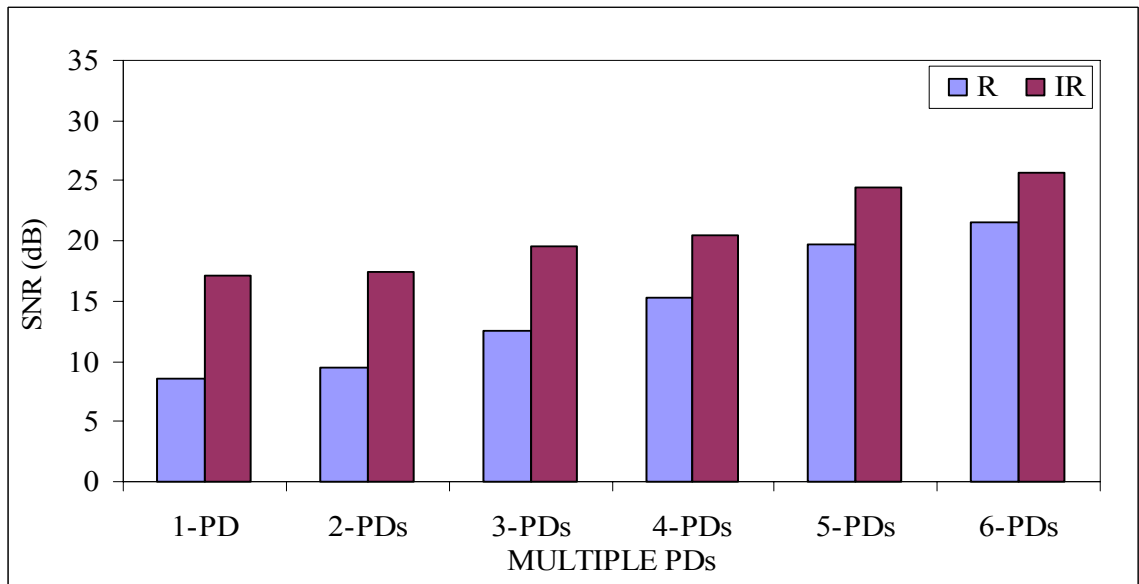


Figure 7.8(b). SNR improvement observed with increasing PD area in reflection mode.

In order to calculate the SNR, the RMS PPG signals (S) were acquired from the left index finger of a volunteer. The RMS noise was calculated from the dark current which was used as the noise factor (N). The SNR analysis demonstrates that by increasing the active area of the PD used in either transmission or reflection type sensors it is possible to lower the minimum currents required to drive the LEDs without compromising the quality of the detected PPG signals. The LED peak drive currents necessary to produce acceptable PPGs signals utilizing larger PDs are summarized in Table 7.3. Power consumption was estimated using the PSPU's LED duty cycle of 12.5% ($T_{ON}=0.128\text{ms}$, $T_{ON+OFF}=1.024\text{ms}$) for a typical 220mAh lithium type coin-size battery assuming that a similar battery would be used to power the optical components of a wearable pulse oximeter. With the estimated power consumption it can be conveniently determined which sensor mode consumes the lowest amount of power while the LEDs are pulsed at a frequency ($f=1/T_{ON}$) of 7.8 kHz.

Table 7.3. Comparison of LED peak drive currents and power consumption for different sensor modes.

Sensor Mode	$I_{R_{Peak}}$ (mA)	R_{Peak} (mA)	Duty Cycle (DC) (%)	Average I_{Avg} $(I_{R_{Peak}} + R_{Peak}) * (DC/100)$	Estimated power consumption (days) (Battery capacity: 220mAh)
Reflection	1.9	3.0	12.5	0.6	15
Transmission	19.6	46	12.5	8.2	1

7.3 Testing Multiple PD Performance Using a Prototype 6-PD Reflectance Sensor

The RMS values corresponding to the amplitude of the AC components measured from each PD are plotted in Figure 7.9. During darkness, the average noise generated by an individual PD was estimated to be about 0.114V. In comparison, as discussed in section 6.3.2, the average PPG AC amplitude measured *in vitro* by the 6 individually

connected PDs under a spatially uniform illumination field produced by the external LED source was equal to 0.647V. Figure 7.10 shows the signals detected *in vitro* with multiple PDs using a simulated uniform illumination. The right-side bars represent the measured RMS values corresponding to different PD areas. For comparison, the left-side bars were computed using the ideal relationship $0.647n$, where n corresponds to the number of PDs connected in parallel.

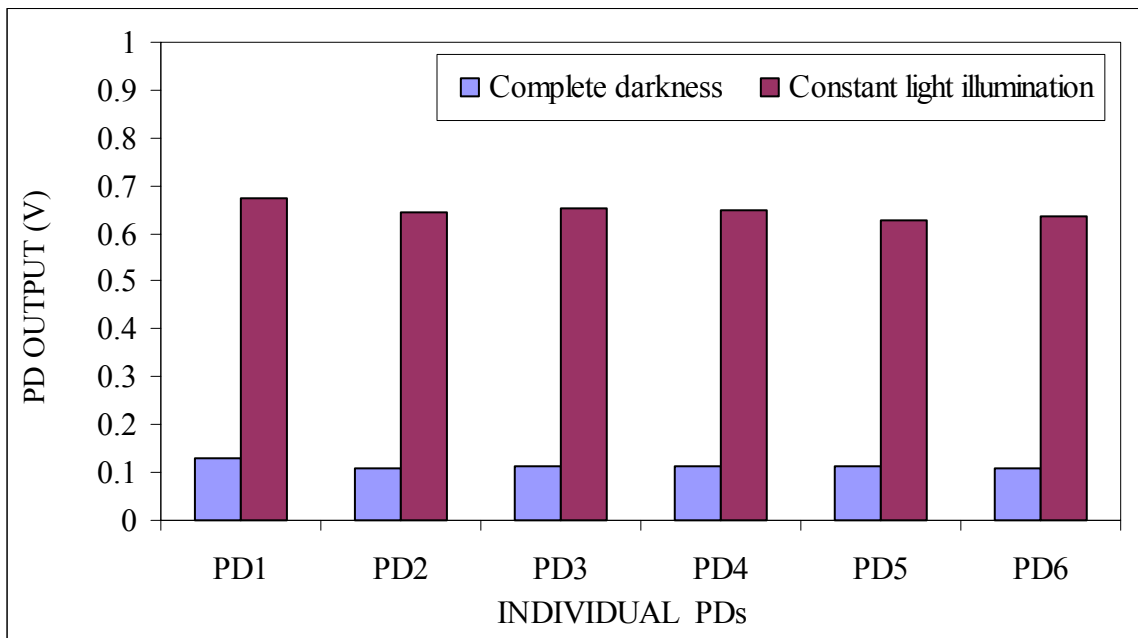


Figure 7.9. Individual PD performance under complete darkness and a constant light illumination.

The trend observed in Figure 7.10 provides sufficient evidence of a linear improvement in signal intensity as a function of a proportional increase in the active area of the PDs. The magnitude of the pulsatile R and IR PPGs measured *in-vivo* from a finger for different combinations of PD is shown in Figure 7.11. From the data presented, it can be observed that the overall increase in the reflected PPG signals achieved *in vivo* when all 6 PDs were connected in parallel is smaller and does not follow the same linear relationship observed *in vitro* as shown in Figure 7.10. We postulated that this deviation

was probably caused by the non-uniform backscattered light distribution emanating from the finger.

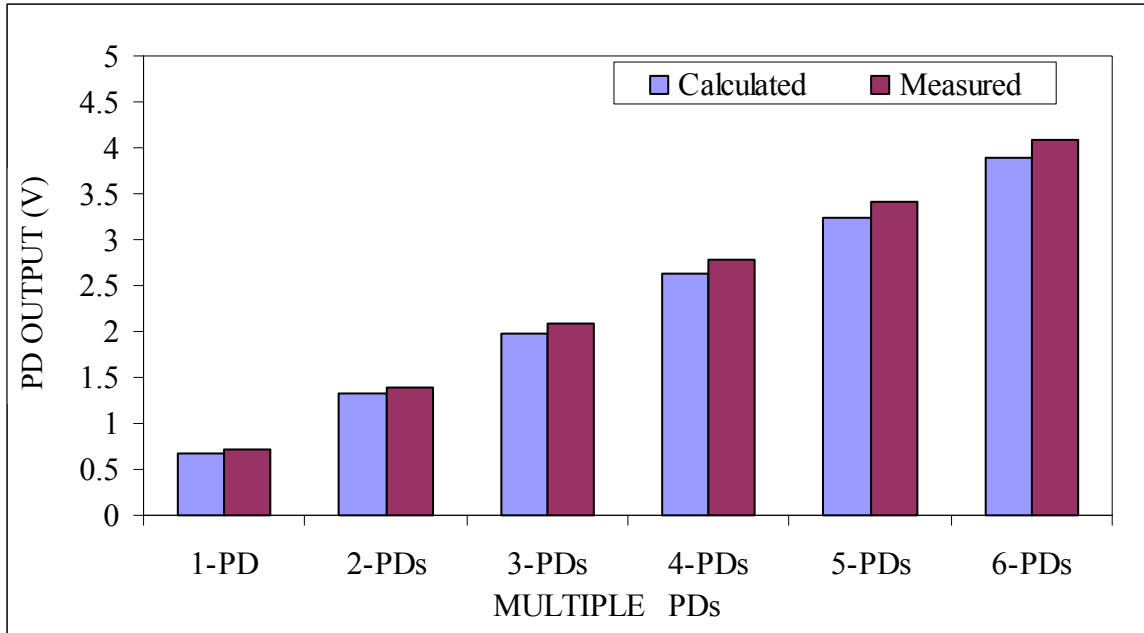


Figure 7.10. Signal improvement observed in-vitro with multiple photodetectors.

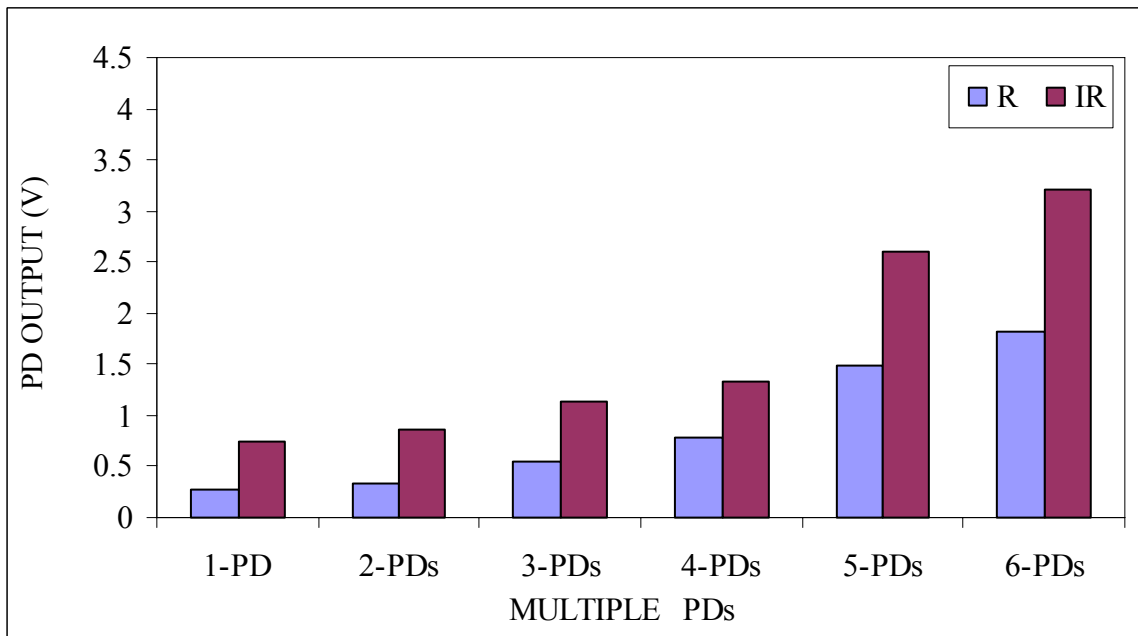


Figure 7.11. Signal improvement observed in vivo with multiple photodetectors.

7.4 Effects of PD Size and Measurement Site on Power Consumption

Typical examples of reflected PPG signals measured from the forehead and wrist by the inner set of 6 PDs in the 12-PD reflectance prototype sensor for constant peak LED drive currents (R: 8.5mA, IR: 4.2mA) are plotted respectively in Figure 7.12. For comparison, the relative RMS amplitudes of the PPG signals measured by the 6 near (N) and far (F) PDs, and the combination of all 12 PDs (N+F) are plotted in Figures 7.13(a) and (b) for a peak R & IR LED drive current of 8.5mA and 4.2mA, respectively.

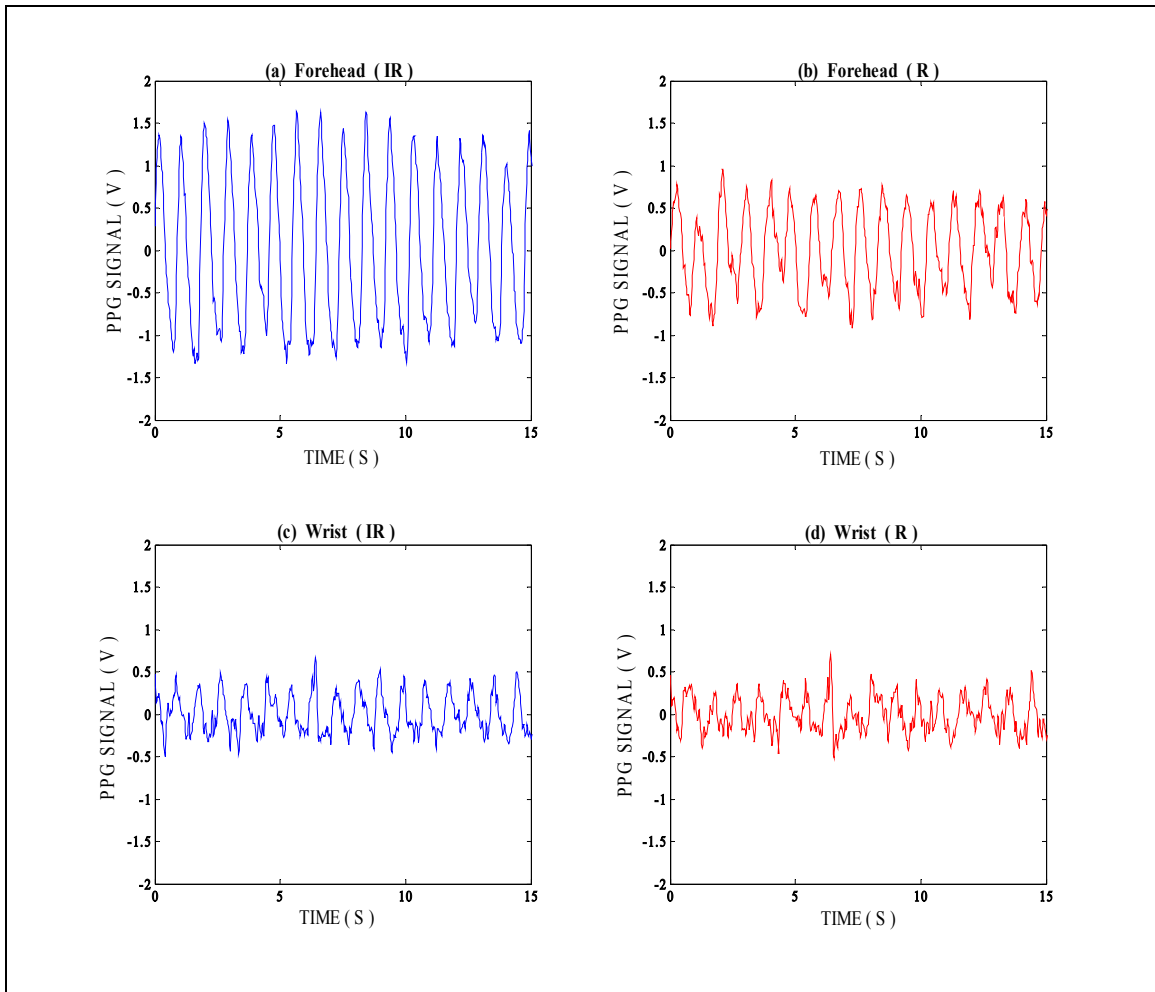


Figure 7.12. PPG signals measured from the forehead (a and b) and wrist (c and d) for constant LED driving currents.

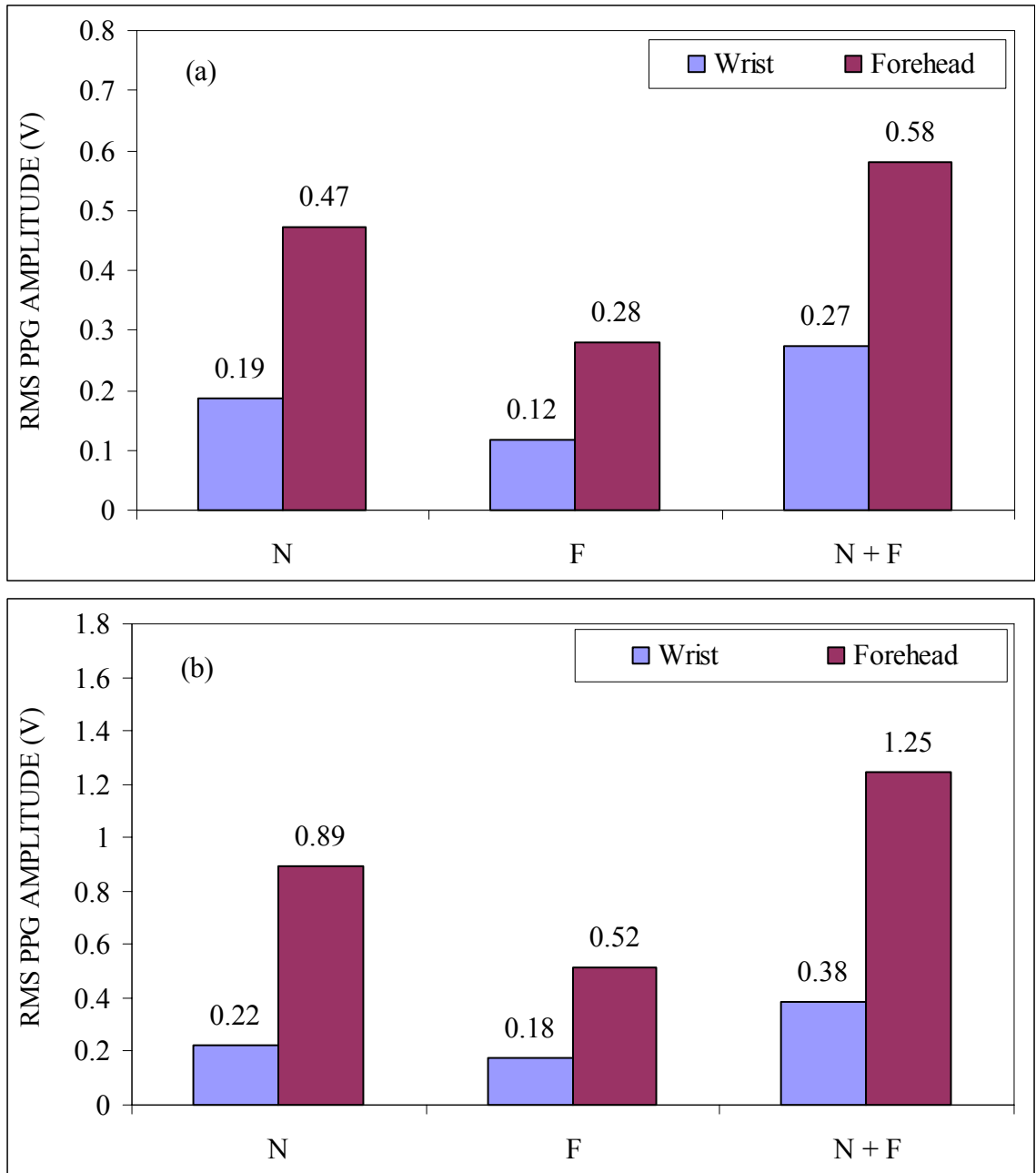


Figure 7.13. RMS values calculated from the PPG signals measured by the near (N), far (F) and combination (N+F) PDs from the wrist and forehead for constant R and IR LED drive currents corresponding to 8.5mA (a) and 4.2mA (b), respectively.

Analysis of the data revealed that there is a considerable difference between the signals measured by each set of PDs and the relative amplitude of the respective PPG signals depends on measurement site. Figure 7.14 compares the relative peak LED

currents required to maintain a constant AC RMS amplitude of approximately 0.840 (± 0.017) V measured from the forehead by the N, F and (N+F) PDs.

The LED peak driving currents plotted in Figure 7.14 were used to estimate the expected battery life of a typical 220mAh Lithium coin size battery. Table 7.4 summarizes the estimated battery life for the different PD configurations tested in this study. The calculations are based on LEDs pulsed continuously at a typical duty cycle of approximately 1.5% where $T_{ON}=0.2\text{ms}$ and $T_{ON+OFF}=13.2\text{ms}$. The timing values (T_{ON} and T_{ON+OFF}) were calculated from the EPO unit representing a low power consuming commercial pulse oximeter.

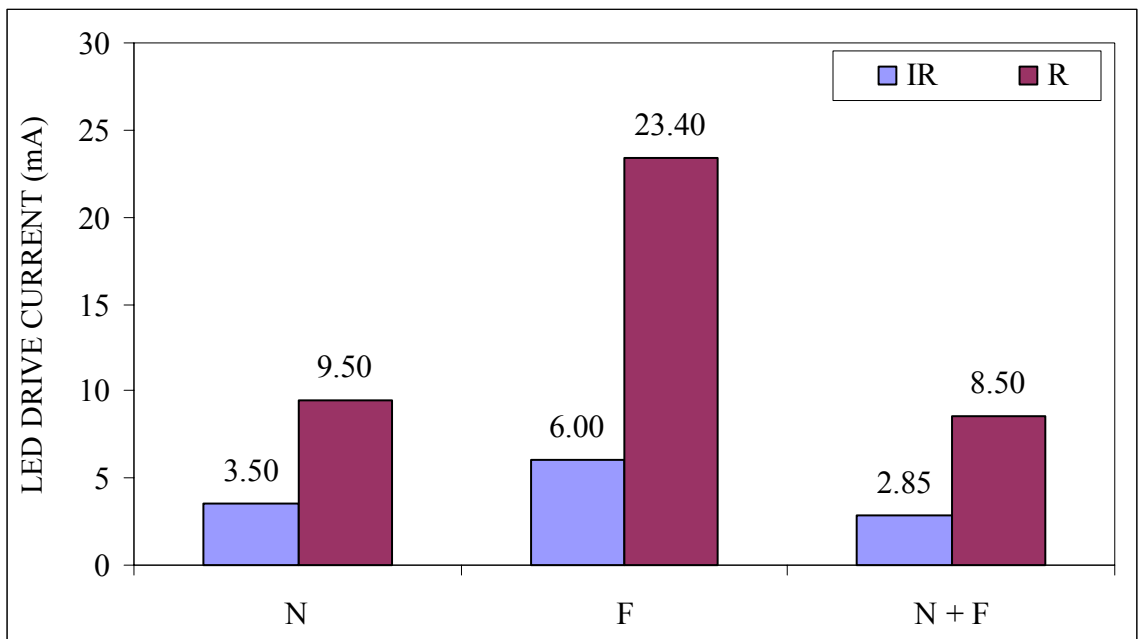


Figure 7.14. Relative LED peak driving currents required to maintain a constant PPG amplitude of 0.840V RMS for the near (N), far (F) and combination (N+F) PD configurations. Measurements were obtained from the forehead.

Table 7.4. Comparison of estimated battery life for different PD configurations. Values based on forehead measurements for a typical 220mAh coin size battery.

PD Configuration	$I_{R_{Peak}}$ (mA)	R_{Peak} (mA)	Duty Cycle (DC) (%)	Average I_{Avg} $(I_{IR}+I_R)*(DC/100)$ (mA)	Battery Life (Days)
Near	3.50	9.50	1.5	0.195	47
Far	6.00	23.40	1.5	0.441	21
Near+Far	2.85	8.50	1.5	0.170	54

7.5 Multiple PD Evaluations

Figures 7.15(a) and (b) show the readings obtained from the RPO and EPO as described in section 6.5 where similar control sensors (RS-10) were attached to the forehead of a volunteer (Case 1). Figures 7.16 (a) and (b) show the results obtained for case 2 and 3, respectively. A correlation coefficient (r) equal to 0.98 was calculated by comparing SpO_2 values obtained from the RPO and EPO in case 2 where both pulse oximeters were connected with similar control sensors (RS-10). Similarly, in case 3, the data obtained from the EPO while using the prototype sensor were relatively consistent ($r = 0.97$) when compared to the data obtained from the RPO with the control sensor. In case 4, representing a significant drop in LED drive currents, a considerable error in SpO_2 readings using a single PD reflectance sensor was observed. As shown in Figure 7.17 with 100% (24mA) current drive delivered to the LEDs, adequate stability was observed with a single PD setup. On the other hand, the readings from the single PD prototype sensor with only 6% (1.44mA) drive current supplied to the LEDs were unreliable and inaccurate in comparison to the readings observed from the control sensor with a 100% drive current. However, with an increase in the number (i.e. active area) of PDs, accurate SpO_2 readings can be obtained even with significantly lower LED drive currents, as

illustrated in Figure 7.17. The corresponding changes measured in the LED optical power due to the drop in drive current for different PD areas are summarized in table 7.5.

Table 7.5. Optical powers for different PD areas corresponding to a drop in peak LED drive currents.

Percentile (%)	LED Drive Current (mA)	Peak Optical Power/Area ($\mu\text{W}/\text{cm}^2$)		Average Optical Power/Area ($\mu\text{W}/\text{cm}^2$) for 1.5% duty cycle		Optical Power (μW) (Normalized to PD area)
		IR	R	IR	R	
100	24.41	1.48	1.48	0.0222	0.0222	0.016
75	18.42	1.216	1.088	0.01824	0.01632	0.0125
50	12.05	0.72	0.632	0.0108	0.00948	0.0074
25	6.44	0.312	0.28	0.00468	0.0042	0.0032
6	1.44	0.016	0.032	0.00024	0.00048	0.0003

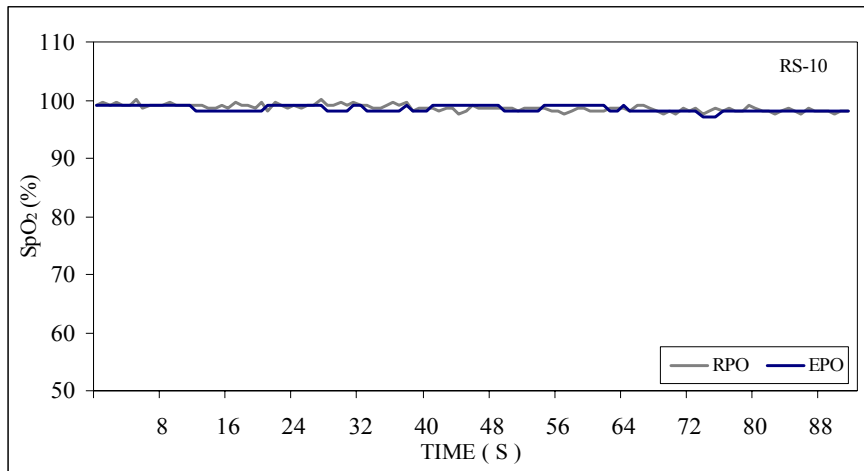


Figure 7.15(a). SpO_2 obtained from the RPO and EPO using similar control sensors.

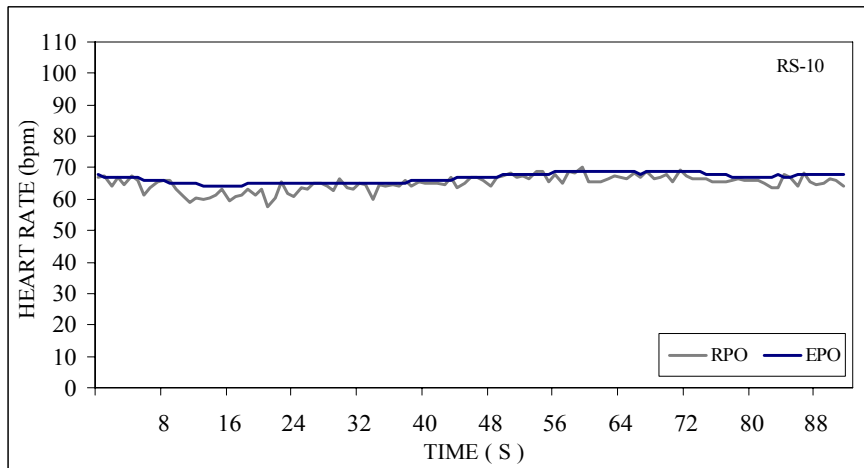


Figure 7.15(b). HR readings obtained from the RPO and EPO pulse oximeters using similar control sensors.

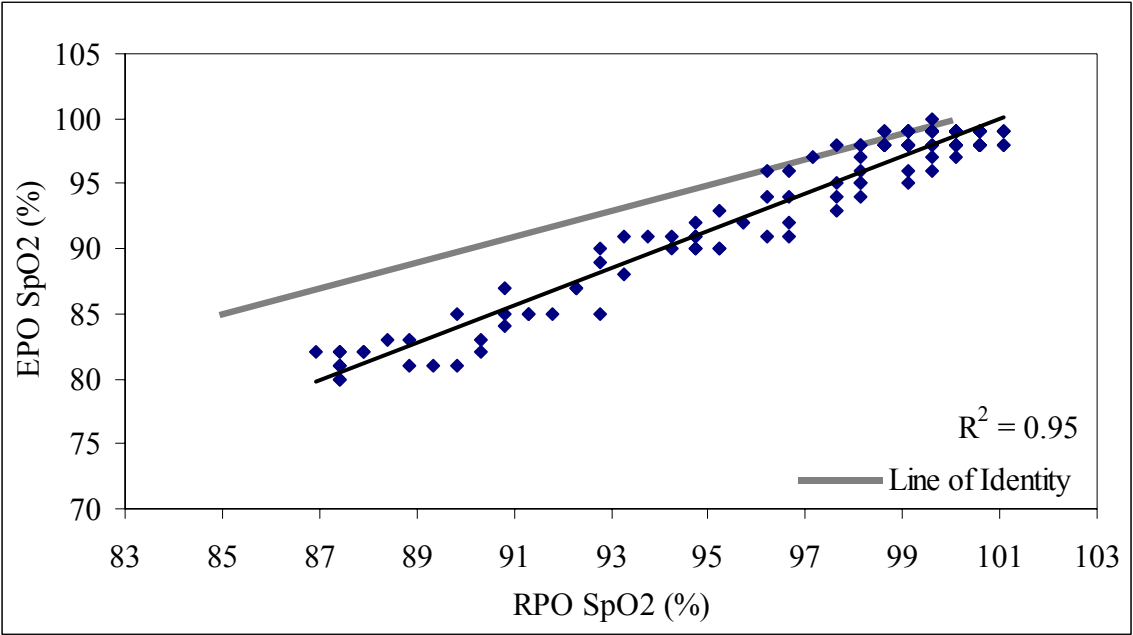


Figure 7.16(a). Comparison of SpO₂ readings for case-2 obtained from the control sensor (RS-10) connected to the EPO vs. a control sensor (RS-10) connected to the RPO.

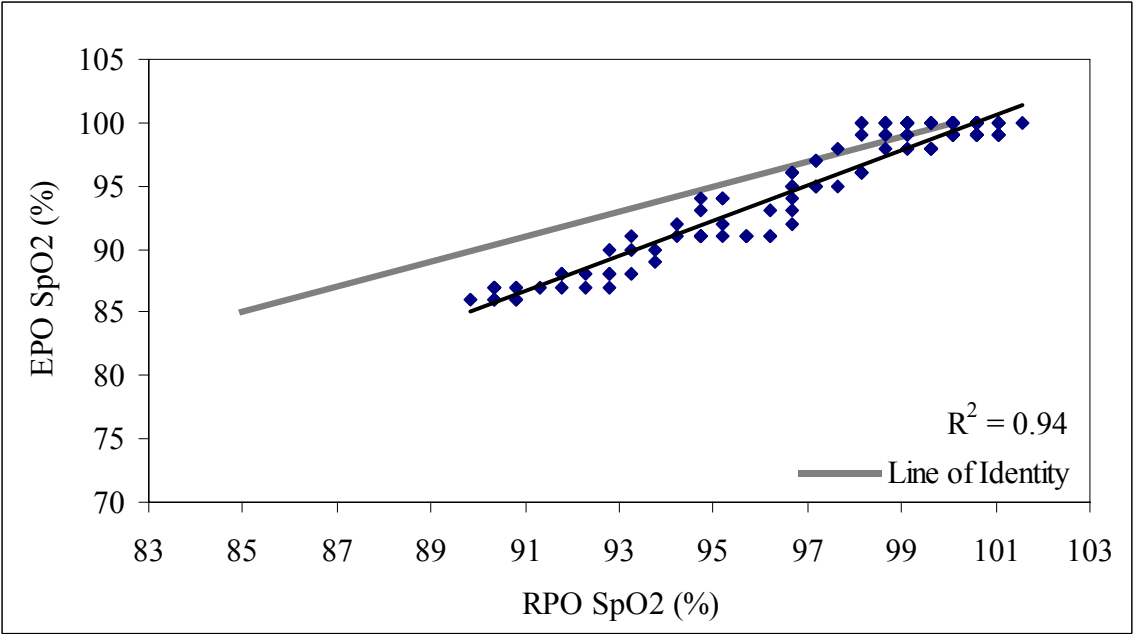


Figure 7.16(b). Comparison of SpO₂ (%) readings obtained from the prototype sensor (6-PDs) with 100% LED current drive (case-3) connected to the EPO vs. a control sensor (RS-10) connected to the RPO.

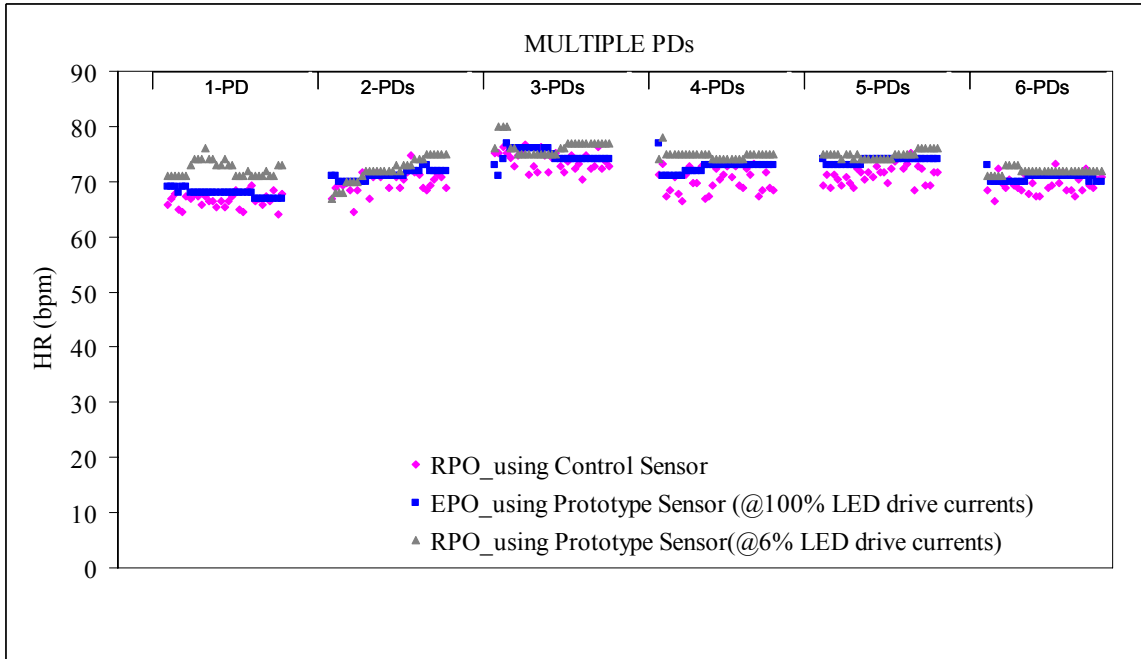


Figure 7.17(a). Comparison of HR (bpm) measured from the control sensor (RS-10) and prototype 6-PD reflectance sensor with varying number of PDs at different LED drive currents.

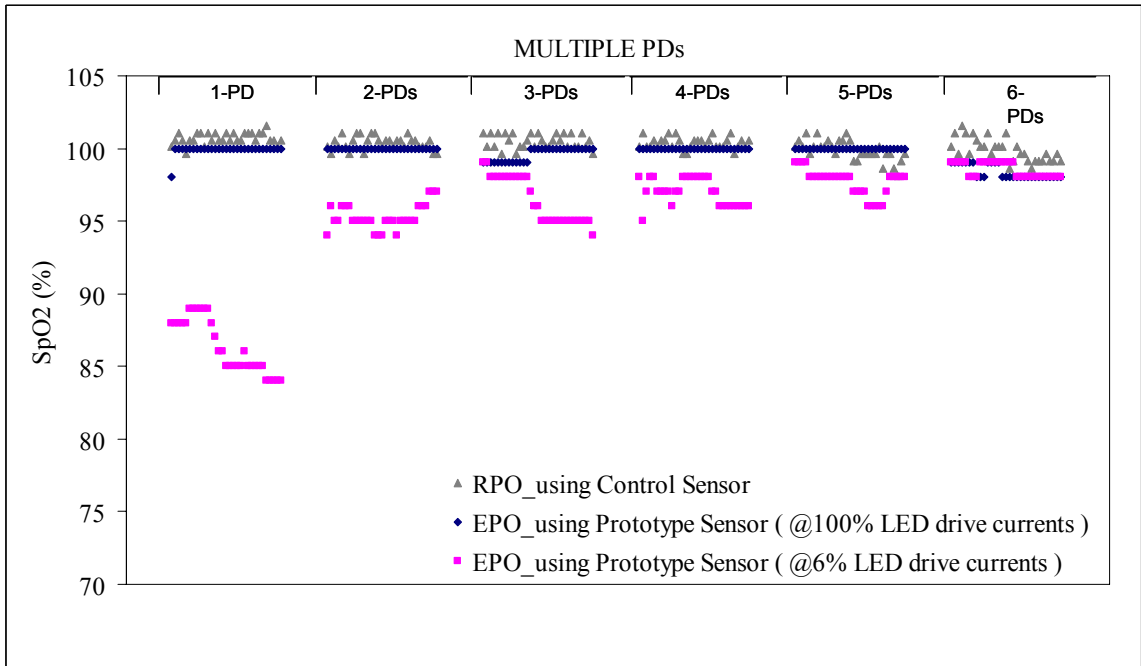


Figure 7.17(b). Comparison of SpO_2 measured from the control sensor (RS-10) and prototype 6-PD reflectance sensor with varying number of PDs at different LED drive currents.

8. DISCUSSION

8.1 Decision Matrix

Site selection and power consumption play a crucial role in optimizing the design of a wearable pulse oximeter for long-term telemedicine application. A decision matrix was used to select an appropriate location for sensor placement while considering compatibility with the end-user and the stringent need for power optimization in designing a wireless pulse oximeter.

Backscattered light intensity can vary significantly between different anatomical locations. For example, optical reflectance from the forehead region is typically strong because of the relatively thin skin covering the skull combined with a high density of blood vessels. By contrast, other anatomical locations, such as the limbs or torso, have a much lower density of blood vessels and, in addition, lack a dominant skeletal structure in close proximity to the skin that helps to reflect some of the incident light. Therefore, the relative AC components of the reflected PPGs from these body locations are considerably smaller. Consequently, it is more difficult to perform accurate pulse oximetry measurement from these body locations without enhancing cutaneous circulation using for example artificial vasodilatation. In a comparative study performed by Tur *et al*, 52 anatomical sites were subjected to PPG measurement, where an increase in blood perfusion was registered by an enhancement of the PPG amplitude [33]. Although direct comparison of anatomical sites are quite awkward because of the inconsistencies in the subject population and measurement conditions, the factor that led to the consideration of Tur's study for the location selection was the application of a PPG technique to distinguish basal perfusion at different anatomical sites [40]. Furthermore,

top locations from the comparative study were pre-tested to determine if SpO₂ measurements could be acquired using a commercial reflectance sensor and a table top pulse oximeter. Thus, the comparative study facilitated the construction of an initial decision matrix (table 4.2), which primarily considered different anatomical sites for attachment of a pulse oximeter sensor.

Features such as signal quality, attachment techniques, physical location, safety, portability, durability and cost were listed in an organizational tree, as shown in Figure 4.1. These features were scored for their importance level in the design process using a pairwise comparison technique. From the pairwise comparison table shown in table 4.1 it was concluded that the design should consider the following features

Signal quality > Attachment Convenience > Location > Safety > Portability > Durability > Cost

where > denotes the order of importance.

The selected locations from the initial decision matrix were compared with the features of the pulse oximeter sensor and the end-user requirements to construct a final decision matrix. It provided a hierarchy for the 5 pre-selected anatomical sites for application of a pulse oximeter sensor, as shown in table 4.3. The finger and earlobe formed a set of standard locations which are clinically accepted while the forehead, chin and wrist were locations where reflectance sensor placement and attachment is relatively easy using articles that are part of a soldier's gear. For example, the Kevlar helmet, or chin strap, can become potential means for attaching a reflectance sensor to the skin. Due to the improved PPG signal quality, the forehead followed by the finger gained precedence in comparison to other locations such as the chin, wrist and earlobe. Although

high quality signals can be obtained from a finger sensor, it cannot be used as a potential location for sensor placement in combat applications because it restricts normal hand motion and is highly susceptible to motion artifacts. Also, the ears and fingers are affected by thermo-regulatory vasoconstriction and have slower response to changes in central oxygenation compared to the forehead sensors which may be critical for rapid detection of hypoxemia [40, 41]. Therefore, from the final decision matrix, it was concluded that the following locations are important

Forehead > Chin > Finger > Earlobe > Wrist

where > represents the order of importance.

Thus, given this particular design challenge, it was concluded that the forehead of a soldier is the most suitable location for sensor placement.

8.2 Sensor Mode Studies

Designing a practical wearable pulse oximeter for long-term monitoring presents several unique challenges. In addition to user acceptability and site selection, the other most important issue to consider was power consumption. Rhee *et al* developed a miniaturized double-ring sensor intended for long term continuous monitoring of SpO₂ and HR from the base of a finger utilizing wireless reflection pulse oximetry [26-28, 36, 51]. The idea to design a pulse oximeter sensor based on a ring shaped configuration was motivated by the need to develop a comfortable wearable device for the aging population that the majority of people will accept to wear for an extended period of time. Additionally, utilizing a ring configuration approach has a unique benefit since the sensor can be securely attached to the body without the need to use disposable tape which is normally used to affix reflectance type sensors. Although the unique sensor developed by

Rhee and co-workers has adequately addressed the issue of susceptibility to motion artifacts by devising a double ring design, their optical sensor is based on R and IR LEDs positioned adjacent to a single PD chip as is commonly employed in reflection type commercial sensors. Furthermore, Rhee *et al* did not justify why they chose a reflection mode rather than relying on the more popular transmission approach.

Even though the decision matrix primarily suggested the application of a reflection mode sensor to the forehead, it was imperative to test different sensor modes to compare signal quality and estimate power consumptions for each mode. The ring shape sensor configuration of the wireless pulse oximeter provided the initial inspiration to test the different modes in terms of power consumption and signal quality. The physical configuration of a prototype ring-shaped sensor provided space for mounting several discrete PDs in three distinct orientations relative to the position of the LEDs. Therefore, it was important to investigate which configuration would be more desirable in terms of overall power efficiency. From the data presented in Figures 7.4(a-b) and 7.5, it can be observed that the amplitude of the AC components depends on the location of the PDs inside the ring. It was found that with a constant LED drive current and the same active area of 12mm^2 for each PD pair to facilitate easy comparisons, the RMS magnitude of the PPGs was the highest in reflection mode and their values decreased considerably when measurements were obtained from the PDs positioned in transflection or transmission modes. Statistical calculation using a single factor ANOVA in table 7.2(a-b) proved that the ‘ratio of ratio’ (R/IR) had no significant variance due to the change in sensor mode even though varying amplitude PPG signals were acquired from different sensor modes with constant LED drive currents.

After comparing the three different detection modalities, it was found that transflection and transmission modes consume approximately 4-6 times more current compared to reflection mode. This result was anticipated since higher incident light intensities must be produced in order to overcome the larger optical attenuation encountered in transmission compared to transflection or reflection modes. The current consumed by the LEDs in a battery operated wearable pulse oximeter is inversely proportional to the battery life. Therefore, the LED peak drive current plotted in Figure 7.6 were used to estimate the expected battery life of a typical 220mAh Lithium type coin-size battery (Duracell: DL2032). It should be noted also that the LEDs in a pulse oximeter are alternately switched on and off by high-speed digital circuitry in order to allow synchronized detection of the light by a single photodetector. Synchronizing the detection reduces the on time (T_{ON}) of each LED, and thereby helps to reduce the overall power consumption. Table 8.1 summarizes the estimated battery life for the different operating modes tested in this study assuming that the LEDs are pulsed continuously at a typical duty cycle of approximately 1.5%. This typical duty cycle was calculated using a lower power consuming commercial pulse oximeter (EPO) where $T_{ON} = 0.2\text{ms}$ and $T_{ON+OFF} = 13.2\text{ms}$.

Table 8.1. Comparison of estimated battery life for different operating modes.

Sensor Modes	LED drive current (mA)		Estimated Battery Life (Days) DL2032 (220mAh)
	$I_{R_{Peak}}$	R_{Peak}	
Reflection	7.0	24.1	19
Transflection	26.0	77.8	6
Transmission	44.5	143.8	3

Overall, the sensor mode study showed that in order to produce similar PPG amplitudes, increasingly more current was required for measurements performed in

transmission compared to reflection or transflection modes. The considerable differences in the estimated power consumptions shown in table 8.1 clearly points out the practical advantage gained by using a reflection rather than transflection or transmission mode in extending battery longevity. Thus, it can be concluded that reflection mode is more power efficient in comparison to other modes.

Practically, however, a requirement that the ring sensor must be attached to the finger imposes restrictions on hand motions. Utilizing disposable tape or a reusable spring-loaded device for attachment of a pulse oximeter sensor to the fingertip, as commonly practiced in clinical medicine, poses significant limitations and therefore is not compatible for an austere battlefield environment. Thus, even though the prototype ring sensor sounds like an excellent alternative in terms of attachments, it is unlikely that it could meet the necessary requirements for physiological monitoring of a soldier during combat.

8.3 Effect of Large PD Area on Power Consumption for Different Sensor Modes

High brightness LEDs are the preferred light sources commonly used in commercial pulse oximeters. To obtain the high light intensity required to overcome the strong optical absorption by blood and tissue, these LEDs must be driven by relatively high peak current pulses, typically in the range between 100-200mA. Hence, the LEDs will consume a large portion of the power in a battery-operated pulse oximeter. Therefore, minimizing the drive currents supplied to the LEDs would contribute considerably toward the overall power saving in the design of a wearable pulse oximeter. In addition to lowering the duty cycle of the LEDs, to ensure low power consumption, it is also possible to lower the peak driving currents of the LEDs. However, lowering the

intensity of the LEDs reduces the area of illumination which leads to significant deteriorations in the overall SNR. As a result of this design tradeoff, measurements could become more susceptible to external interferences and thus could affect the overall accuracy and reliability of the oximeter.

Besides lowering the duty cycle and driving currents supplied to the LEDs, the conventional approach for reducing power consumption in portable electronics, such as in calculators and notebook PCs, is to power-down non essential circuitry when the device is not in use over a certain period of time. However, while sleep-mode power reduction techniques are appropriate for consumer electronics, this specific approach may not be acceptable in certain medical applications. For example, SpO₂ and HR readings by a pulse oximeter are used to monitor potentially dangerous physiological trends since changes in SpO₂ can occur in a relatively short time span. Moreover, the readings of a pulse oximeter are based on a time averaging technique and, therefore, pulse oximeters require a few seconds of stable signals before they can process and display accurate physiological information. Hence, by switching the oximeter on and off intermittently to conserve power, critical clinical information may be compromised or lost.

Sensors used with commercial transmission or reflection pulse oximeters employ a single PD element, typically with an active area of about 6-10mm². Normally, a relatively small PD chip is adequate for measuring strong transmission PPGs since most of the light emitted from the LEDs is diffused by the skin and subcutaneous tissues predominantly in a forward direction. However, in reflection mode, only a small fraction of the incident light is backscattered by the subcutaneous tissues. Additionally, the backscattered light intensity reaching the skin surface is normally distributed over a

relatively large area surrounding the LEDs. Hence, the design of a reflectance-mode pulse oximeter depends on the ability to fabricate a sensor that has improved sensitivity and can detect sufficiently strong PPGs from various locations on the body combined with robust digital signal algorithms to process the relatively weak and often noisy signals.

Figures 7.7 and 7.8 (a-b) clearly demonstrates that by increasing the active area of the PD in either transmission or reflection type sensors it is possible to lower the minimum currents required to drive the LEDs without compromising the quality of the detected PPG signals. Noise measurements were performed with an increment of the PD area in complete darkness. Approximately 10-15 dB increase in SNR was observed in both transmission and reflection modes with lower current drives. In comparing the two operating modes shown in table 7.3, it was found that transmission mode required approximately 10-15 times more current compared to reflection mode. To overcome the larger optical attenuation encountered in transmission compared to reflection mode, higher light intensities are required. But in order to optimize power budgeting, low light intensities are preferred, since LED drive current is inversely proportional to the battery life and directly proportional to the emitted light intensity. Thus, the lowest LED drive currents in reflection mode with large PD area of 36mm^2 are 1.9 mA and 3.0 mA for IR and R, respectively. Likewise, in transmission mode the corresponding currents are approximately 19.6 mA and 46 mA for the IR and R LED, respectively. As indicated in table 7.3, the estimated battery life using a larger PD area in reflection mode is approximately 18 times longer compared to transmission mode. Thus, this study clearly suggests that a reflection pulse oximeter sensor with a larger PD area is preferred over a

transmission type sensor with a similar size PD for extending the battery life of a wearable pulse oximeter.

8.4 Effect of Measurement Site on Power Consumption

Several studies have shown that oximetry readings may vary significantly according to sensor location [37, 39, 45, 49]. For example, tissue blood volume varies in different parts of the body depending on the number and arrangement of blood vessels near the surface of the skin. Other factors, such as sensor-to-skin contact pressure and LED intensity can affect the of PPG signal. Thus, sensor site is considered a major factor in calculating the power consumption as well as attachment technique. From the data presented in Figure 7.12, it is evident that the amplitude and the quality of the recorded PPGs vary significantly between the forehead and the wrist. While using relatively low peak LED driving currents, a considerable amount of external pressure on the sensor was applied in order to measure discernable PPG signals from the wrist. In contrast, using minimal contact pressure and similar LED driving currents produced significantly larger and less noisy PPG signals from the forehead. These noticeable differences are due to the lower density of superficial blood vessels found on the arms compared to the highly vascular forehead skin combined with a stronger light reflection from the forehead bone. Additionally, during conditions of peripheral vasoconstriction, a sensor placed on the forehead can maintain stronger PPGs longer compared to a finger sensor. Furthermore, a possible technique for attaching a forehead reflectance sensor could be achieved using the inner foam of the soldier's Kevlar helmet. In addition, disposable tape would not be required to attach the reflectance sensor to the skin, leaving out problems related to sensor detachment over time, particularly in sweaty conditions.

8.5 Effect of Varying LED-PD Separation on Power Consumption

Despite the noticeable differences between the PPG signals measured from the wrist and forehead, the data plotted in Figure 7.13 also revealed that considerable stronger PPGs could be obtained by widening the active area of the PD which helps to collect a larger proportion of backscattered light intensity. The additional increase, however, depends on the area and relative position of the PD with respect to the LEDs. For example, utilizing only the outer-ring configuration, the overall increase in the average amplitudes of the R and IR PPGs measured from the forehead region was estimated to be about 23% and 40%, respectively. Similarly, the same increase in PD area produced an increase in the PPG signals measured from the wrist, but with a proportional higher increase of 42% and 73%, respectively. The data presented in Figure 7.14 confirmed that in order to produce similar PPG amplitudes, significantly higher peak LED driving currents are required when backscattered light is measured by the outer PD set compared to the inner set. This observation was expected since the backscattered light intensity measured is inversely related to the separation distance between the PD and the LEDs [29]. In the R/IR calculation, the outer (F) PDs showed higher R/IR values in comparison to the inner (N) or the combination (N+F) PDs. This variation was anticipated because the luminous intensity of the LED is diminished as the distance of the PDs increased relative to the position of the LED. Also, from the spectral response of the PDs shown in Figure 2.4, it is obvious that the PD has a higher spectral sensitivity to the IR wavelength (930nm) compared to the R wavelength (660nm). Thus, with a decrease in LED illumination and an increase in the separation distance between the PD and the LEDs, there is a significant increase in the IR DC component of the PPG signal in

comparison to the R DC component. This difference in the DC components causes an increase in the R/IR values. Even though there is an increase in the PD distance for the combined (N+F) arrangement of PDs, the variation in the R/IR was not observed because the total detection area is doubled. Thus, the R/IR variations observed due to the reduction in LED illumination can be compensated by increasing the detection area.

In comparing the three different PD configurations, it was found that by combining both PD sets to simulate a single large PD area, it was possible to further reduce the driving currents supplied the LEDs without degrading the quality of the reflected PPGs. The considerable differences in the estimated power consumptions shown in table 7.4 clearly points out the practical advantage gained by using a reflection sensor comprised of a large ring-shaped PD to perform accurate measurements from the forehead. A continuous ring-shaped PD could be used to simulate a larger active area rather than using discrete PDs as shown in Figure 8.1. If the annular width of the ring-shaped PD is maintained at 2mm, then the increment in the PD area would be approximately doubled assuming the distance from the LEDs is equal to 6mm. Table 8.2 shows the estimated area covered by the 12-PD in the prototype reflectance sensor based on discrete elements in comparison to a continuous ring-shaped PDs configuration that can be used in a future sensor design.

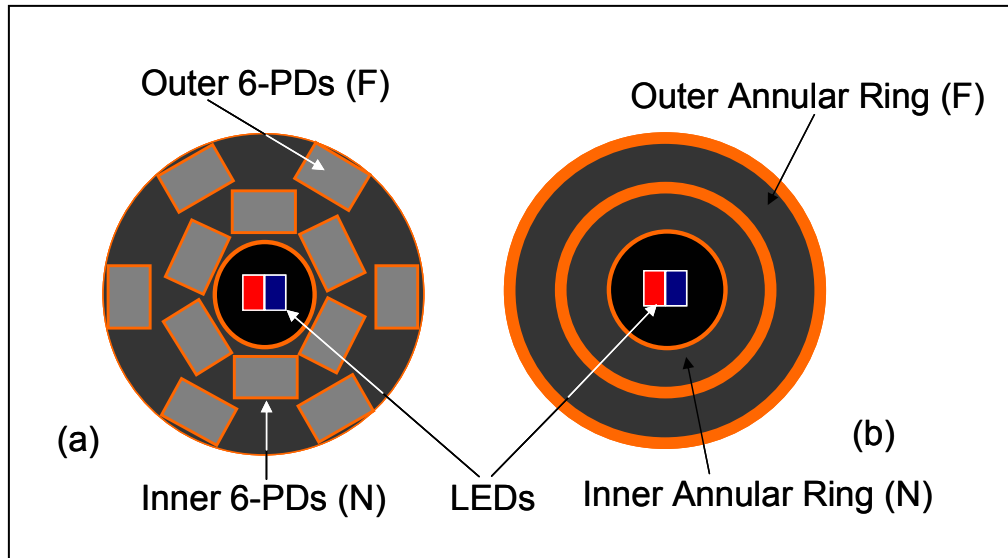


Figure 8.1. (a) Multiple PDs simulating a large PD area (b) equivalent configuration utilizing ring-shaped continuous PDs.

Table 8.2. Equivalent detections area calculated for the inner and outer ring-shaped reflectance sensor configuration illustrated in Figure 8.1.

PD Position	Area for 6-PDs setup (mm ²)	Area for ring-shaped PD (mm ²)
Inner (N)	36	63
Outer (F)	36	114
Inner + Outer (N+F)	72	176

8.6 Evaluation of Large Area PD Sensor Prototype

Table 8.3 summarizes the 3 experimental cases, with each case providing information regarding the bias (accuracy) and standard deviation (precision) of the prototype reflectance sensor evaluated using the EPO.

Case 1: Data collected during normal breathing while using the controlled RS-10 sensor for both pulse oximeters (RPO and EPO) provided information related to the difference in SpO₂ readings. Based on this analysis, it was determined that the EPO tends to overestimate SpO₂ with a bias of 0.28%. The 95 % confidence limit of 1.29% shows that the EPO produce reading differences ranging between -1.00 and 1.57% compared to the values measured by the RPO.

Table 8.3. Statistical analysis of SpO₂ values obtained during various breathing maneuvers for different sensor setups.

CASE	Type of breathing	Sensor		Total number of data points (N)	Accuracy (%) [Bias]	Precision (%) [Standard Deviation (SD)]	95% confidence limit (%) ~2*SD		
		RPO (Nellcor N-100)	EPO (Nonin X-pod)				Limit	-Ve	+Ve
1	Normal	RS-10	RS-10	115	0.28	0.65	1.29	-1.00	1.57
2	Breath holding (40sec)	RS-10	RS-10	115	3.11	2.27	4.45	-1.34	7.57
3	Breath holding (40sec)	RS-10	6PD Prototype	115	-2.03	1.88	3.68	-5.71	1.65

Case 2: When attached to the EPO during breath holding experiments, the control sensor tends to overestimate SpO₂ by 3.11%. With a 95 % confidence limit of 4.45%, the EPO produced inaccuracies ranging between -1.34 and 7.57% compared to the true value measured by the RPO using a control sensor.

Case 3: With different sensors connected to the pulse oximeters, data collected during breath holding provided information related to the difference in SpO₂ between the control and prototype sensors. For example, a bias of -2.03% indicates that the EPO with the prototype sensor tends to underestimate SpO₂. Using a 95 % confidence limit of 3.68%, it was observed that the differences in the readings measured by the EPO ranged between -5.71 and 1.65 % compared to the true value measured by the RPO using the control sensor.

It was also observed that while using low LED drive currents, considerable improvement in PPG signal was achieved by increasing the area of the PDs [52-55]. But with a lower LED current and a relatively small PD used as a control sensor, the systemic error was significant. However, as demonstrated in Figure 7.17, by increasing the number of PDs in the prototype sensor, it is possible to decrease this error considerably even with

lower LED driving currents. The data from case 4, summarized in Table 8.4, shows the variation in the accuracy of the pulse oximeters observed with different LED drive currents using a reflectance sensor with a large PD area.

Table 8.4. Statistical analysis for low LED drive current and its effect on SpO₂ accuracy.

CASE 4 Normal Breathing	6-PDs Prototype sensor	LED Current (%)	Total number of data points (N)	Accurac y (%) [Bias]	Precision (%) [Standard Deviation]	95%confidence limit (%) ~2SD		
						Limit	-Ve	+Ve
a	1-PD	100	31	0.792	0.826	1.652	1.687	-0.103
	6-PDs	100	31	1.506	0.65	1.300	2.807	0.206
b	1-PD	6	31	14.03	1.876	3.753	17.78	10.27
	6-PDs	6	31	0.763	0.668	1.336	2.1	-0.57

Case 4(a): Data collected during normal breathing with a 100% (24mA) LED drive current provided information related to the difference in accuracy between a single PD sensor prototype compared to multiple PDs. A bias of 0.792% was obtained for a single PD sensor compared to a control sensor attached to the RPO, thus producing smaller bias while using 100% LED drive currents. A 95 % confidence limit of 1.652% demonstrated that the single PD sensor connected to the EPO produced inaccuracies in the range between -0.103 and 1.687 % compared to the true values measured from the RPO with the control sensor. With 6 PDs used in the prototype sensor and 100% current supplied to the LEDs, a bias of 1.506 % was produced indicating an overestimation of SpO₂. A 95 % confidence limit of 1.652% showed that the 6-PDs prototype sensor connected to the EPO produced reading differences in the range between -0.103 and 1.687 % compared to the true value measured by the RPO with the control sensor.

Case 4(b): Data collected during normal breathing with a 6% LED drive current provided information related to the difference in accuracy between the single PD prototype sensor compared to the multiple PDs prototype. A bias of 14.03% was observed for the single

PD sensor compared to a control sensor attached to the RPO. This shows that with less current supplied to the LEDs, the SpO₂ obtained is less accurate. Using a 95 % confidence limit of 1.652% showed that the single PD sensor connected to the EPO produced reading differences ranging between 10.103% and 17.78 % compared to the true values measured by the RPO with the control sensor. However, with the 6 PDs prototype sensor and only 6% LED drive currents, a bias of only 0.763% was produced that led to a small and insignificant overestimation in SpO₂. Thus, the addition of multiple PDs simulating large PD area helps to overcome the inaccuracy caused by the loss of LED illumination. The close correlation observed between the prototype reflectance sensor at 6% drive current and the control sensor with a 100% current drive proves that with a larger detection area, the accuracy is increased even with low LED drive currents.

The driving currents tabulated in Table 8.4 were also used to estimate the expected battery life of a typical 220mAh Lithium type coin battery assuming that a similar battery could be used eventually to power the optical components of a wearable wireless pulse oximeter sensor. The values in Table 8.5 were estimated assuming that the LEDs are pulsed continuously at a typical duty cycle of approximately 1.5%. The considerable differences in the estimated power consumptions clearly points out the practical advantage gained in extending the battery longevity by using a large PD area sensor with low LED driving currents.

Table 8.5. *Estimated battery life for different LED operating currents.*

Prototype sensor (6-PDs)	Estimated Battery Life (Days)
100% current (24mA)	13
6% current (1.44mA)	212

Note that the estimated values given in Table 8.5 are very conservative since they rely only on the power consumption by the LEDs and do not take into consideration additional power demands imposed by other components of a wearable pulse oximeter. Typically, the power consumed by the other electronic components of a wearable pulse oximeter such as processing unit (CPU) and RF transmitter are significantly less in comparison to the power consumption by the LEDs of a commercial sensor. For example, the CPU draws approximately 0.153 mA and the RF transmitter consumes approximately 0.10mA whereas average current required for a single PD sensor is approximately 0.36mA [28]. But with the development of the prototype sensor, the current values have reduced considerably while using only 6% of current drive where the average current is approximately 0.021mA.

9. CONCLUSIONS AND RECOMMENDATIONS

A key requirement in the optimal design of a wearable pulse oximeter is low power management without compromising signal quality. This research investigated the advantages gained by using multiple PDs to simulate a larger active area at relatively low peak LED driving currents in order to reduce the overall power requirement of a wireless reflectance mode pulse oximeter sensor. Using a decision matrix to help organize the requirements for designing a pulse oximeter sensor from a mobile soldier, it was concluded that the forehead was the most appropriate location for future sensor placement.

In vivo experiments demonstrated that by increasing the PD area it is possible to reduce the overall power requirement of a wireless sensor without compromising the quality of the PPG signal. The study showed that a reflection sensor with a large area PD can be used to extend the battery life by approximately 6 times in comparison to a transmission mode sensor with an equivalent PD area. With low LED intensities, a commercial pulse oximeter sensor would normally provide deteriorated PPG signals whereas the prototype 6-PD sensor evaluated in this study provided a 10-15 db SNR improvement. Thus, it was concluded that a reflection sensor employing a larger area PD would be preferable over a similar transmission or transflection type sensor for extending the battery life of a pulse oximeter intended for future telemedicine applications.

Even though considerable SNR improvement was obtained from a prototype reflectance sensor utilizing 6-PD, it was essential to evaluate the sensor by comparing it to a commercially available pulse oximeter sensor. The initial benchmarking results indicated a good agreement for both HR and SpO₂ measurements. The close correlation

between the prototype reflectance sensor at 6% drive current compared to a control sensor with a 100% current drive proved that with larger detection area, the measurement accuracy increased even with considerable lower peak LED drive currents.

Different large area PD components were selected from manufacturers for testing, but drilling a hole in the centre of the PD to place LEDs with optical guard was a daunting task. The second problem was varying the area size using an iris ring without creating an error due to optical interference or loss of sensor -to- skin contact. According to manufacturers, even if it was possible to drill a hole in the PD, the process would have changed PD's typical specifications such as sensitivity, efficiency and noise level. Secondly, application of LEDs without an optical guard would alter the PPG signal quality with large noise interference. Thus, discrete components were used in experiments which were a major constraint as a limited number of PDs could be used simulating a specific area. To overcome this constraint, a custom built annular PD would be required. An improved reflection sensor that can be constructed with a continuous PD ring surrounding the area of illumination is shown in Figure 9.1. The total size of the prototype sensor may be around 27mm (dia.) which would provide sufficient area to fix it to the Soldier's helmet lining and obtain maximum signal strength. The total area of the continuous PD ring (width of the PD@ 6-8mm) is estimated to be $265\text{-}400\text{mm}^2$ (i.e. $84\pi\text{-}128\pi$) while a minimum distance of about 4mm from the LEDs. An optical guard protects the PDs from detecting light shunted directly through the sensor rather than propagating through the tissue.

Further *in vivo* testing must be performed to evaluate the prototype reflectance sensor on mobile soldiers in austere environments. Also, most of the pulse oximeters

perform well at high values of SaO_2 which may not remain consistent at lower SaO_2 . Thus, further clinical evaluations of the continuous ring PD sensor with a commercial battery-operated pulse oximeter are recommended.

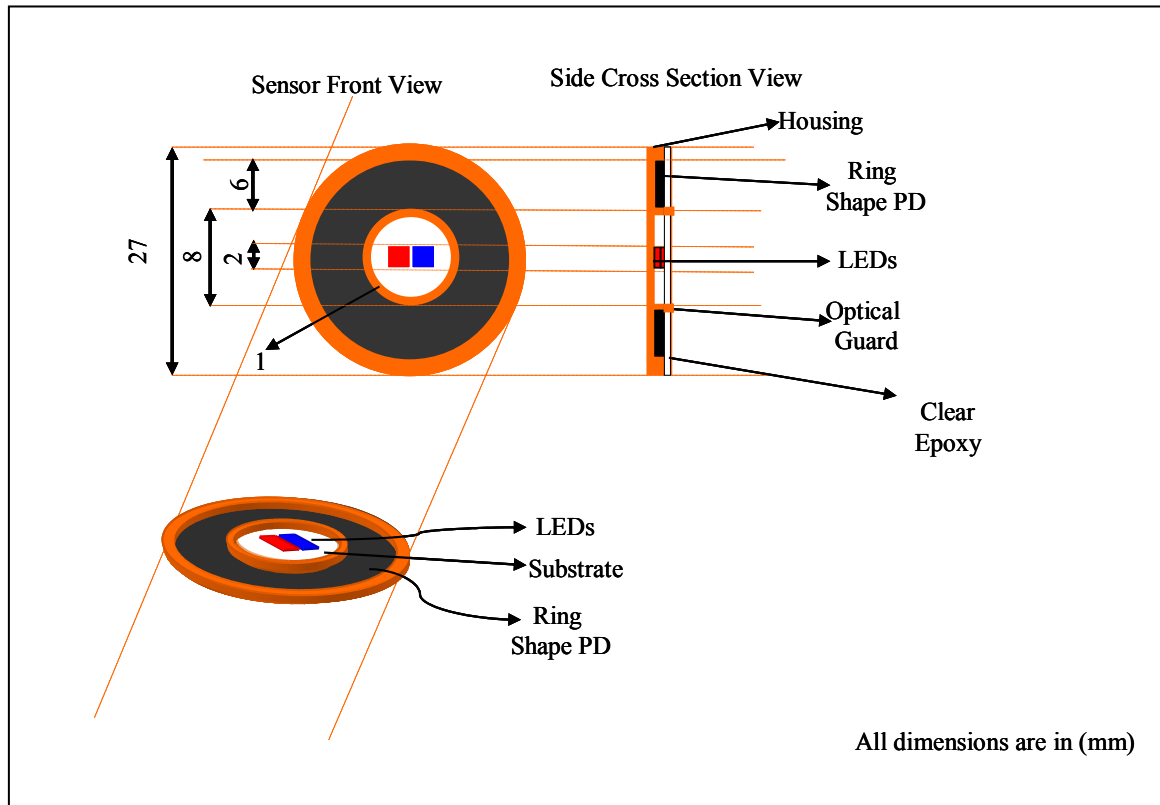


Figure 9.1. Forehead reflectance sensor using a continuous ring-shaped PD for SpO_2 and HR measurements with low LED intensity for optimum power budgeting.

APPENDIX A

Pros and cons for different anatomical locations considering a soldier as the end user.

Site	Advantages	Disadvantages
Forehead	<ul style="list-style-type: none"> • Flat and large region • Easy attachment (helmet) • Stable region (low motion artifact effects) • Strong PPG signals • Clinically available sensors 	<ul style="list-style-type: none"> • Only reflectance mode • Dirt and sweat may cause errors
Temple	<ul style="list-style-type: none"> • Flat region • Easy attachment (helmet) • Clinically available sensors 	<ul style="list-style-type: none"> • Subject dependent (presence of hair) • Only reflectance mode • Dirt and sweat may cause errors
Nose	<ul style="list-style-type: none"> • Stable region (low motion artifacts) • Both T & R modes • Clinically available sensors 	<ul style="list-style-type: none"> • Attachment restrictions • Visible location (non concealable) • May be obstructive (vision)
Chin	<ul style="list-style-type: none"> • Flat region • Easy attachment (helmet straps) • Strong PPG signals 	<ul style="list-style-type: none"> • Subject dependent (presence of hair) • Only Reflectance mode • Dirt and sweat may cause error
Ear Lobe	<ul style="list-style-type: none"> • Non obstructive • Less size restrictions • Both T & R modes • Strong PPG signals 	<ul style="list-style-type: none"> • Attachment difficulties • Subject dependent • Motion artifact (due to neck movement) • Obstructive (hearing canal)
Nape	<ul style="list-style-type: none"> • Flat and large region • Less size restriction • Concealed location 	<ul style="list-style-type: none"> • Only Reflectance mode • Dirt and sweat may cause error • Presence of hair • Weak signal
Jaw line	<ul style="list-style-type: none"> • Easy attachment (helmet straps) 	<ul style="list-style-type: none"> • Attachment restrictions • Visible location (non concealable) • May be obstructive (vision) • Weak signal
Chest	<ul style="list-style-type: none"> • Flat and large region • Less size restriction • Concealed location 	<ul style="list-style-type: none"> • Motion artifact • Only reflectance • Weak signal
Abdomen	<ul style="list-style-type: none"> • Flat and large region • Less size restriction 	<ul style="list-style-type: none"> • Poor signal (very weak) • Motion artifact

	<ul style="list-style-type: none"> • Concealed location 	<ul style="list-style-type: none"> • Weak signal • Only reflectance
Arm	<ul style="list-style-type: none"> • Flat and large region • Less size restriction • Concealed location 	<ul style="list-style-type: none"> • Weak signal • Motion artifact • Only reflectance
Forearm	<ul style="list-style-type: none"> • Concealed location • Respiration & PPG signal • Easy attachment (Arm band) 	<ul style="list-style-type: none"> • Weak signal • Motion artifact • Only reflectance
Wrist	<ul style="list-style-type: none"> • Concealed location • Easy attachment (Wrist watch technique) • Less size restriction 	<ul style="list-style-type: none"> • Site prone to motion artifact • Only reflectance
Palm	<ul style="list-style-type: none"> • Flat and large region • Less size restriction • Concealed location 	<ul style="list-style-type: none"> • Weak signal • Site prone to motion artifact • Obstructive (normal motion) • Only reflectance
Finger base	<ul style="list-style-type: none"> • Strong signal • Respiration & PPG signal • Easy to apply • Both T & R modes • Clinically available sensor (gold standard) 	<ul style="list-style-type: none"> • Site prone to motion artifact • Obstructive (normal motion)
Finger tips	<ul style="list-style-type: none"> • Strong signal • Respiration & PPG signal • Easy to apply • Both T & R modes • Clinically available sensor (gold standard) 	<ul style="list-style-type: none"> • Site prone to motion artifact • Obstructive (normal motion)
Thigh	<ul style="list-style-type: none"> • Flat and large region • Less size restriction • Concealed location 	<ul style="list-style-type: none"> • Weak signal • Site prone to motion artifact • Obstructive (normal motion)
Calf	<ul style="list-style-type: none"> • Flat and large region • Less size restriction • Concealed location 	<ul style="list-style-type: none"> • Weak signal • Site prone to motion artifact • Obstructive (normal motion)

Foot	<ul style="list-style-type: none"> • Flat and large region • Less size restriction • Concealed location 	<ul style="list-style-type: none"> • Weak signal • Site prone to motion artifact • Obstructive (normal motion)
Toe	<ul style="list-style-type: none"> • Less size restriction • Concealed location 	<ul style="list-style-type: none"> • Weak signal • Site prone to motion artifact • Obstructive (normal motion)

APPENDIX B-1

RPO SPECIFICATION

Unit Name:	Nellcor Pulse Oximeter Model N-100:
%Saturation Range:	0-100%
Pulse Rate Range:	20-250 beats/minute (BPM)
Readout:	Two 3-digit, 7 segment LED Displays - 0.8cm (0.3") high characters; Pulse Amplitude Display, Pulse Search and Battery in Use Indicators
Alarm Limit Range:	LO SAT: 50-99% HI RATE: 40-250 BPM LO RATE: 40-250 BPM
Measurement Wavelengths:	RED - 660nm (nominal) IR - 925nm (nominal)
Accuracy (%SaO ₂ +/- 1 SD):	100-70%: +/-2% 70-50%: +/-3% 50-0%: Unspecified
Temperature:	Instrument: 0-40 ⁰ C Oxisensor: within physiologic range (28-42 ⁰ C) for accurate measurement
Humidity:	Operates at all levels of humidity where no condensation is formed
Altitude:	0-10,000 ft
Power Requirements:	Model N-100: 90-130 V _{AC} 50-60 Hz
Power Consumption:	75 watts

Leakage Current:	50 μ A max, chassis to main ground
Patient Isolation:	Measured from any part of Oxisensor or its connector to ground: > 12 megohms, 2500 VRMS at 60 Hz, 40 ⁰ C and 95% relative humidity
Battery Pack:	Internal 12V sealed, starved electrolyte lead acid batteries. Discharge life: Minimum 1 hour on a full charge. Recharge Period: 8 hours continuously
Dimensions:	10.7cm (4.2") high X 30.5cm (12") wide X 30.5cm (12") deep
Weight:	7.3 kg (16 lb)
Preamplifier Cable Length:	4 m (12 ft)
Oxisensor Cable Length	0.5 m (18")

APPENDIX B-2

NELLCOR INTERFACE SPECIFICATION

Unit Name:	NELLCOR Interface, Model N-8000
Power Requirements:	100-120VAC 50/60Hz
Power Consumption:	<35 Watts
Leakage Current:	<50 μ A Chassis to Main Ground
Temperature:	0 ⁰ to 40 ⁰ C (Operating) -25 ⁰ to 70 ⁰ C (storage/shipping)
Humidity:	Any, non-condensing
Altitude:	0 to \pm 20,000 Feet (Operating)
Full Scale Output:	Within 20mV of nominal Full Scale on any range.
Zero Output:	20mV Maximum any Range
Accuracy: (Referred to Oximeter Display)	<0.5% of Full Scale Range (5/10V) Within 20mV max (1/3V)
Dimensions:	6.6cm (2.6"), High 30.5cm (12"), Wide 26.7cm (10.5).
Weight:	3.6Kg (8 lb)
Optical Cable Length:	0. 5m (18 ")

APPENDIX B-3

EPO SPECIFICATION

Unit Name:	Nonin Xpod Patient Cable Oximeter
Oxygen Saturation Range:	0 to 100%
Pulse Rate Range:	18 to 300 pulses per minute
Measurement Wavelengths:	Red - 660 nm Infrared - 910 nm
Accuracy SpO ₂ (± 1 Standard Deviation)*:	70 - 100% ± 2 digits for adults using the Finger Clip Sensor 70 - 95% ± 3 digits for neonates using infant or neonatal sensors 70 - 100% ± 3 digits for adults using Flex or Reflectance Sensors 70 - 100% ± 4 digits using Ear Clip Sensor Below 70% is not specified for all sensors
Rate Accuracy:	± 3% ± 1 digit
*Standard Deviation is a statistical measure: up to 32% of the readings may fall outside these limits.	
Temperature	
a) Operating:	0° C to +50° C
b) Non Operating:	-20° C to +50° C
Humidity	
a) Operating:	10 to 90% Non Condensing
b) Non Operating:	10 to 95% Non Condensing
Power Draw:	60 mW - typical operating
Voltage Input:	2 to 6 volts dc operating
Note: Sensor is not isolated from input voltage	
Output Digital Signals:	0 - 5 volts (nominally)
Patient Isolation:	Greater than 12 megohm
Leakage Current:	Not applicable

Dimensions: 2.1" x 0.8" x 0.6" (53 x 20 x 15mm)
Weight: 75g (including 6' cable and connector)
Ruggedness immersion
a) Shock: Per IEC 68-2-27
b) Vibration: Mil-standard 810C, method 514-2
Sensors: Designed to use *Nonin* sensors only

INPUTS:

Red Wire: V+ (2-6VDC, 60mw typical)
Black Wire: Ground
Cable Shield: Ground
(Both Black wire and cable shield must be attached to ground on the host device)
Yellow Wire: ECG Sync (Optional)

REFERENCES

- [1] S. Fox, *Human Physiology*: Oxford: W.C. Brown Publishers, 1993.
- [2] J. Webster, "Design of Pulse Oximeters," in *Medical Science Series*, W. J. G, Ed.: IOP Publishing Ltd, 1997.
- [3] J. Peterson, "The development of pulse oximetry," in *Science*, 1986, pp. G135-40.
- [4] G. Millikan , J. Pappenheimer, A. Rawson, and J. Hervey, "Continuous measurement of oxygen saturation in man," *American Journal of Physiology*, pp. 133:390, 1941.
- [5] E. Wood and J. Geraci, "Photoelectric determination of arterial oxygen saturation in man," *The Journal of Laboratory and Clinical Medicine*, vol. 34, pp. 387-401, 1949.
- [6] E. Merrick and T. Hayes, "Continuous, non-invasive measurements of arterial blood oxygen levels," *Hewlett-Packard Journal*, vol. 28, pp. 2-9, 1976.
- [7] T. Aoyagi, M. Kishi, K. Yamaguchi, and S. Watanabe, "Improvement of earpiece oximeter," presented at 13th Annual Meeting Jpn. Soc. Med. Elec. Biomed. Eng, 1974.
- [8] S. Nakajima, Y. Hirai, H. Takase, A. Kuse, S. Aoyagi, M. Kishi, and K. Yamaguchi, " New pulse-type ear oximeter," *Kokyu to Junkan*, vol. 23, pp. 709-713, 1975.
- [9] I. Yoshiya , Y. Shimada, and K. Tanaka, "Spectrophotometric monitoring of arterial oxygen saturation in the finger tip," in *Medical & Biological Engineering & Computing*, vol. 18, 1980, pp. 27-32.
- [10] V. Heines, "Investigation spurs interest in blood-oxygen monitors," in *Times News*.
- [11] Y. Mendelson, "Pulse Oximetry: Theory and Applications for Noninvasive Monitoring," *Clinical Chemistry*, vol. 38, pp. 1601-1607, 1992.
- [12] Philips Medical Systems, "Understanding Pulse Oximetry SpO2 concepts," Philips Medical Systems.
- [13] R. Brinkman and Zijlstra, "Determination and continuous registration of the percentage of the percentage of the oxygen saturation in small amounts of blood," *Arch. Chir.Neerl.*, vol. 1, pp. 177-183, 1949.

- [14] J. Payne and J. Severinghaus, *Pulse Oximetry*. New York: Springer, 1986.
- [15] W. McKay and W. Noble, "Critical incidents detected by pulse oximeter during anesthesia," *Canadian Journal of Anesthesia*, vol. 35, pp. 265-9, 1988.
- [16] N. Johnson , V. Johnson, J. Bannister, and R. Lilford, "The accuracy of fetal pulse oximetry in the second stage of labor," in *Neonatal Intensive Care*, 1992, pp. 46-49.
- [17] Y. Mendelson and R. Peura, "A combined transcutaneous SaO₂/PO₂ sensor," presented at Proceedings of the XIV ICMBE and VII ICMP, Espoo, Finland, 1985.
- [18] USAMRMC, " <http://mrmc-www.army.mil/index.asp?EntryURL=/mrdrads.asp>," United States Army Medical Research and Materiel Command (USAMRMC).
- [19] C. Leedham, C. Blood, and C. Newland, "A descriptive analysis of wounds among U.S Marines treated at second-echelon facilities in the Kuwaiti theater of operations," *Military Medicine*, vol. 158(8), pp. 508-12, 1993.
- [20] MEDLINEplus, "<http://www.nlm.nih.gov/medlineplus/ency/article/000039.htm>," MEDLINEplus Health information system.
- [21] J. Wilson and J. Hawkes, in *Optoelectronics: An Introduction*, 3rd ed. Essex: Pearson Education Limited, 2000, pp. 293-358.
- [22] M. Ott, "Capabilites and Reliability of LEDs and Laser Diodes," NASA Goddard Space Flight Center 1997.
- [23] P. Mannheimer, J. Casciani, M. Fein , and S. Nierlich, "Wavelength selection for low-saturation pulse oximetry," *IEEE Transactions on Biomedical Engineering*, vol. 44, pp. 148-58, 1997.
- [24] R. Bonner, R. Nossal, S. Havlin, and G. Weiss, "Model for photon migration in turbid biological media," *Journal of the Optical Society of America A: Optics, Image Science, and Vision*, vol. 4, pp. 423-432, 1987.
- [25] J. Schmitt "Simple photon diffusion analysis of the effects of multiple scattering on pulse oximetry," *IEEE Transactions on Biomedical Engineering*, vol. 38, pp. 1194-1203, 1991.
- [26] S. Rhee, B. H. Yang, and H. Asada, " The Ring Sensor: A new Ambulatory Wearable Sensor for twenty Four Hour Patient Monitoring," presented at Proc. of

- the 20th Annual International Conference of the IEE Engineering in Medicine and Biology Society, Hong Kong, Oct. 1998.
- [27] S. Rhee, B. H. Yang, and H. Asada, "Artifact-resistant, Power-efficient design of finger-ring plethysmographic sensors, part-2," presented at Proceedings of the 22nd Annual International Conference of the IEEE Engineering in Medicine and Biology, Chicago, USA, 2000.
- [28] S. Rhee, B. H. Yang, and H. Asada, "Artifact-resistant, Power-efficient design of finger-ring plethysmographic sensors, part-1," presented at Proceedings of the 22nd Annual International Conference of the IEEE Engineering in Medicine and Biology, Chicago, USA, 2000.
- [29] Y. Mendelson, J. Kent, B. Yocum, and M. Birle, "Design and Evaluation of New Reflectance Pulse Oximeter Sensor," *Medical Instrumentation*, vol. 22, pp. 167-173, 1988.
- [30] UDT, " Photodiode characteristics," in *UDT sensors: Application Notes*: www.udt.com, 2003, pp. 1-10.
- [31] F. Perry, "Predicting the performance of a photodetector," Boston Electronics Corporation, www.boselec.com, 2003.
- [32] Pacific silicon sensor Inc, "Series 6: Low dark Current (Id) Photodiodes," Pacific silicon sensor Inc, Data sheets. 2003.
- [33] Y. Mendelson and B. Ochs, "Noninvasive Pulse Oximetry Utilizing Skin Reflectance Photoplethysmography," *IEEE Transactions on Biomedical Engineering*, vol. 35, pp. 798-805, 1988.
- [34] G. Ling, B. Day, P. Rhee, and J. Ecklund, "In Search of Technological Solutions to Battlefield Management of Combat Casualties," presented at Part of the SPIE Conf. on Battlefield Biomedical Technologies, April 1999.
- [35] Col. J.Obusek, "Warfighter Physiological Status Monitoring," in *The Warrior*, Nov.-Dec.2001, pp. 6-8.
- [36] S. Rhee, B. H. Yang, and H. Asada, "Design and evaluation of artifact-resistant finger-ring plethysmographic sensor," 2000.
- [37] M. Mahlmeister, "Sensor Selection in Pulse Oximetry," *The Journal For Respiratory Care Practitioners*, Dec-Jan1998.

- [38] C. Dym and P. Little, *Engineering Design : A project-based introduction*. New York: John Wiley & Sons, Inc., 1999.
- [39] Y. Mendelson, R. Lewinsky, and Y. Wasserman, "Multi-Wavelength Reflectance Pulse Oximetry," *Anesthesia & Analgesia*, vol. 94, pp. S26-S30, 2002.
- [40] E. Tur, M. Tur, H. Maibach, and R. Guy, "Basal Perfusion of the Cutaneous Microcirculation: Measurements as a Function of Anatomic Position," *The Journal of Investigative Dermatology*, vol. 81, pp. 442-446, 1983.
- [41] B. Winer, *Statistical Principles in Experimental design*, 2nd edition ed. New York: McGraw-Hill, 1971.
- [42] Nellcor Inc. Product catalog for nellcor pulse oximetry sensors, "<http://www.nellcor.com/Catalog/PDF/Product/SensorSelectionGuide.pdf>," Nellcor Inc.
- [43] A. Awad, M. Ghobashy, W. Ouda, R. Stout, D. Silverman, and K. Shelley, Ph.D, "Different Response of Ear and Finger Pulse Oximeter Wave Form to Cold Pressor Test," *Anesthesia & Analgesia*, vol. 92, pp. 1483-1486, 2001.
- [44] A. Hertzman and L. Roth, "The absence of vasoconstrictor reflexes in the forehead circulation: effects of cold," *American Journal of Physiology*, vol. 136, pp. 692-697, 1942.
- [45] D. Bebout, P. Mannheimer, and C. Wun, "Site-dependent differences in the times to detect changes in saturation during low perfusion," *Critical Care Medicine*, vol. 29, pp. A115, 2001.
- [46] R. Tobin, J. Pologe, and P. Batchelder, "A Characterization of Motion Affecting Pulse Oximetry in 350 Patients," Datex-Ohemda, Louisville, Colorado, USA, Case study.
- [47] D. Bebout, P. Mannheimer, and N. Asbagh, "Detection of Hypoxemia during Peripheral Vasoconstriction at the Radial Artery and Various Pulse Oximeter Sensor Sites," *Critical Care Medicine*, vol. 31, pp. A72, 2003.
- [48] D. Bebout and P. Mannheimer "Effects of Cold Induced Peripheral Vasoconstriction on Pulse Amplitude at Various Pulse Oximeter Sensor Sites." 4280 Hacienda Drive, Pleasanton, CA 94588: Nellcor Oximetry, Tyco Healthcare.

- [49] Y. Mendelson and M. McGinn, "Skin reflectance pulse oximetry: in vivo measurements from the forearm and calf,," *Journal of Clinical Monitoring and Computing*, vol. 37, pp. 7-12, 1991.
- [50] Nellcor Inc, *N-100 Manual*: Nellcor , Inc.
- [51] B.Yang, S. Rhee, and H. Asada, "A twenty-four hour tele-nursing system using a ring sensor," presented at Proceedings of 1998 IEEE, International Conference on Robotics and Automation, Leuven, Belgium, May 1998.
- [52] M. Savage, C. Pujary, and Y. Mendelson, "Optimizing Power Consumption in the Design of a Wearable Wireless Telesensor: Comparison of Pulse Oximeter Modes," presented at 29th Annual Northeast Bioengineering Conference, March 2003.
- [53] C. Pujary, M. Savage, and Y. Mendelson, "Photodetector Size Considerations in the Design of a Noninvasive Reflectance Pulse Oximeter for Telemedicine," presented at 29th Annual Northeast Bioengineering Conference, NJIT, Newark, NJ, March 2003.
- [54] Y. Mendelson and C. Pujary, "Measurement Site Photodetector Size Considerations in Optimizing Power Consumption of a Wearable Reflectance Pulse Oximeter," presented at 25th Annual International Conference of the IEEE Engineering in Medicine and Biology Society, Cancun, Mexico, Sept 2003.
- [55] Y. Mendelson, C. Pujary, and M. Savage, "Minimization of LED Power Consumption in the Design of a Wearable Pulse Oximeter," presented at Proceedings International Association of Science and Technology for Development, International Conference. BioMED, Salzburg, Austria, June 2003.